

Development of a Material Jetting 3D Printer with Magnetic Orientation Capabilities

by

Alejandro Federico Eufrazio Aguilera

A thesis submitted in partial fulfillment of the requirements for the degree of

Master of Science

Department of Mechanical Engineering

University of Alberta

© Alejandro Federico Eufrazio Aguilera, 2018

Abstract

Additive manufacturing (AM) has come to be considered one of the most groundbreaking technologies nowadays, revolutionizing the traditional manufacturing and opening the doors to a new generation of complex freeform engineered functional part. The AM process shows a high correlation between material, design, and the manufacturing process. This relationship offers the possibility to tailor and engineer localized material properties within one part. Currently a number of AM processes are available to deliver tailored mechanical properties through multi-material printing. In this work a novel integrated material-manufacturing-control system to print parts with functional Ferro-magnetic properties is presented. The proposed AM system, based on material jetting, photo polymerization, real time control system, and active magnetic alignment control allows the manipulation of the local orientation of a specialized photosensitive magnetically responsive resin to fabricate objects with locally controlled anisotropic particles arrangement. The proposed system builds upon the standard slicing and path planning algorithms used by open source 3D printing software and extends it by adding two extra dimensions related to the orientation of the magnetic particles within the printing process itself enabling the real-time control of the particles orientation of the printed parts.

To my father

Contents

1	Introduction	1
1.1	Magnetic materials	2
1.2	Additive Manufacturing	2
1.2.1	Additive manufacturing technologies review and comparison	3
1.3	Recent advances	6
1.3.1	Study and fabrication of magnetic anisotropic composites	7
1.3.2	Isotropic magnetic composites additive manufacturing	8
1.3.3	Anisotropic magnetic composites additive manufacture	13
1.4	Motivation	14
2	Magnetic-material deposition system design	15
2.1	Dispensing system	15
2.2	Ultraviolet (UV) curing light	18
2.3	Magnetic alignment jig	19
2.4	Printing Head	21
2.5	Motion platform	24
2.6	Control drivers	28
2.6.1	Motion control module	29
2.6.2	Digital and Analog Input/output modules	33
2.7	Power Supply	33
2.8	System Integration	34
3	Control Software	36
3.1	ADaM Lab - Particles Control Center	38
3.2	ADaM Lab - Motion Control Center	45
3.2.1	CompactRIO and LabView	45
3.2.2	Software workflow	47
3.2.3	Project Explorer files tree	48
3.3	VI's internal description	50
3.3.1	Motion control	50
3.3.2	Essential function blocks	54
3.4	VI description	57
3.4.1	FTP Loader VI	57
3.4.2	Main VI	59
3.4.3	FPGA VI	73
4	Experimental validation	76
4.1	Printing test	76
4.2	Particles alignment test	80
4.2.1	Alignment characterization	81
4.3	Conclusion	83

References	87
Appendix A	90
A.1 Ultimus V	90
A.2 UV LED Driver	97
A.3 Permanent Magnets Setup	102
A.4 Final Assembly Images	104
A.5 SISU-1004 FPGA VI code	109
A.6 Deposition Test	115
A.7 Particles orientation test G-Code	117
A.8 Alignment characterization images	120
A.9 Permission letters	121

List of Tables

3.1	XY common configurations	51
3.2	Z axis configurations	53
3.3	C axis configurations	54
3.4	G-Codes cases.	67

List of Figures

1.1	Single and multi step process principle	3
1.2	Single-step AM polymer processing	4
1.3	Vat photopolymerization schematic	5
1.4	Binder jetting Schematic	5
1.5	Material jetting schematic	6
1.6	Field-structured composites	7
1.7	Process of bonded Nd-Fe-B magnets by injection	8
1.8	3D printed magnet vs commercial magnet	10
1.9	Hysteresis loops	11
1.10	3D printed magnet vs commercial magnet	11
1.11	BAAM system	11
1.12	Demagnetization curves for both BAAM and injection molding	12
1.13	Drop-on-demand apparatus	13
1.14	Hysteresis loops	14
1.15	3D printed magnet vs commercial magnet	14
2.1	Ultimus V precision dispenser	17
2.2	UV LED and development kit	19
2.3	FEMM simulation of the Halbach array	21
2.4	Halbach array inside of gear	22
2.5	Printing head bottom view	23
2.6	Printing head front view	24
2.7	C-Beam linear actuator	25
2.8	Gantry configuration	26
2.9	Design drawing of the XYZ gantry	27
2.10	Deposition System CAD model	28
2.11	CompactRIO controller	29
2.12	SISU-1004 pin-out	30
2.13	EM705 stepper motor drive	31
2.14	Incremental torque per Micro-step/Full-step	32
2.15	A4988 carrier minimum wiring diagram	33
2.16	Integration diagram	35
2.17	Final assembly	35
3.1	3D printing workflow	38
3.2	Example of a G-Code line	39
3.3	Particles Control Center - GUI	40
3.4	Toolpath example and alignment options	42
3.5	Post-processing algorithm	44
3.6	VI front panel, connector pane and back panel	46
3.7	LabView data flow example	47
3.8	VI's block diagram	48
3.9	Project explorer files tree	49
3.10	Machine coordinate system	51

3.11	X-axis direction configuration	52
3.12	Y-axis direction configuration	53
3.13	Softmotion VI's pallet	55
3.14	Ultimus V VI pallets	56
3.15	PWM block diagram	57
3.16	FTP VI front panel	58
3.17	FTP VI back panel	58
3.18	Main VI front panel	59
3.19	Manual control interface	60
3.20	Manual control block diagram	62
3.21	Homing block diagram	64
3.22	Printing control interface	65
3.23	Read file block diagram	65
3.24	String parsing block diagram	66
3.25	Cases diagramm	67
3.26	Case F block diagram	68
3.28	Case Z block diagram	69
3.27	Case E block diagram	70
3.29	Case L block diagram	71
3.30	Main VI graph indicator	72
3.31	Main VI additional controls	73
3.32	FPGA front panel	74
3.33	FPGA back panel	75
4.1	UofA CAD model	77
4.2	Deposition test	78
4.3	UofA logo printing test	79
4.4	Grid used for directionality test	79
4.5	Grid used for directionality test	81
4.6	Optical microscopy images of aligned particles in cured resin	82
4.7	Magnetic particles directionality data	83
A.1	Permanent magnets setup side view	103
A.2	Permanent magnets setup top view	103
A.3	Assembly view 1	105
A.4	Assembly view 2	106
A.5	Assembly view 3	107
A.6	Assembly view 4	108
A.7	FPGA VI - section 1	110
A.8	FPGA VI - section 2	111
A.9	FPGA VI - section 3	112
A.10	FPGA VI - section 4	113
A.11	FPGA VI - section 5	114
A.12	Zero degree alignment	120

Abbreviations

A Ampere. 18, 19

AM Additive Manufacturing. 1, 3, 14, 15, 24

BAAM Big Area Additive Manufacturing. 11, 12

CAD Computer-Aided Design. 23, 27, 28, 36

cc Cubic Centimetre. 17, 84

FEA Finite Element Analysis. 27

FEMM Finite Element Method Magnetics. 20

FSC Field Structured Composites. 7

GUI Graphical User Interface. 40, 59

NdFeB Neodymium Iron Boron. 20, 22

PWM Pulse Width Modulation. 28, 33

STL Stereolithography. 36

T Tesla. 20

UV Ultraviolet. iv, 1, 4, 6, 17, 18, 21, 23, 34

V Volt. 18

VI Virtual Instrument. 18

Glossary

3D printing The act of using an additive manufacturing machine (3D printer) to produce a solid object one layer at a time (also known as additive manufacturing). 2, 13

Br Remanence is the magnetization left behind in a ferromagnetic material (such as iron) after an external magnetic field is removed. 12

Combo box It is a combination of a drop-down list or list box and a single-line editable textbox, allowing the user to either type a value directly or select a value from the list. 40

cRIO CompactRIO is a real-time embedded industrial controller made by National Instruments for industrial control systems. 29

FPGA Field Programmable Gate Arrays can be reprogrammed to desired application or functionality requirements after manufacturing. 45, 56

FTP File Transfer Protocol, is a standard network protocol used for the transfer of computer files between a client and server on a computer network. 47

Hc The magnetic coercivity is a measure of the ability of a ferromagnetic material to withstand an external magnetic field without becoming demagnetized. 12

LabView Laboratory Virtual Instrument Engineering Workbench is a system-design platform and development environment for a visual programming language from National Instruments. 16, 18

PR48 The Autodesk Standard Clear Prototyping Resin. 18, 81

RJ45 Computers, a commonly-used name for the 8P8C modular connector used in Ethernet and other data links. 29

RS232 Recommended Standard 232 is a standard introduced in 1960 for serial communication transmission of data. 16, 28

Ultimus V Provides high-precision benchtop fluid dispensing control for advanced applications of fluids that change viscosity. 16–18

XML Extensible Markup Language is a markup language that defines a set of rules for encoding documents in a format that is both human-readable and machine-readable. 41

Chapter 1

Introduction

In the present work, an additive manufacturing (Additive Manufacturing (AM)) process involving a magnetically loaded ultraviolet (UV) sensitive resin was investigated. The goal was to manufacture anisotropic permanent magnets with enhanced characteristics that eventually could find their way to the industry. Such permanent magnets would exploit the advantages of additive manufacturing, featuring complex geometries not achievable, nor economical, by traditional manufacturing methods. Furthermore, this new manufacturing approach would enable the user to tailor localized properties in the AM magnet. Then, all this effort could be translated, as an example, to an increase in the performance of electric motors, having a direct impact in energy consumption and therefore, a decrease in the devastation of natural resources required to generate it.

The positive impact that magnetic materials can represent for the industry is presented as part of this chapter. The concept of magnetic field structured composites, the improvement that these can offer on the performance of many electrical applications, and some of the different manufacturing methods used to create them are briefly discussed. Along with this, the limitations and challenges on the current fabrication processes are examined. The concept of additive manufacturing (AM) is introduced and proposed as an alternative manufacturing technique to create these anisotropic magnetic composites. The advantages and disadvantages of some of the available technologies are compared; then, the selection of material jetting is justified as the most suitable

from the available options. Following this, an overview of the state of the art in both additive manufacturing of magnetic materials and anisotropic magnetic composites is presented. In this context, the motivation of the ADaM Lab for the development of an original material jetting additive manufacturing system, capable of creating localized magnetic anisotropy is outlined.

1.1 Magnetic materials

Satisfying the increasing demand of humankind for energy has greatly put stress on the Earth's natural resources, causing climate change and other severe effects on the environment. New approaches are then necessary to guarantee the future of our society, and improving the way that we transmit and use energy will be essential for this goal. An effective way to impact energy consumption is through the improvement in energy efficiency. In developed countries, half of the generated energy is consumed by electric motors, and around 60 to 80 % of the electricity used by the industry along with 35 % of the electricity used by the commercial sectors in the European Union, is consumed by electric motors as well [4]. Considering this, functional magnetic materials like advanced hard and soft magnets, magnetic memory alloys, magnetorheological fluids, and elastomers can have an important impact on improving the performance of these technologies [6]. As an example, an improvement of 1 % in electric motor efficiency would result in hundreds of millions dollars of savings and an equivalent reduction of nearly 2.2 million metric tons of carbon emissions [6].

1.2 Additive Manufacturing

Additive manufacturing, also known as 3D printing, is a relatively new technology that has come to disrupt traditional manufacturing methods. Introduced in the 80's, additive manufacturing has been related to the term *rapid* referring to how it is a faster process than the conventional manufacturing methods (for small quantities) that would involve specific tooling. This is how 3D printing has evolved and expanded to include end-user products with

numerous multi-functional characteristics and materials. It is based on the fundamental principle of building an object layer by layer, consolidating material only where needed. Additive manufacturing is then capable of creating highly complex geometries in smaller quantities, and is more economical in comparison to traditional processes.

1.2.1 Additive manufacturing technologies review and comparison

Additive manufacturing processes can be divided into two main groups based on the number of steps required to generate a part with certain properties. These two divisions, as shown in Figure 1.1, are single-step and multi-step AM processes. In a single step process, both the geometry and the properties of a part can be developed in a single fusing material operation. In a multi-step process, for example, the geometry can be created in a primary operation and the material properties can be developed in a secondary operation and depending on the application, further post-processing operations might take place [1].

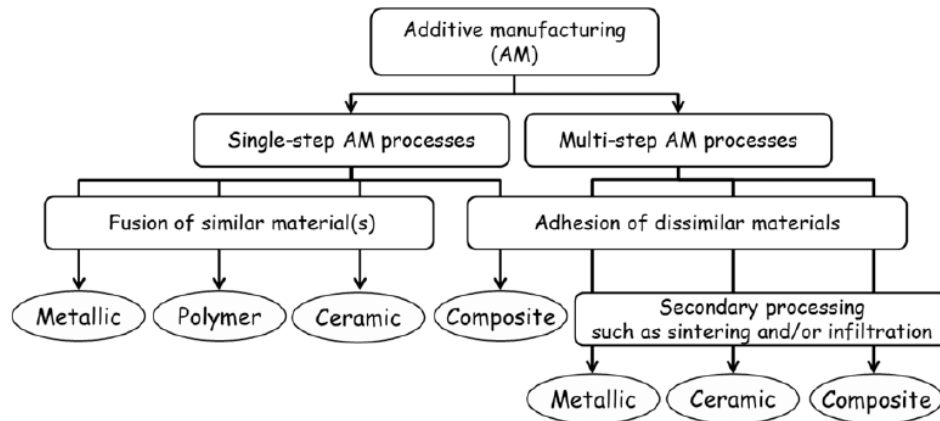


Figure 1.1: Single and multi step process principle [1] ¹.

In a further division, single-step processes are divided depending on the type of material being used. These divisions includes metallic, polymer, ceramic, and composite materials. The general processing principles for each one of these materials are further divided so each individual AM method can

be clearly defined and identified. Based on the polymeric nature of the UV sensitive resin selected for this research, the polymer processing principles were closely analyzed to select the most suitable material for our application. A detailed sub-division of the processing principles for polymer materials is shown in Figure 1.2. From these different processes, the ones that can be applied to our liquid resin were analyzed and will be described next.

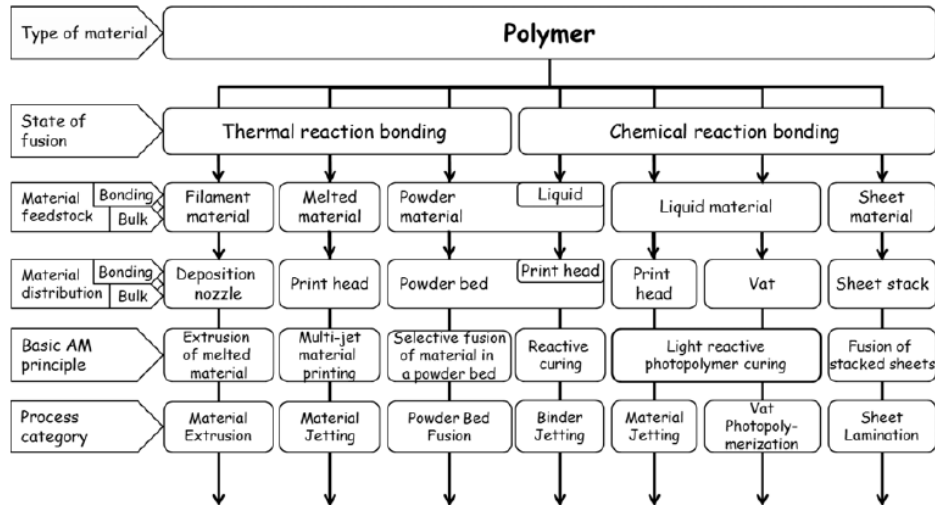
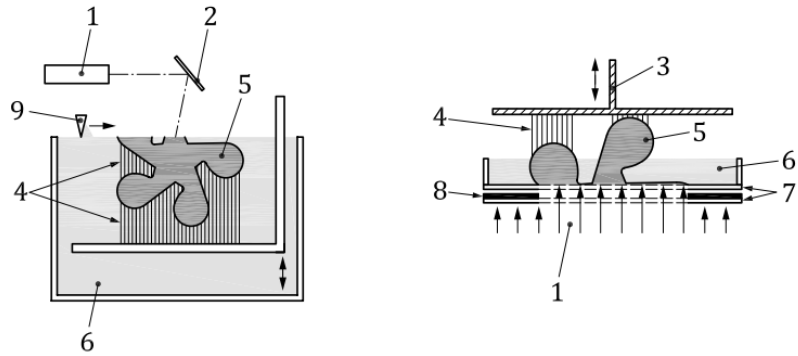


Figure 1.2: Single-step AM processing for polymer [1] ¹.

Vat-photopolymerization shown in Figure 1.3 is a process in which liquid resin in a vat is selectively exposed to light (with a projector or a laser typically), which triggers a polymerization process that solidifies the exposed areas. Then, a new layer of resin is added and again, it is selectively solidified. This technique offers a high level of accuracy and complexity, but it is usually constrained to relatively small building areas. Technologies like SLA, DLP, 3SP and CLIP are included in this category.

¹Copied by Alejandro Eufrazio Aguilera at the University of Alberta with the permission of the Standards Council of Canada (SCC) on behalf of ISO.



a) Vat photopolymerization by laser light source

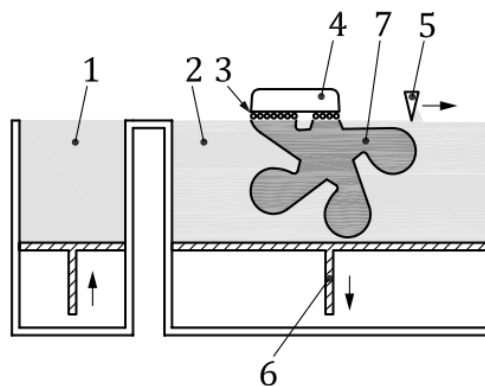
b) Vat photopolymerization by controlled area light source

Key

- | | |
|-------------------------------|---|
| 1 energy light source | 6 vat filled with liquid photocurable resin |
| 2 tilted mirror with focus | 7 transparent plates |
| 3 build platform and elevator | 8 photo mask |
| 4 support structure | 9 recoating and surface levelling mechanism |
| 5 product | |

Figure 1.3: Vat photopolymerization schematic [1] ².

Binder jetting shown in Figure 1.4 is a process in which a liquid bonding agent is selectively deposited to join thin layers of powdered material, then a new thin layer of the powder is spread, and the process is repeated. One of the advantages of this process is the diversity of materials that can be used together, e.g., powdered plastic, metal, ceramics, and sand.

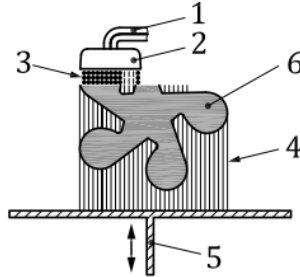


Key

- | | |
|--|-------------------------------|
| 1 powder feeding system | 5 powder spreading device |
| 2 powder material distributed in a powder bed | 6 build platform and elevator |
| 3 liquid bonding agent | 7 product |
| 4 dispensing apparatus including connection to bonding agent feed system | |

Figure 1.4: Binder jetting schematic [1] ².

By definition, material jetting refers to the process of selectively depositing droplets of material layer by layer as shown in Figure 1.5. Usually this process involves UV curable resins and thermally molten materials.



Key

- | | | | |
|---|---|---|-----------------------------|
| 1 | feedstock delivery system for build and support material (optional dependent on the specific process) | 4 | support structure |
| 2 | dispensing apparatus (radiation light or thermal source) | 5 | build platform and elevator |
| 3 | droplets of build material | 6 | product |

Figure 1.5: Material jetting schematic [1] ².

From the described process, different aspects were analyzed, such as the complexity of the technology, the flexibility of the process, and the compatibility with our goals. This is how, based on the fundamental requirement of being able to tailor local properties in the printed part while this is being manufactured, we concluded that, neither a binding nor a vat-photopolymerization process would allow local tailoring and that the technologies themselves were not flexible enough to be further modified. This is how the material jetting process was selected for this application.

1.3 Recent advances

Studies of magnetic anisotropic composites and reports of additive manufacturing systems capable of fabricating permanent magnets have been published [7] [8]. In this work, the most relevant study cases are summarized and their limitations are identified. Then, a custom material jetting based system with capabilities to dispense and align a magnetic-resin is presented.

²Copied by Alejandro Eufrazio Aguilera at the University of Alberta with the permission of the Standards Council of Canada (SCC) on behalf of ISO.

1.3.1 Study and fabrication of magnetic anisotropic composites

Martin et al. [12], presented data describing Field Structured Composites (Field Structured Composites (FSC)'s). These composites are magnetic particle suspensions formed by aligning the particles inside of a resin mixture, applying an uniaxial or biaxial magnetic field, and setting the particles in place via polymerization [12]. As part of this study, both soft and hard magnetic particles were used. Soft magnetic carbonyl iron powder with a size between 3-5 μm in concentrations between 2-30 vol% and hard magnetic SmCo with a concentration of 2.5 vol% were used [12]. The particles were mixed with the epoxy resin Epon 28; combined with a series of hardeners and dispersant; and mixed using an ultrasonic bath, mechanical stirring, and degassed in a vacuum oven. The suspensions were then deposited in polystyrene cuvettes. Using two magnets, a uniaxial 150 G field was applied to the samples, and those were cured for 20 hours and post-cured for another 6 hours.

Figure 1.6 shows the chainlike particles structure created by the applied uniaxial magnetic field on the sample in the cuvette. Using this sample, Martin et al. [12] studied the effect of the anisotropic structures, concluding that both magnetic remanence and susceptibility increase along the alignment axis [12].

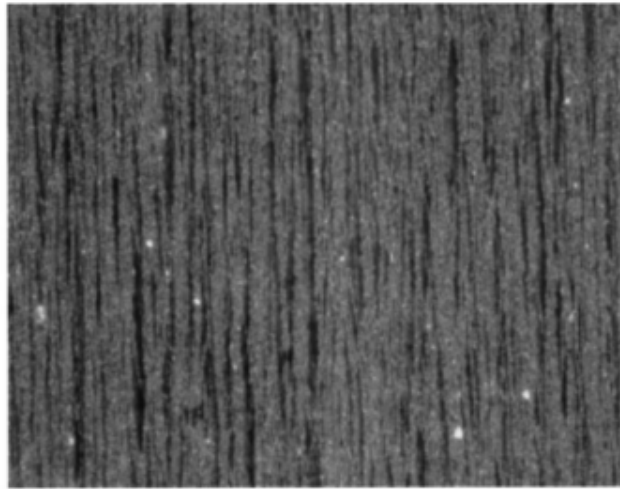


Figure 1.6: Field-structured composites of particles structured by a uniaxial magnetic field [12].

Xiao-lei et al. [25] briefly describe a fabrication method for anisotropic hard magnetic bonded magnets through an injection molding process. Their study is based on the usage of anisotropic Nd-Fe-B magnetic powder. Figure 1.7 shows the process diagram. It can be seen that after mixing the anisotropic Nd-Fe-B powder with additives and binders, prilling it at a temperature of 205-215 C, and injecting it into the mold [25], an external electromagnetic field is generated around the mold to promote some degree of alignment of the particles inside. Finally, the injected part is magnetized by a pulsed magnet and its characteristics are analyzed.

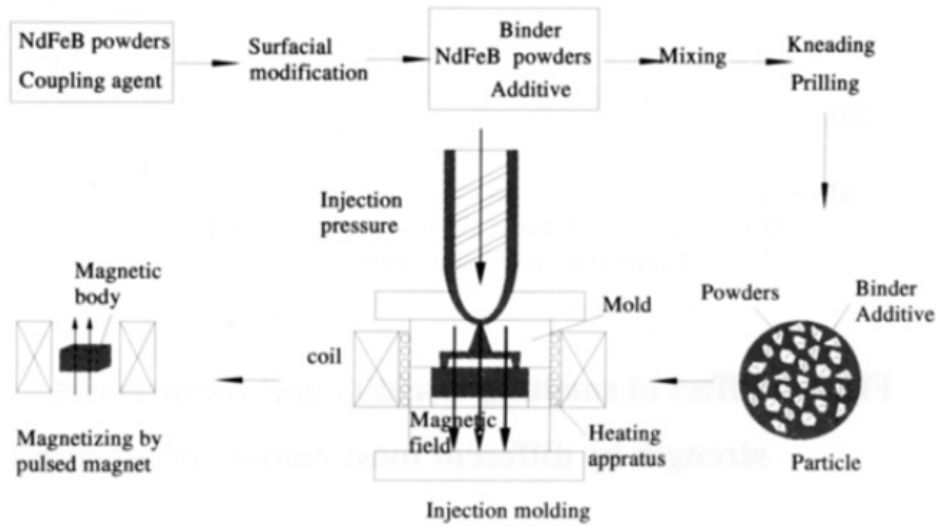


Figure 1.7: Process of bonded Nd-Fe-B magnets by injection [25].

The effects of powder loading, particle size, and the kind of binder used were examined. Their method resulted in anisotropic bonded magnets with a field of $B_r=0.72$ T and $H_c=983$ KA/m.

1.3.2 Isotropic magnetic composites additive manufacturing

The traditional methods for manufacturing permanent magnets have a series of limitations, e.g., the injection molding process tooling of a new mold is required every time that a new design needs to be fabricated, making it a very expensive and slow process. Additionally, the geometry of the mold itself is limited by the

traditional manufacturing methods. Furthermore, techniques such as sintering generate significant waste of magnetic material as part of the tooling needed to achieve net-shape geometries. Motivated by the goal of reducing the waste of this critical material and enabling the creation of complex geometries and sizes, Paranthaman et al. [19], started a new research with the sole purpose of fabricating near-net-shape isotropic NdFeB bonded magnets using additive manufacturing to compete with the conventional injection molding methods [19]. For this study, Parantham [19] selected the binder jetting technique due to its versatility, feasibility, and performance to fabricate the near-net-shape magnets. This method, previously described in section 1.2.1, was then tailored to produce the desired bonded magnets. As described, the first step consisted of preparing a CAD model of the desired part (magnet, in this case); then, the CAD file was exported as an STL file which divides the object into triangles that subsequently, the printer's software separates into layers. An ExOne X1-Lab printer was then used to print the generated shapes [19]. A resin-coated isotropic NdFeB magnetic powder (MQP-B-20173-070) with an average diameter of approximately $70 \mu\text{m}$ was then used in the powder bed for the building area. For this study, several combinations of parameters were tested: the powder layer thickness, the powder packing rate, the binder saturation, the spread speed, and the drying time between layers [19]. A square and a ring shaped magnet were printed and then thermally cured in an oven for 4-6 hours at a temperature ranging between 100-150 C and finally dip-coated with a clear resin.

Figure 1.8 shows a comparison of the binder jet magnets that were 3D printed within the Oak Ridge National Laboratory (on the left) and commercial nickel-coated sintered NdFeB magnets (on the right).

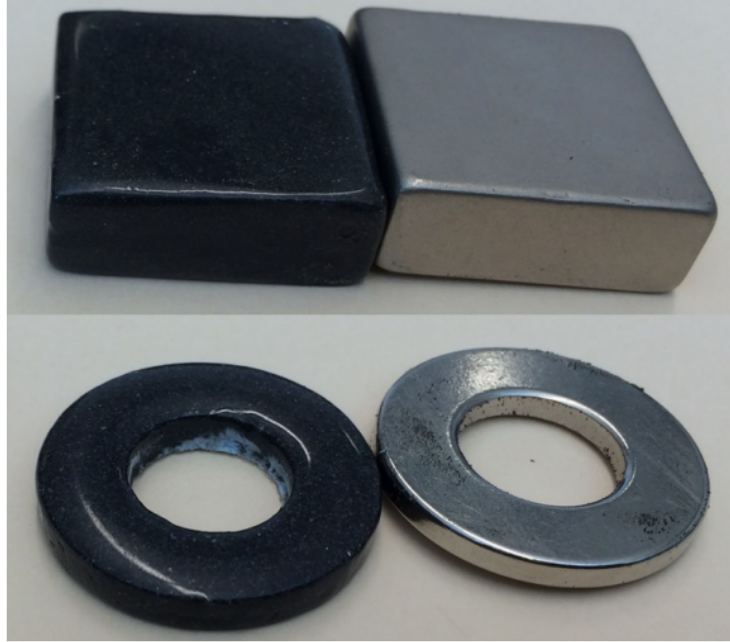


Figure 1.8: 3D printed magnet vs commercial magnet [19].

The above samples were then analyzed. Figure 1.9 shows the hysteresis loop for the printed parts. It was found that the printed parts had a coercivity of 716.2 kA/m that corresponds to the range of values of the initial powder (MQP-B-20173-070) that ranges between 692.3-748.0 kA/m. These results are important because they prove that the coercivity of the powder is not decreased by the process itself. The resultant density of the parts turn out to be 3.47 g/cm, around 46 vol.% of the density of the NdFeB itself (7.6 g/cm). Finally, Figure 1.10 shows a remanent magnetization of about 0.3 T for both parts. Using this information, the manufactured magnets were compared with standard injection molded and sintered NdFeB magnets with a typical remanence of 0.5 and 0.64 T and a volume fraction of 0.65 and 0.80 respectively. Such comparison allows one to estimate a volume fraction of approximately 0.45 of NdFeB powder within the printed magnets [19]. With these results, the team at Oak Ridge concluded that no degradation due to the process itself was present and that further investigation is needed to increase the magnetic particle loading to fabricate stronger bonded magnets.

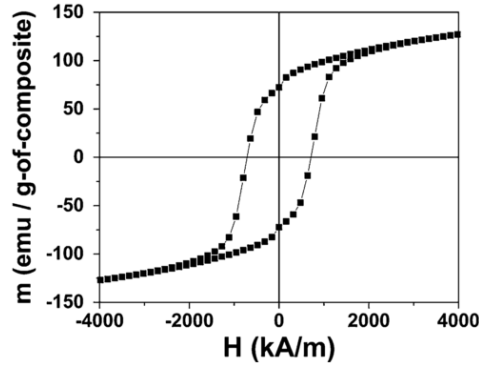


Figure 1.9: Hysteresis loops of a binder jet printed magnet [19].

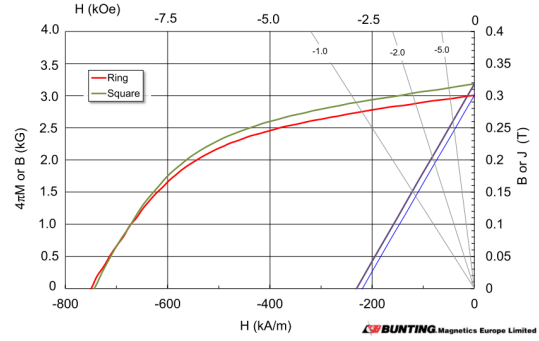


Figure 1.10: Hysteresis loops of the binder jet printed ring and square magnets [19].

The limitations faced with the binder jetting process and the goal of producing more dense parts with better magnetic properties led Ling et al. [9] to start a new project. Named, the Big Area Additive Manufacturing system (Big Area Additive Manufacturing (BAAM)) located at the manufacturing demonstration facility at the Oak Ridge National Laboratory. Combining melting, compounding, and extrusion functions, Ling et al. [9] used this system to extrude magnetic pellets constituted of 65 vol% isotropic NdFeB powder and 35 vol% Nylon-12. Figure 1.11a shows the nozzle dispensing the magnetic material, and Figure 1.11b shows a diagram of the process itself and a hollow cylindrical magnet printed with the BAAM system [9].

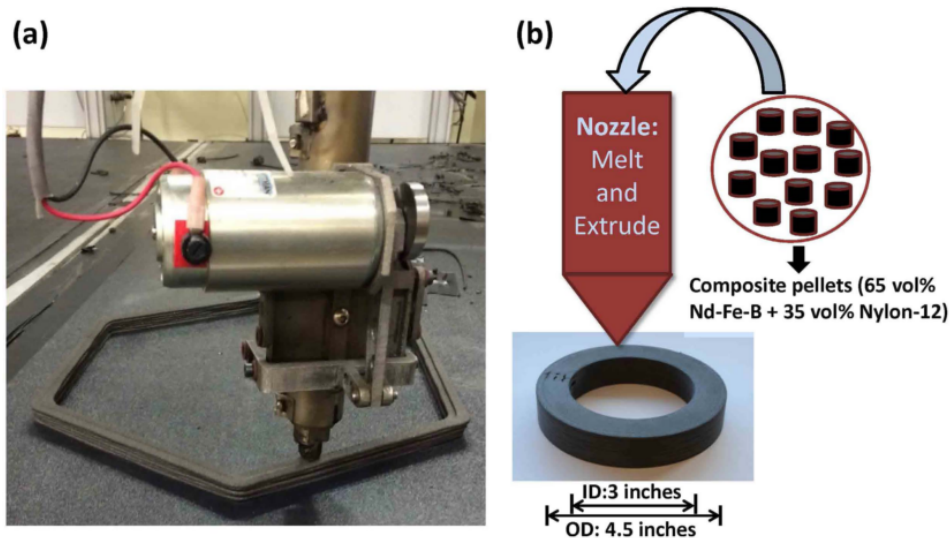


Figure 1.11: BAAM system and process diagram [9].

A comparison of the magnetic, mechanical, and microstructural properties of the 3D printed bonded magnets against commercial injection molded magnets made of the same material was then performed. Starting with the part density, the BAAM magnet resulted in a very similar density as the injection molded magnet with values of 4.8 g/cm and 4.9 g/cm [9]. The most meaningful part from this analysis was the hysteresis loop. Figure 1.12 shows the demagnetization plot of both the BAAM and the injection molded magnets, showing that the BAAM magnet had slightly better magnetic properties, with a coercivity $H_c=688.4$ kA/m and remanence of $B_r=0.51$ T [9].

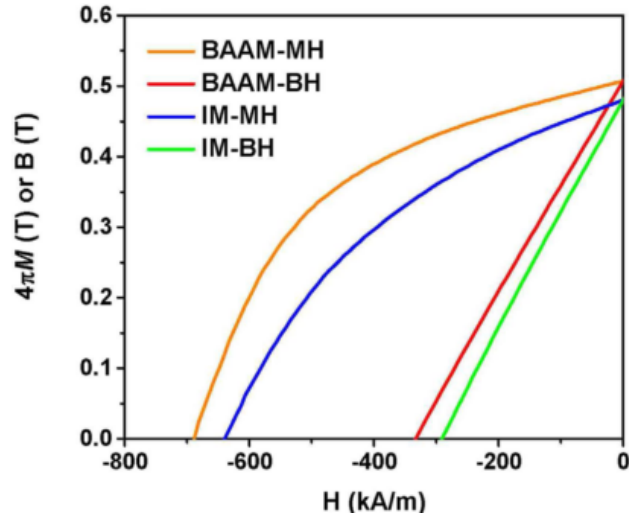


Figure 1.12: Demagnetization curves for both BAAM and injection molded magnets [9].

With these and another series of characterizations, Ling et al. [9] showed that BAAM magnets can outperform injection molded magnets. In addition, these AM magnets have all the advantages that additive manufacturing itself has to offer. These advantages include the reduction of material waste and the capability of producing parts of unlimited size and shapes [9]. Finally, it outlines the agenda for the future work, where the effect of the type of binder used, the loading fraction of the magnetic powder, and anisotropic particles will be investigated.

1.3.3 Anisotropic magnetic composites additive manufacture

Based on a drop-on-demand 3D printing process, Song et al. [23] proposed a methodology aimed at fabricating magnetic composites and components with high permeability and low hysteresis losses, aligning magnetic particles in ink through an external magnetic field during the jetting process [23]. Employing a Thermal Inkjet Pipette (by HP) and a 60 μm nozzle, a printing ink is dispensed on the shape of an aqueous suspension of ferromagnetic Cobalt-based 40 vol% [23]. Then, employing a commercial inkjet paper as a substrate, a custom magnetic alignment setup and a high-resolution XY-rotational stage, Song et al. [23] made two sample parts to analyze the performance of the proposed technique. Figure 1.13(a) shows an illustration of the apparatus created and Figure 1.13(b) shows two sample parts.

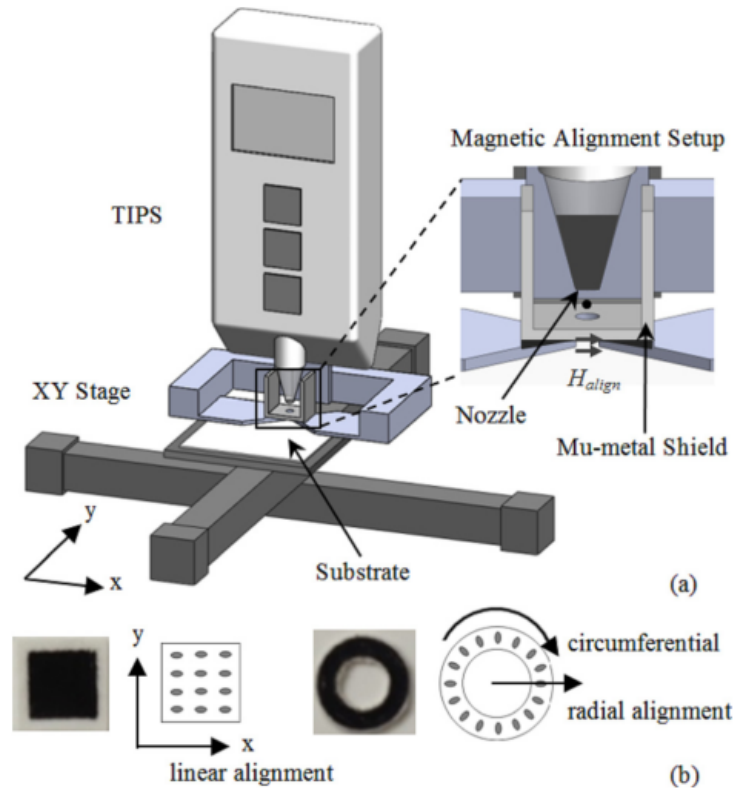


Figure 1.13: Drop-on-demand apparatus [23].

Figures 1.14 and 1.15 show the normalized hysteresis curves of both

sample parts. Both sample parts were cut in to slices to be analyzed. For both of the unaligned samples it was found that the x and y directions of the hysteresis curve overlap with each other. In comparison, for both of the samples printed while applying the 10 mT magnetic field a different pattern is shown for the x and y directions exhibiting anisotropy.

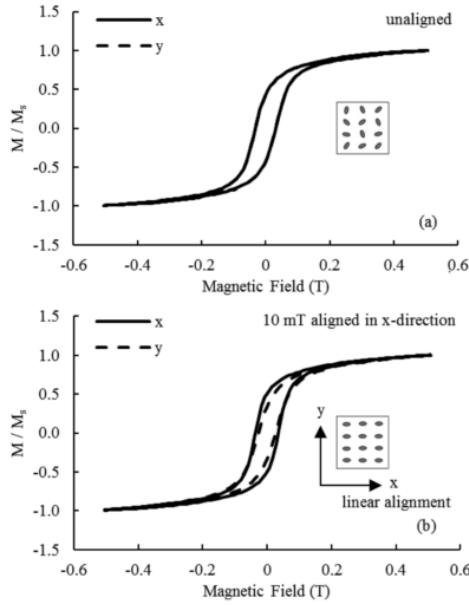


Figure 1.14: Hysteresis loops for the square shape printed sample [23].

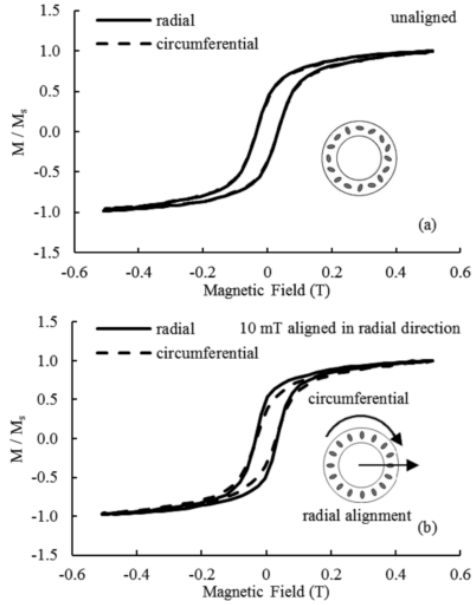


Figure 1.15: Hysteresis loops for the ring shape printed sample[23].

1.4 Motivation

The few but most important research related to additive manufacturing of magnetic composites published at the time that this document was written were presented. The research team at the ADaM lab was able to identify the opportunity of developing an AM system capable of creating in-situ magnetic particle alignment. The goal was manufacturing tailored permanent magnets and magnetic composites with intricate geometries and anisotropic magnetic properties.

Chapter 2

Magnetic-material deposition system design

As detailed in Chapter 1, the material jetting process resulted in the most promising AM method to experiment with magnetic particles suspended in liquid resin where the rheological behavior can be tailored to achieve particle orientation. In this context, there are many consumer-level 3D printers available on the market, but none of them has the flexibility in terms of hardware or firmware to be modified and used as a research tool. This lack of open frame systems was the main motivation to develop our own. As part of this chapter, a detailed explanation and analysis of the design, the parts that integrate our magnetic material jetting system, and their role on the printing process are described. The system was divided into major components, according to their functionality. Dividing them in this way helps to narrow down and select the options that better suit needs for each of the different solutions.

2.1 Dispensing system

For this magnetic material deposition application, the dispensing system was identified as the most critical component. This is because its capabilities in terms of precision, dispensing volume control, and range of viscosity allowable constrain the rheological characteristics of the magnetic-resin that can be used, as well as the level of accuracy that can be achieved in the material deposited.

To be able to select the most suitable option, the required features for the

dispensing system were listed. First, the dispensing system had to be able to jet viscous fluids with embedded particles with a size of up to 200 μm related to the maximum grain size of the available magnetic powder. Second, the dispensing system had to have a construction or a mechanism to prevent the fluid from coming in contact with internal components of the system itself. Such mechanisms could include having a contamination free system or having inexpensive components that could be replaced every time a new variation of the resin had to be tested. With this approach, multiple variations of the resin could be tested without involving deep cleaning. Third, the system had to allow the selection of different nozzle sizes. Fourth, the final dispensing tip or the system itself had to be relatively small and light to be mounted on an aluminum moving gantry platform. Finally, the dispensing system had to have a control driver that could be externally activated through a standard communication protocol like RS232 or could be directly compatible with LabView.

The first kind of dispensing system analyzed was the one known as micro-dispensing valves. We found out that most of these systems are based on electromechanical or piezoelectric actuators combined with a nozzle. We also learned that these kinds of systems require a number of inflow filters to guarantee that the internal mechanism will not jam or get clogged in the presence of contaminants in the fluid. The presence of such filters will constrain the size of the magnetic powders that we could work with. Furthermore, in these kinds of systems, there is a direct contact of the dispensed fluid with the internal mechanism. Therefore, selecting this system would represent a significant increase in the operation time, due to the necessary cleaning process involved in order to avoid contamination caused by running trials with different variations of the magnetic-resin. Besides, most of the control drivers for these systems have close interfaces that do not offer a direct integration or communication with any hardware outside of the control drivers that are sold by the same manufacturer.

Finally, an Ultimius V precision dispenser was selected. This syringe-piston pneumatic system can be equipped with different kinds of syringe barrels that

can be combined with a large selection of dispensing tips made of different materials with different diameters. Next, the components of the system that get in contact with the fluid to be dispensed, including the syringe barrels, pistons, and dispensing tips are designed to be used one time and be disposed. Thus, making it easier to test different fluids without cross contamination. Figure 2.1 shows an image of the components that integrates this dispensing system.



Figure 2.1: Ultimus V precision dispenser [11].

The Ultimus V is capable of regulating air over a piston in a range from 0 to 100 psi and also regulating vacuum in a range from 0 to 18 H₂O making it suitable for dispensing highly viscous fluids. Due to the UV sensitive nature of the magnetic-resin and the presence of the UV light during the curing process, a 30 Cubic Centimetre (cc) amber syringe barrel was selected. This barrel features a UV filter able to block UV and visible light wavelengths up to 550 nm, at the same time it allows one to visually monitor the fluid level inside of the barrel. Following the same reasoning, a specific group of dispensing tips called smooth flow tapered tips were selected. These tips molded of

polyethylene with a UV light block additive are recommended for applications that involve medium to high viscosity UV-cure adhesives and particle filled materials with a range of nominal inner diameters from 0.26 mm to 1.6 mm. Detailed information of the selected parts and further description of the Ultimius V platform is shown in section A.1 in the Appendix. Lastly, a serial port in the Ultimius V driver allows a direct communication with a plug-in to control and manipulate all the settings as well as the dispensing actions from LabView. A LabView Virtual Instrument (VI) was implemented as part of the ADaM Lab Motion Control Center discussed in detail in Chapter 3.

2.2 UV curing light

The selection of a suitable UV curing system was focused on how easy it would be to integrate and control from LabView. In addition, a complete solution that included all the necessary elements to be operated was preferred over standalone UV LEDs. The criteria for selecting the curing system included controllability through a standard communication protocol and an analog signal or a pulse width modulation signal. The wavelength of the emitted UV light had to be 405 nm, matching the wavelength required to trigger the photoinitiator present in the UV sensitive resin (PR48). The last consideration was the minimum power, which was set to be at least 100 W considering that the UV LED will not be directly over the magnetic-resin when this will be deposited, and that there will be significant losses.

A DK-136M series - Development Kit from Luminus was selected. This kit consists of a driver and a heat sink used to dissipate the heat generated by the high power UV LED. The driver was designed to control a high power light source and its intensity is operated by an onboard rotating knob or with an external pulse signal. A full description of the control signal can be found in section A.2 in the Appendix. The driver is powered by 12 Volt (V) and is capable of driving LEDs up to 36 Ampere (A). A compatible CBT-120 UV LED from the same company was selected to be combined with the development kit. This LED was designed for applications that include curing inks,

coatings, and adhesives; as well as, rapid prototyping and 3D printing. This high power density LED allows a variable current up to 30 A and emits a blue light with a peak wavelength of 405 nm. Figure 2.2 shows both the DK-136M development kit and the CBT-120 LED.

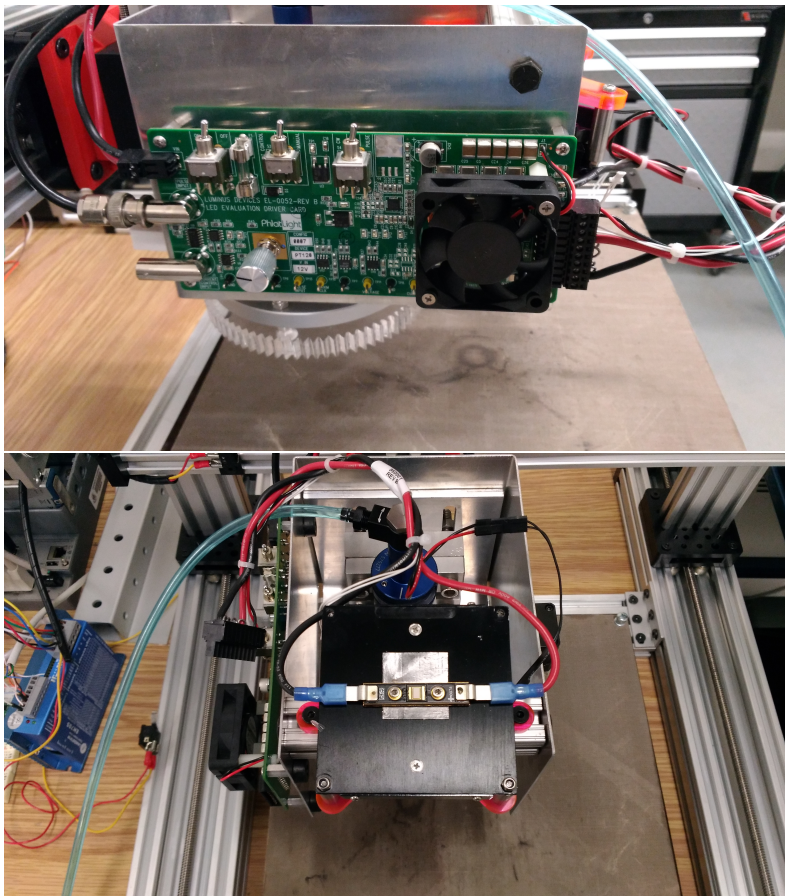


Figure 2.2: UV LED and development kit [22].

2.3 Magnetic alignment jig

As it has been mentioned, the main purpose of this work was to create a machine capable of inducing particle orientation to tailor the magnetic properties of a 3D printed part loaded with magnetic particles. Therefore, initial experiments were conducted to understand what the necessary magnetic field would be to induce the chain like microstructures discussed in Section 1.3.1. Based on these experiments, we were able to prove that by bringing the magnetic

field generated by a pair of permanent magnets to an appropriate distance from a drop sample of the magnetic-resin, the chain like microstructures can be induced. Moreover, we were able to prove that the orientation of the particles can be modified changing the orientation of the magnetic dipole itself. The setup created to run these experiments can be found in the Appendix A.3.

From the previous experiment, we had a first notion of how the particles are oriented applying a magnetic dipole of 0.1 Tesla (T) (estimated through the Finite Element Method Magnetics (FEMM) method). This kind of magnetic dipole was formed by two cubic rare earth magnets with opposite polarities facing each other. From the results obtained, we understood that we would have to generate a stronger field if we wanted to experiment with higher concentrations of particles and more viscous resins. Due to their capability of providing a relatively strong magnetic field within a small volume, the permanent magnet approach was followed. To increase the strength of the field, a special array of eight cubic (1cm^3) Neodymium Iron Boron (NdFeB) N52 magnets was implemented. This special array called a Halbach Array was analyzed using the Finite Element Method Magnetics (FEMM) to determine the magnetic flux density in function of the arrangement among the eight permanent magnets. Figure 2.3 shows the magnets' arrangement and the resulting magnetic flux lines from the FEMM analysis. As it is shown, dipolar uniform flux lines with strength of approximately 0.3 T are generated in the center of the array [16]. Afterwards, the objective was to combine this Halbach Array with a mechanism that allows the array to be rotated and at the same time, moved along the XY plane while the dispensing system deposits the magnetic-resin.

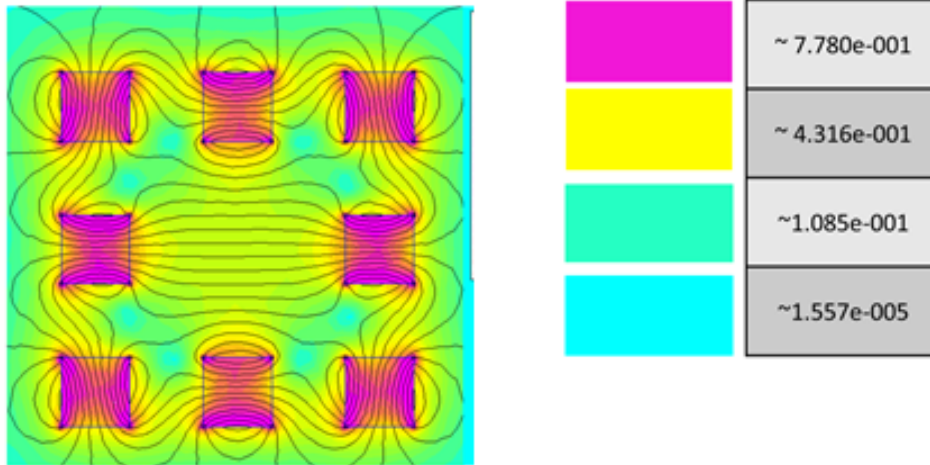


Figure 2.3: FEMM simulation of the Halbach array.

2.4 Printing Head

A modular design where the components needed for dispensing, aligning, and curing the magnetic-resin were put together in a single sub-assembly that is called the printing head. This sub-assembly was required to be light and compact so that a relatively small stepper motor could raise it and lower it down in the Z axis.

Due to its low weight and simplicity to manufacture, aluminum angle and sheet metal were machined to create a support for the syringe barrel, the UV LED, and the Halbach Array. For this proposed design, the syringe barrel was positioned in the center of the printing head. Using two aluminum stanchions, the syringe barrel was secured in place in a parallel position to the Z axis. Furthermore, two slots allowing to modify the distance between the dispensing tip and the bottom of the sub-assembly were machined on the aluminum angle. This feature was included to lower down or bring up the dispensing tip. With this feature, it was possible to modify the distance between the printing bed and the Halbach array, as well as increase or decrease the magnetic flux intensity applied over the dispensed magnetic-resin.

As indicated above, one of the system's requirements was to be able to rotate the magnetic dipole in a programmable way. In order to achieve this,

the previously discussed Halbach Array was embedded into a gear. A half inch transparent acrylic plate was laser cut to create an involute gear profile. At the same time, eight compartments matching the position of the permanent magnets in the Halbach Array, together with a central opening for the dispensing tip to go through, were laser cut in the gear. Using close-fit tolerances for the laser cutting process, the NdFeB magnets were press-fitted and secured in place inside of the acrylic gear. Figure 2.4 shows the manufactured involute gear CAD model with the inserted NdFeB magnets.

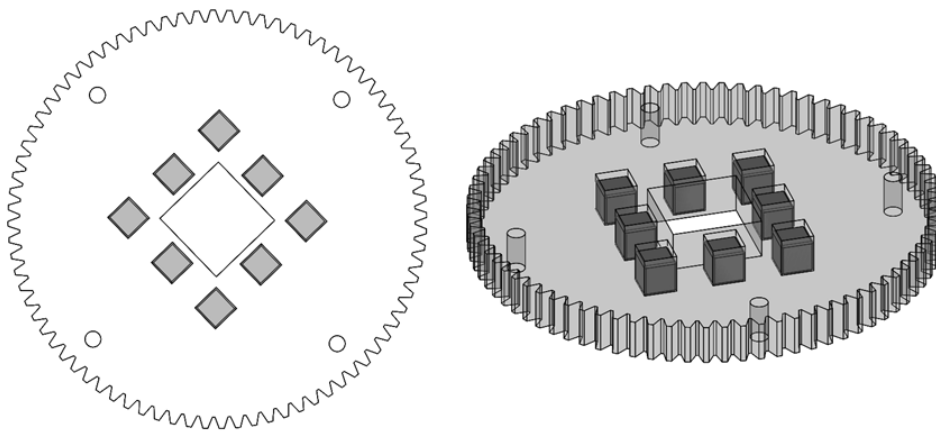


Figure 2.4: Halbach array inside of gear.

To enable the gear to rotate concentrically to the dispensing tip, a swivel bearing was secured in the bottom of the aluminum angle and aligned concentrically to the syringe barrel. Subsequently, the laser cut gear was mounted on the bearing, giving it the freedom to rotate. Finally, to have a precise control of the rotation angle of the gear, a matching pinion cut from the same acrylic plate was attached to a NEMA 14 stepper motor (200 steps/revolution) controlled by a driver with a micro-stepping resolution of down to 1/16-step. For this general configuration, the system was set up for full stepping giving a resolution of 1.8 degrees/step. Figure 2.5 shows the bottom face of the printing head, where the gear containing the Halbach Array and the pinion attached to the Nema 14 stepper motor can be seen.

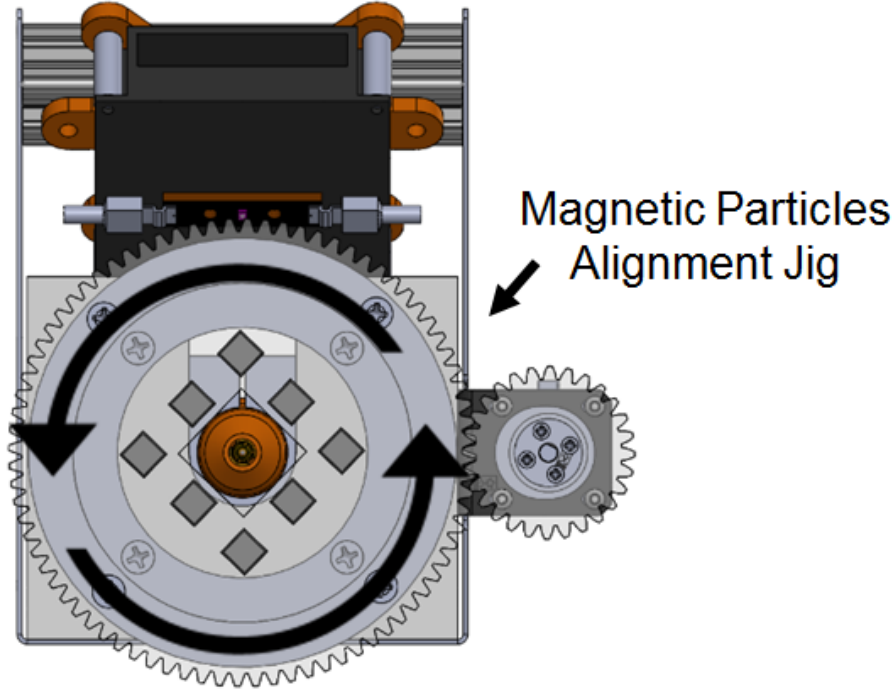


Figure 2.5: Printing head bottom view.

This design combines the mechanical action of a gear with the Halbach Array reducing weight and mechanical elements. At the same time, the transparency of the acrylic plate used allows the light from the UV LED to reach the printing bed, even though the resin is not directly under the dispensing tip, a feature of extreme importance for the curing process.

At last, based on the Computer-Aided Design (CAD) model of the printing head, the appropriate position for the UV LED was determined. That position was found considering the point on the printing bed where the magnetic-resin will be deposited by the dispensing tip, and then drawing a construction line that goes from that point through the opening in the acrylic gear to the center of the UV LED. A T-slotted aluminum profile and a laser cut acrylic support were used to attach the UV LED's heat sink to the aluminum sheet metal. Additionally, the UV LED driver was secured to the side of the sheet metal. Figure 2.6 shows the front view of the printing head's CAD model.

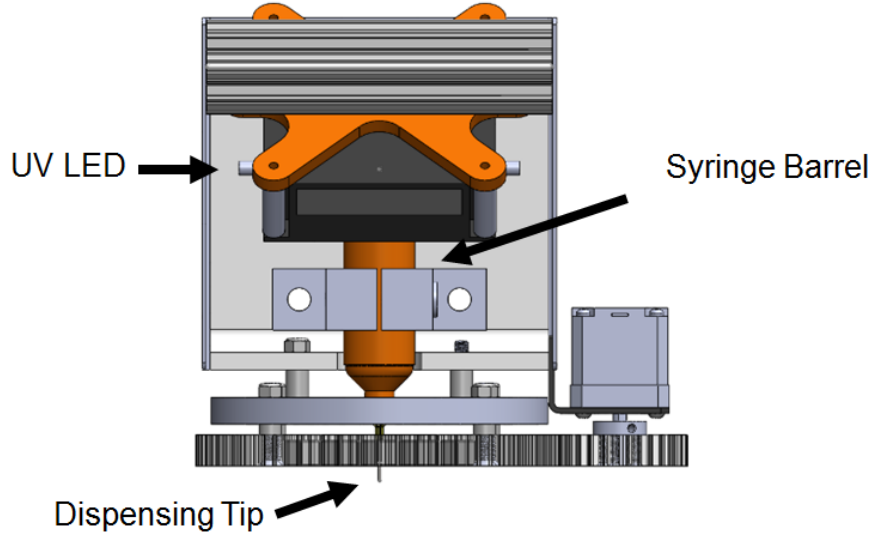


Figure 2.6: Printing head front view.

2.5 Motion platform

As discussed previously, motivated by the close frame construction of the available off-the-shelf motion solutions, we decided to design and build our own open frame system. Based on the modular design of the printing head, the motion platform had to be able to position the whole printing sub-assembly in a controllable way over the X-Y-Z axes. Considering a stable deposition bed, we moved towards a design where the surface on which the magnetic-resin would be deposited remained static, while the printing head would be positioned according to the AM process.

The motion platform was required to be flexible enough that it could be expanded or modified, depending on the needs of the AM process itself. Thus, the system was required to allow cameras, limit switches, and other kinds of sensors to be added. Afterwards, the minimum specifications in terms of force, acceleration, and accuracy were defined to help us with the selection of the best actuator. Considering a maximum payload of 10 kg, and including the printing head and any other extra devices and using conventional 3D printers in the market as reference, we set the minimum acceleration to $500 \text{ mm}/\text{sec}^2$ [2]. Then, the minimum force required for the linear actuators was determined

to be 10 N considering efficiency losses. Finally, we decided upon a minimum accuracy of 100 μm , considering that actuators with higher accuracies would have higher cost. With these considerations, different linear actuators on the market were analyzed. In the end, A C-Beam linear actuator from OpenBuilds was chosen, shown in Figure 2.7. Constructed over a C shape T-slotted aluminum profile, this actuator allowed us to combine it with other T-slotted profiles to design the motion table. Such versatile elements assure us that making later modifications would result in a relatively easy task. Featuring a high torque lead screw, these actuators though not ideal, resulted in the best characteristics in terms of price/performance relationship. Powered by a NEMA 23 stepper motor, the linear actuator is capable of exerting a maximum force of 294 N, and travelling at a maximum speed (under no load) of 5500 mm/min, all this with an accuracy of 119 μm and a repeatability of $\pm 42 \mu\text{m}$ [24].

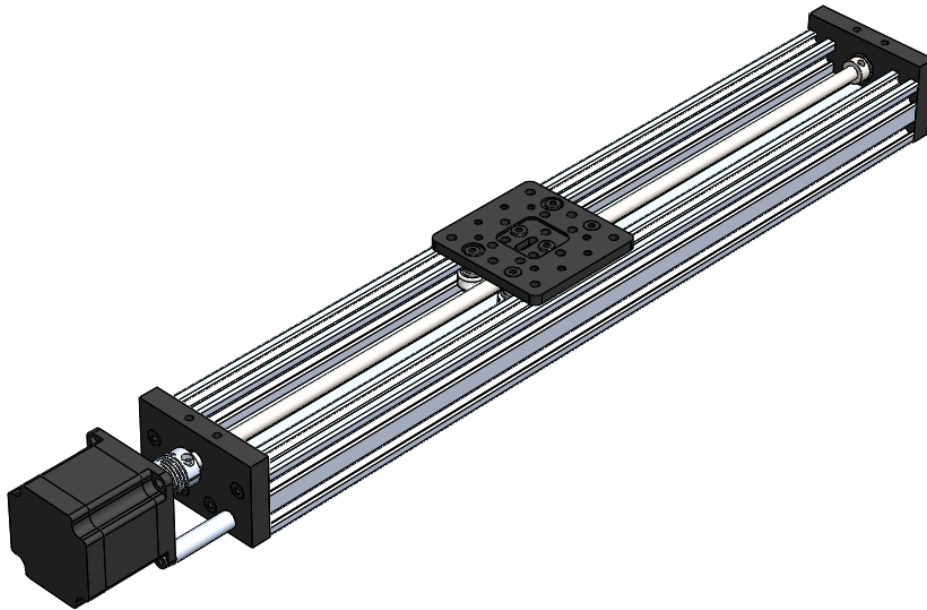


Figure 2.7: C-Beam linear actuator.

Considering the design constraints of a fixed deposition surface and a moving printing head, a gantry configuration was selected. Figure 2.8 shows a schematic of this configuration. As it can be seen, the main characteristic of a

gantry is a bridge-like overhead structure with supports on both ends. In this case, this is useful for separating any component mounted on the top beam from the dispensing surface.

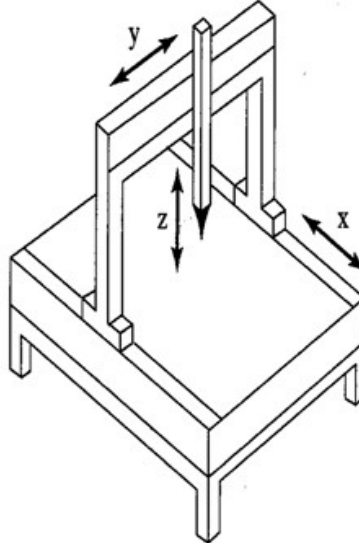


Figure 2.8: Gantry configuration.

To reproduce such a configuration, three C-Beam actuators with travel distances of 400 mm were combined with T-slotted linear rails working as the supports. Two out of the three C-Beam actuators were combined in a parallel configuration over the Y-axis, keeping a separation distance enough to match the length of the linear actuator itself. The third actuator designated to power the X-axis was combined with two vertical supports and secured on the top of the moving carriages of Y-axis actuators to recreate the overhead structure.

The next element of the motion platform was the one that connects the motion platform itself with the printing head and at the same time allows the printing head to be lowered and raised during the printing process. For this task, a lead screw linear actuator with an effective travel distance of 100 mm and powered by a NEMA 14 stepper motor was attached to the moving carriage of the C-Beam actuator on the X-axis. With a screw pitch of 1 mm and driving at full step by a 200 steps/rev NEMA 14 stepper motor, this actuator can modify the height of the printing head with a resolution of 5 μm under ideal conditions. Figure 2.9 shows the designed gantry configuration of

the motion platform previously described.

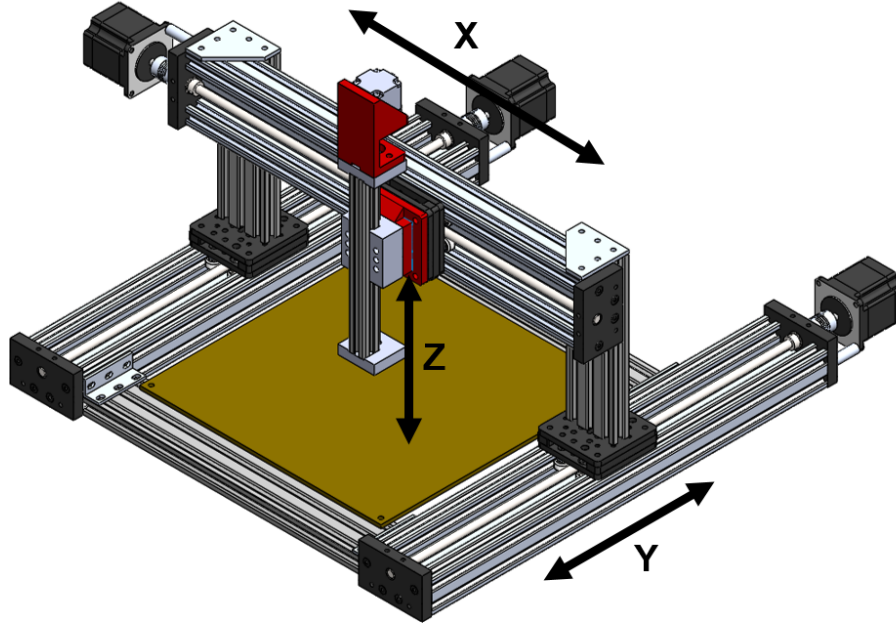


Figure 2.9: Design drawing of the XYZ gantry.

As a last component of the motion platform, an appropriate surface for depositing the magnetic-resin was needed. Using the Finite Element Analysis (Finite Element Analysis (FEA)) to find the appropriate material and geometrical characteristics for the deposition surface, a 1/8 inch thick acrylic plate of 30 cm x 30 cm was chosen. To extend the life of the plate this covered with an anti-sticking film. This plate, called the printing bed, was mounted upon a set of leveling supports. These spring based supports allows for fine leveling compensations to assure that the distance between the dispensing tip and the printing bed will remain within tolerance all around the printing area. Figure 2.10 shows a CAD model of the complete deposition system combining all the previously described elements in a design that allows us to run different kinds of experiments without being limited by a closed frame or a pre-established workflow.

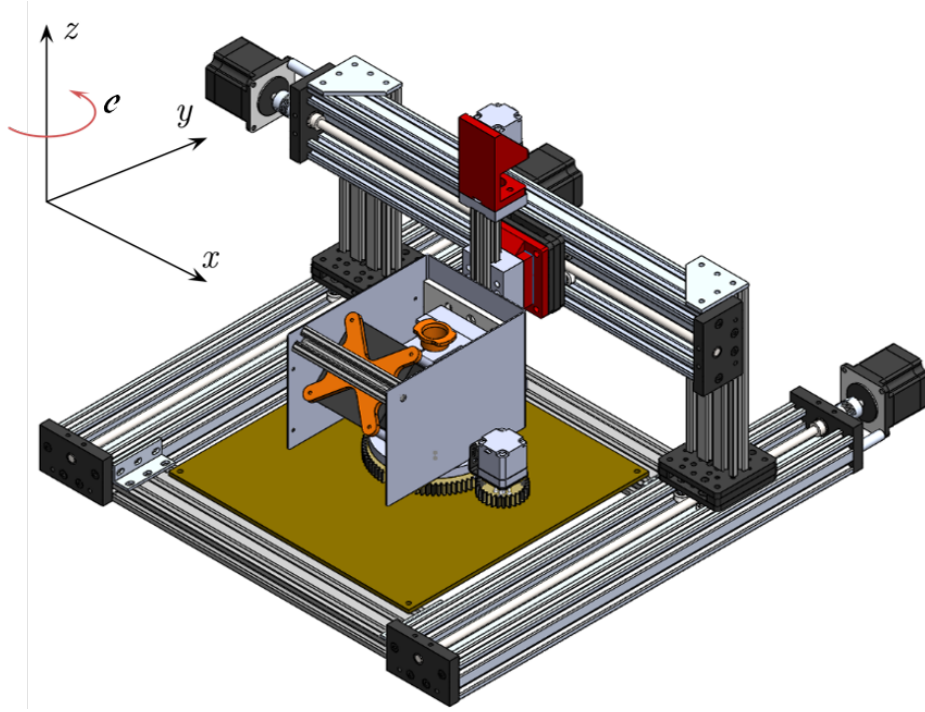


Figure 2.10: Deposition System CAD model.

2.6 Control drivers

Several CNC controllers were initially analyzed to be used in our application. For selecting one of the many options available, we required the controller to have: first, the capability to control no less than 4 motion axes necessary for our CNC application; second, the capability to control external devices through standard communication protocols such as RS232; third, the ability to receive and generate both digital and analog signals to read or control simple digital sensors like limit switches as well as analog sensors. Finally, the controller had to be able to generate Pulse Width Modulation (PWM) signals. The PWM or Pulse Width Modulation is a technique used to generate an analog voltage out of a digital signal. This is achieved by generating a square signal and modifying the time of the cycle in which the signal stays on the high position versus the time that it stays on the low position. Many drivers use this as an input to set the speed of a motor, or in our case, to configure the intensity of the LED.

Ultimately, a solution from National Instruments was preferred, mainly mo-

tivated by the initial decision of using LabView as a development environment. From the options offered by National Instruments, a cRIO-9066 was selected. Shown in Figure 2.11, this FPGA based controller with a 667 MHz dual-core CPU, 256 MB of DRAM, and 512 MB of storage, features eight slots to which different modules can be connected [15]. These modules include digital I/O, voltage and current outputs, motion, removable storage, counter measurements/pulse generation, timing and synchronization, wireless measurements, serial communication, temperature, resistance, and others. The flexibility and expansibility of this controller, along with its real-time processor running a NI Linux real-time operating system, makes it more than adequate to control our platform. A further description of the cRIO, in terms of its architecture and software, is given in the next chapter.



Figure 2.11: CompactRIO controller [15].

Three modules for the cRIO were selected to fully control the devices present in our platform. These modules included a motion control module, a digital input/output module, and an analog input/output module.

2.6.1 Motion control module

A SISU-1004 motion control module was selected. This four-axis stepper motor interface allows synchronized control of all axes using its Softmotion control plugin for Labview. Using RJ45 connectors, this module features all the necessary inputs and outputs per axis to control the X-Y-Z coordinated axes from the motion platform and the rotation of the magnetic alignment jig. Figure

2.12 shows the pinout diagram of one of the four ports of the SISU-1004. The outputs include step, direction, and enable; and the inputs include forward limit, reverse limit, and drive fault.

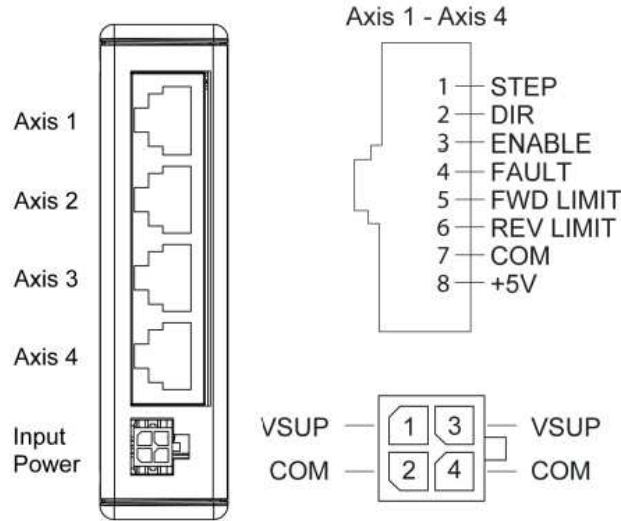


Figure 2.12: SISU-1004 pin-out [14].

These low voltage control signals cannot directly run a stepper motor. For this, an intermediate device capable of receiving such signals and translating them to power outputs that can be applied to terminals of the stepper motors is necessary. First, three drivers with the necessary characteristics to drive three Nema 23 stepper motors that run the X-Y axes were selected. The EM705 from Leadshine, shown in Figure 2.13, is a two-phase digital stepper drive capable of delivering 0.35 to 5 A of current in the range from 20 to 70 V, sufficient to control the 495 Oz-in and 5 A Nema 23 stepper motor used in our application. Featuring the exact same inputs/outputs like the SISU-1004, the EM705 drive can be configured to set a determined output current depending on the specifications for the stepper motor to be controlled. The EM705 has the capability of configuring the micro-stepping resolution for the stepper motor. Ranging from 200 steps/rev up to 25,000 steps/rev, it has the capability of configuring such resolution through dip switches physically located on the driver.



Figure 2.13: EM705 stepper motor drive [5].

The capability of generating micro-stepping can be reflected into reduced vibrations and higher resolution in the system, combined with the 8 mm metric Acme lead screws with a pitch of 2 mm belonging to the C-Beam linear actuators. The stepper motor/EM705 drive combination could reach a resolution that is calculated as:

Considering a screw pitch of 2 mm and a selected micro-stepping resolution of 25000 steps/rev

$$1rev = 2mm \text{ (linear displacement)}$$

$$1rev = 25000steps$$

$$1step = \frac{2mm}{25000steps}$$

$$1step = 80\mu m \text{ (linear displacement)}$$

Such resolution seems to be much higher than the minimum required for our application, but it is important to understand that there is a disadvantage when it comes to the use of micro-stepping. When the number of micro-steps per revolution is increased, there is a loss of incremental torque per micro-step. This means that depending on the load, a number of successive micro-steps would have to be sent until the accumulated torque exceeds the load torque

plus all the other forces related to the friction of the mechanism itself. Figure 2.14 shows the negative effect of micro-stepping on the incremental torque per micro-step as a function of the increment on micro-steps per full step.

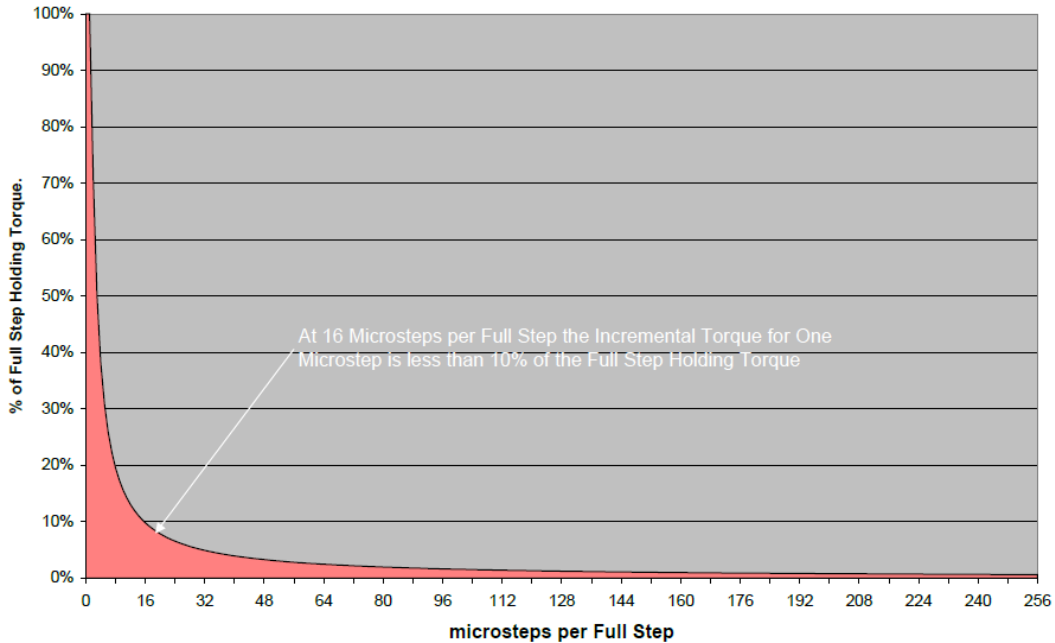


Figure 2.14: Incremental torque per Micro-step/Full-step [13].

Finally, a different driver with matching capabilities to control the 20 Oz-in and 1 A Nema 14 stepper motors used in the Z axis of the motion platform and in the magnetic alignment jig was selected. The A4988 Stepper Motor Driver Carrier shown in Figure 2.15 is a breakout board sold by Pololu for the Allegro’s A4988 bipolar stepper motor drive. This drive is capable of operating with voltages from 8 to 35 V and delivering up to 2 A per coil if sufficient cooling is provided. It features the same input signals as the SISU-1004 and has the capability of micro-step resolutions down to 1/16 step.

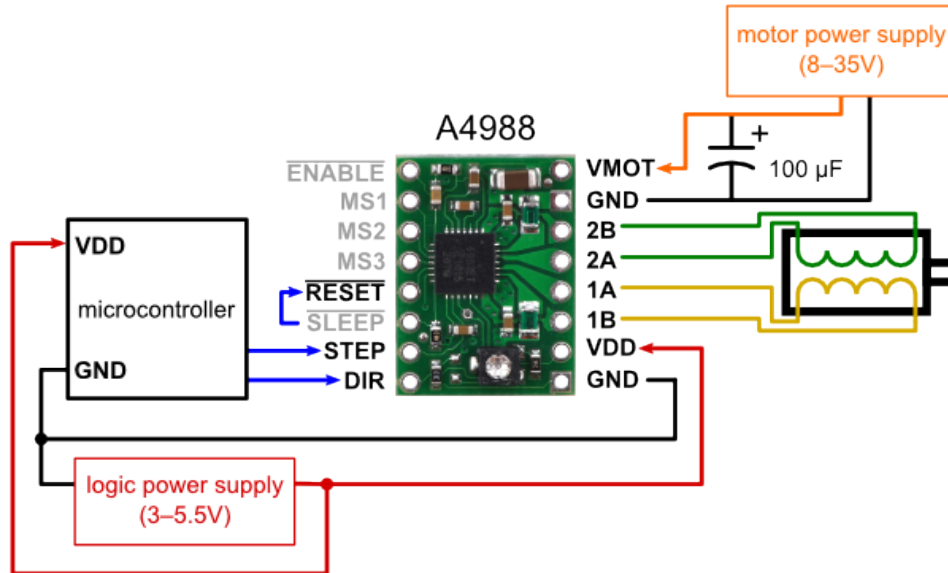


Figure 2.15: A4988 carrier minimum wiring diagram [20].

It is important to highlight that the initial configuration for the stepper motors was set to full step.

2.6.2 Digital and Analog Input/output modules

A 32-channel digital input/output module (NI-9403) and a 32-channel analog input/output module (NI-9201) were selected. Based on the need of generating a PWM signal to control the light intensity of the LED, one of the ports from the digital input/output module was configured using software to generate such a signal at a frequency of 2.8 kHz. Then, the duty cycle was manipulated to obtain the desired light intensity. The remaining inputs are then available to include external devices or sensors in the future.

2.7 Power Supply

With all the actuators, drivers, and devices in place, a selection of the appropriate power supplies that satisfied the voltage and current requirements of each of the components was conducted. Three different power supplies were included in the platform. First, a PS-15 power supply from National Instruments with an output voltage of 24 V and 5 A was used to power the real-time

controller cRIO and the SISU-1004 motion controller, both with acceptable input voltages from 18 to 30 V and relative low power consumption. Second, an RPS4810 from Leadshine with a supply voltage of 48 V, a rated current of 10.4 A, and a peak current of 12.5 A was used to power the three Nema 23 stepper motors through the EM705 drives. With different voltage outputs and current capabilities for each output, a 500 W ATX power supply was used to provide a 12 V and 35 A input for the UV LED DK-136M series development kit, which had to supply up to 30 A to the CBT-120 UV LED. Lastly, a 5 V output from the ATX power supply was used to power the logic stage of the A4988 stepper motor driver carrier and another 12 V output was used to power the Nema 14 stepper motors driven by the A4988 driver.

2.8 System Integration

Once the components were received, manufacturing drawings were created and sent along with either raw material or off-the-shelf components to be fabricated. With all the manufacturing completed, the motion platform was assembled. The 3-axis CNC system was wired and interfaced with the drivers and controllers. Then, the remaining components like the dispensing system, the LED, and the printing head were integrated one by one, developing the appropriate control software and optimization for the best configurations. In the next chapter, a detailed explanation of this interface and the software developed is presented. Figure 2.16 an interaction diagram of all the components described in this chapter.

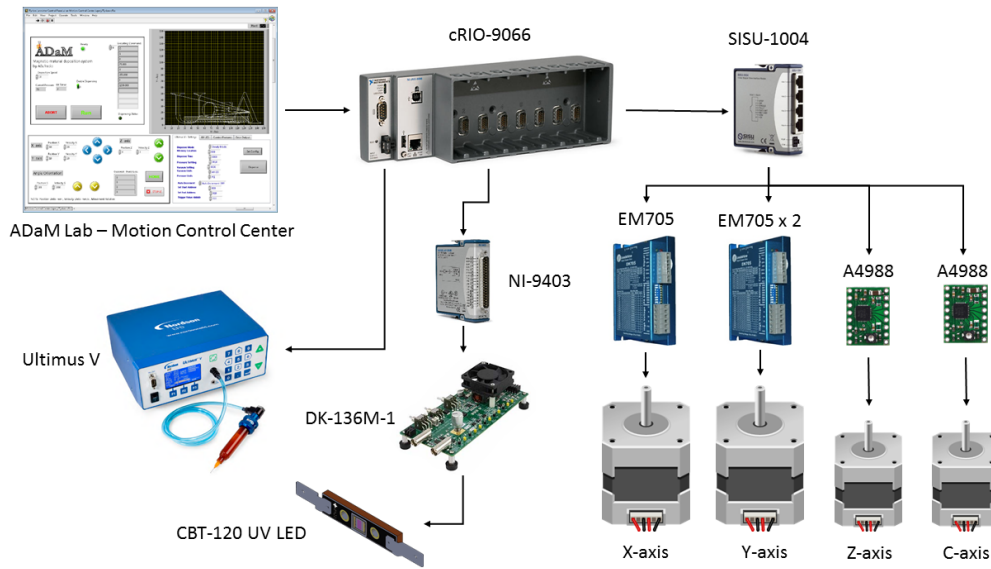


Figure 2.16: Integration diagram.

Finally, Figure 2.17 shows a picture of the final assembly as described in this chapter. More images of the system can be found in section A.4 in the Appendix.

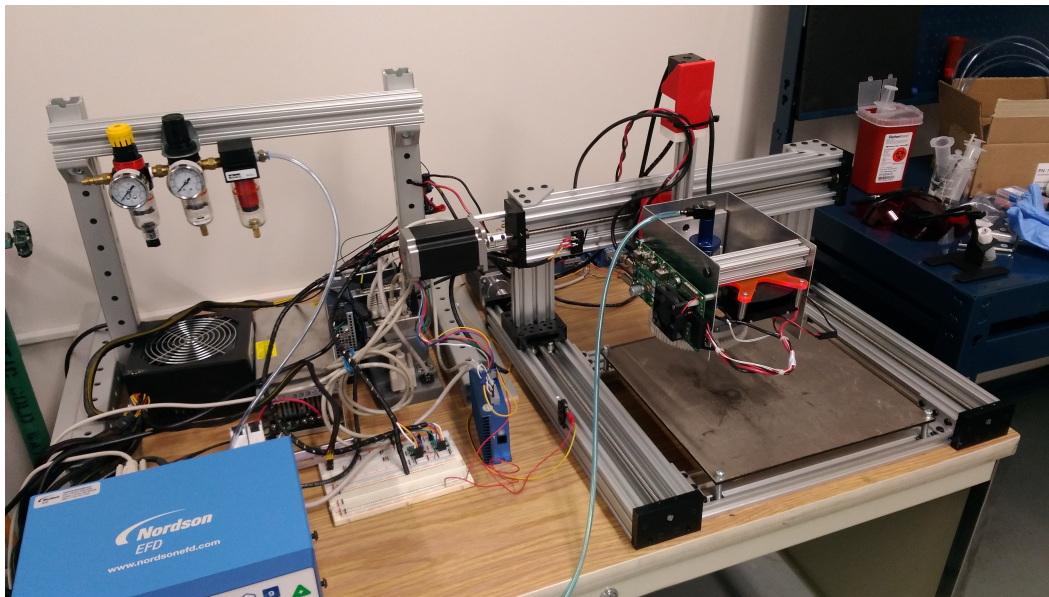


Figure 2.17: Final assembly.

Chapter 3

Control Software

AM processes regularly start with the generation of a CAD model of the geometry to be printed. From the CAD model, an Stereolithography (STL) file is generated. This file format is a triangulated version of the geometry found in the CAD file. Changing the CAD model to this format allows the geometry to be interpreted by other software. The next step is the slicing process where the 3D geometry from the STL file is divided normal to the Z-axis into a series of 2D layers coplanar to the XY plane. Then, the slicer generates a set of instructions to control the toolpath along the XYZ planes and to deposit material where it is required. This path that the extrusion head must follow to construct a desired part, along with the additional set of instructions, is called G-Code.

The concept of G-Code itself was inherited into additive manufacturing from the computer-aided subtractive manufacturing industry. In that industry G-Code has been used as a language to give instructions to the automated machines of "how" to create something. It is important to understand that G-Code itself has a strong hardware dependency as a programming language which is used in a large variety of machines with very different capabilities and constructions. This means that at some point most of the companies dedicated to build automated machines had to create their own G-Code version to match their hardware. Then it is clear that G-Code is a proprietary language that is not under any standard and that it was inherited in to additive manufacturing following the same philosophy, allowing to each developer to

include the necessary instructions to control their own system.

As part of the slicing process, the user is also able to modify different settings for the print, e.g., the layer height, filament width, printing speed, infill pattern, number of extruders, and a number of other options to deal with many aspects of the print itself. Such settings are reflected in the G-Code and later interpreted by the control software. Once that the G-Code is generated, it can be loaded into the software tasked with controlling the 3D printer. There are many ways in which a 3D printer can be operated. The most common are: first, an embedded driver with an external memory reader, such as an SD card reader or a USB port where a storage device containing the G-code can be plugged in; second, a host computer running a control software GUI through which the user can explore the local file tree and find the generated G-Code. Usually this interface allows the user to operate the 3D printer and modify the printing parameters. Some systems even possess both interfaces. With the G-Code loaded, it is just a matter of initiating the 3D printing process. At that point, the task of the control software is to sequentially execute the G-Code and send the necessary instruction to the 3D printer controller to perform the operations required.

As a part of the standard process described, we can identify two points in which our magnetic material deposition process is not compatible with the available software solutions. The first point of incompatibility is the 3D Slicer software. Even with the great flexibility offered by some open-source and proprietary slicing software, it results too complicated to deal directly with additional degrees of freedom. This is the case with our application, where the orientation of magnetic particles has to be included as a part of the G-Code itself. The second point is the control software. Due to the different additional drivers and devices included in our system, a generic software controller for a 3D printer doesn't have the capability, nor flexibility, to be expanded or extensively modified to work as a research platform.

In this chapter, two different software programs developed to address our need for custom solutions that suit our process are presented. The first program is a post-processing software called "ADaM Lab - Particles Control Cen-

ter”. This software was created to enable the user to configure the desired orientation of the particles as part of our AM process and at the same time to provide a tool for generating an “extended” version of a standard G-Code quickly and easily. The second is a full printer control software called “ADaM Lab - Motion Control Center”, featuring a complete control GUI and a custom G-Code interpreter design to operate our magnetic material deposition printer.

3.1 ADaM Lab - Particles Control Center

Figure 3.1a shows the diagram of the previously described process followed by most of the 3D printers available on the market, and Figure 3.1b gives a visualization of where the post-processing software described next is included in this process.

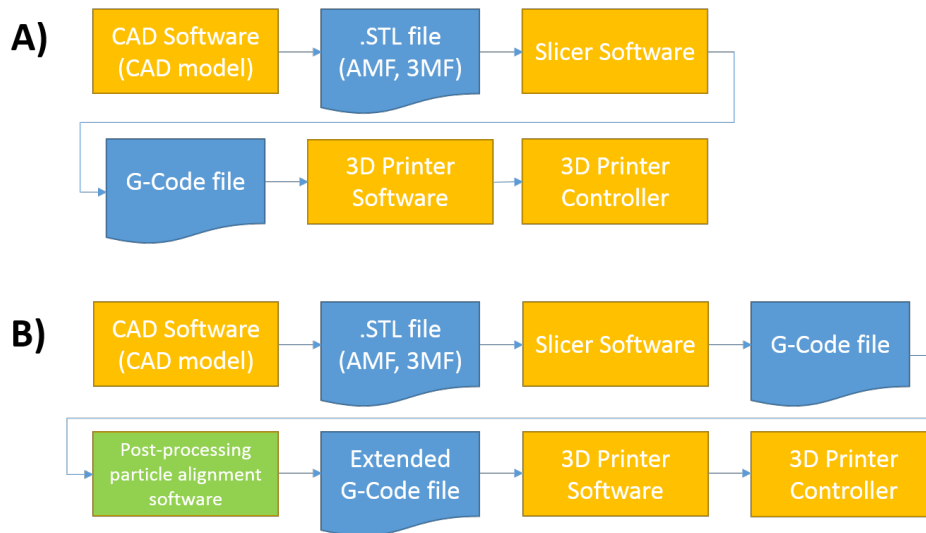


Figure 3.1: a) 3D printing typical workflow b) Extended 3D printing workflow.

As mentioned before, the first step is the generation of a CAD model of the part to be printed, then this model is exported to an STL file. The STL format and other similar standards offer the advantage of being a raw geometrical representation of the CAD model which usually has a proprietary format. The STL files can be interpreted by most of the slicing software. In

the slicing process, the orientation of the part and other printing settings can be configured, affecting the resulting G-Code.

Slic3r [3] was the slicing software selected to generate the basic G-Code instructions. The core of these instructions is a series of linear interpolations between points across the XY plane that describe the material extrusion routine and the tool-path that the printing head must follow. These linear interpolations are the fundamental operations required to construct the three-dimensional object, layer by layer, moving in the Z direction to step from one layer to the next one. An example of a typical G-Code line is shown in Figure 3.2.

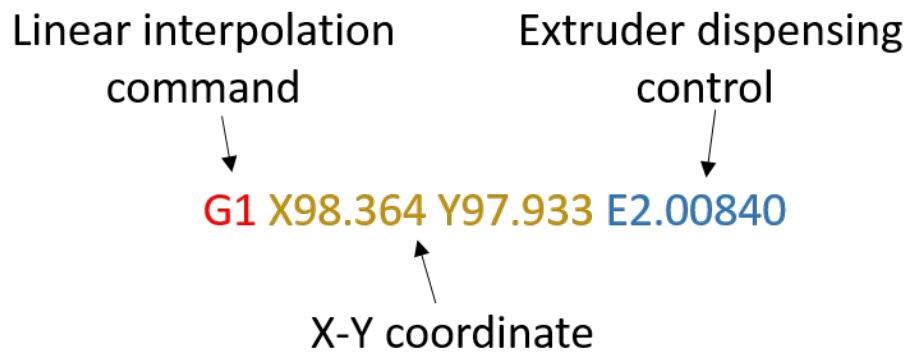


Figure 3.2: Example of a G-Code line.

The open-source nature of the software, the flexibility of the infill options that it offers, and the capability of triggering post-processing scripts were the main reasons that this software was incorporated in this additive manufacturing process.

The material deposition process for which the post-processing software was designed requires a particular kind of infill. Here is where the versatility of the slicing software is useful, allowing the selection of the required concentric shape infill pattern. Now, to exploit another feature of the slicer software, our post-processing software is configured to be executed once the basic G-Code is generated. With this last option selected and the parameters specific to the dispensing configured, the G-Code can be generated. Once that Slic3r finishes the creation of the basic G-Code file, the main panel of the post-processing

software will be displayed to the user, so the extra configurations to manipulate the magnetic particles' orientation can be modified.

Figure 3.3 shows the graphical user interface (Graphical User Interface (GUI)) which was based on the popular programming language, Python. This GUI was developed to allow the user to manipulate a number of parameters related to the multi-functional AM process. To code the GUI, the TkInter Python package [10] was used and then combined with a class-based algorithm that allowed us to iterate through the G-Code file, and identify and perform different operations according to the selected options. The first control in this software is a directory browser at the top of the window that allows the opening of any existing G-Code. This feature avoids having to go through the entire slicing process every time a change on the configuration has to be made or every time that a different particle orientation has to be selected using the same G-Code.

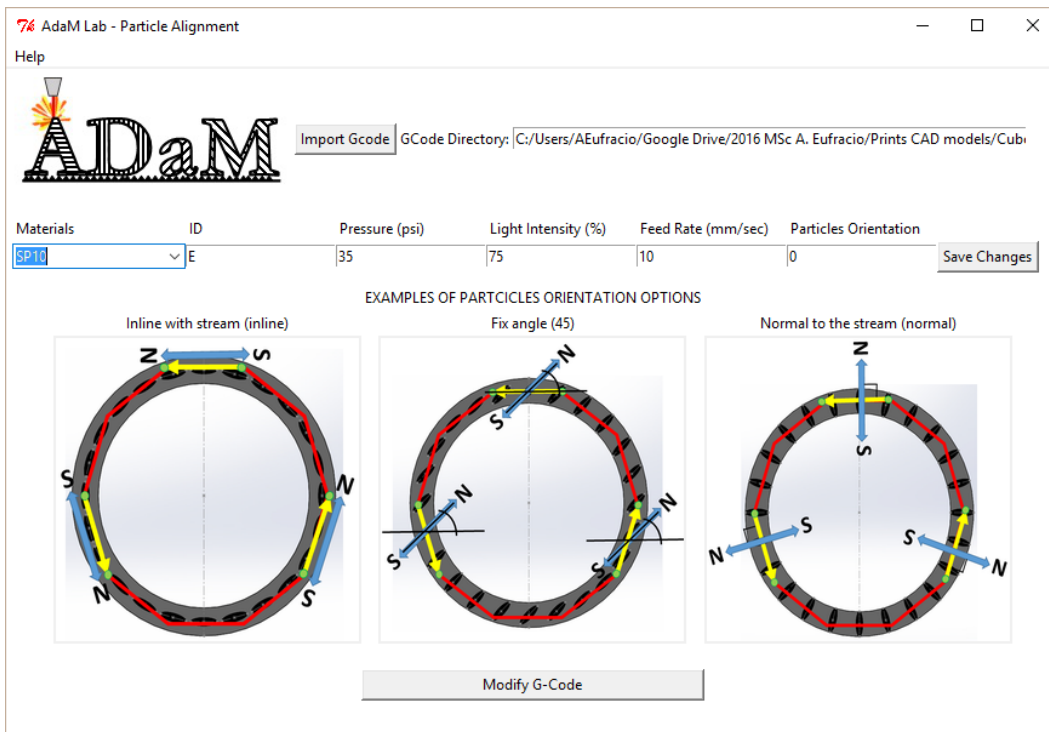


Figure 3.3: Particles Control Center - GUI.

A Combo box with the tag “materials” on the GUI gives the possibility of working with up to three different resin variations and to set individual

configurations for each of them. The configuration values are saved or updated to an extensible markup language (XML) library so they can be easily retrieved for subsequent iterations. This multi-material approach was conceived to give the flexibility to scale up the number of dispensing actuators that the printer itself can handle. Then, depending upon the type of suspension, the user can optimize the best parameters for each of the suspensions individually. Incorporating the style of other multi-material 3D printers, an ID letter is assigned to each of these suspensions. This ID is used later as part of the printing process itself, to generate the proper signals to trigger the different actuators.

The available settings on the main panel are: pressure, measured in psi with valid input values from 0 to 100, related to the maximum physical capabilities of the dispensing device (100 psi) [11]; intensity of the light source, controlled by a percentage from 0 to 100; angular velocity for the magnetic jig axis, measured in deg/sec, and the desired particles' orientation. The first three parameters are embedded in a G-Code command line with this structure:

```
G1 L50 P5 F10.0
```

In this command, the value next to the identifier “L” indicates the light intensity, the value next to the identifier “P” represents the dispensing pressure, and the value next to the identifier “F” defines the velocity for the C-axis.

Three possible orientations for the magnetic particles are presented as part of the first version of the software. These are Inline, Fixed Angle, and Normal alignment. As mentioned, the deposition process is determined by a series of 2D linear interpolations that the slicer software creates based on the imported STL file. The reason why the concentric infill pattern was selected for the slicing process is for its ability to use the same approach for the magnetic orientation on a given contour across the whole test part, by just iterating through the whole geometry. Figure 3.4a shows the solid body and the representation of the toolpath for a cylindrical test part. In the Figures 3.4b and 3.4c, the infill percentage was configured to 30% to make the visualization of the toolpath more clear. The red contours are the concentric loops where the stream of resin is dispensed and on which the particles are oriented.

Figures 3.4d, 3.4e, and 3.4f, give a graphical representation of the alignment options over a single loop of the printing head. The red line shows a coarse representation of the linear interpolations created by the slicer which represent the geometry of the part to be printed. The green dots symbolize the 2D points present in the standard G-Code, and the yellow arrows indicate the direction that the printing head follows to move between points. The core of this post-processing software is the manipulation of the orientation of the blue double arrow, which represents the angle of the dipolar magnetic field and therefore, the intended orientation of the magnetic particles inside of the resin stream.

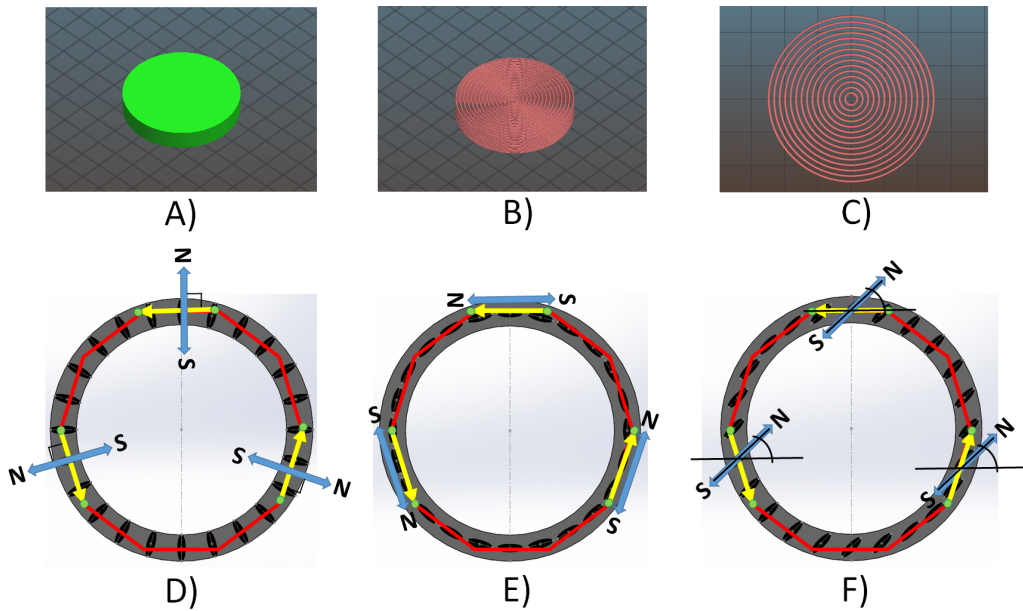


Figure 3.4: Toolpath example and alignment options.

Figure 3.5 shows the algorithm followed to iterate through the source G-Code. The process consists of identifying the lines where the material is extruded. It is during this deposition process that the angle of the magnetic jig must be calculated. The rest of the linear interpolations where no material is being extruded are directly included in the G-Code, having the next structure:

```
G1 X98.364 Y97.933 F10.0
```

For the extrusion cases, the XY coordinates of a pair of subsequent points are extracted and the angle between them is calculated. This calculation is

done by considering a right triangle and using the arctangent function and computing the quotient of the opposite sides as shown in the Equation (3.1). Then, depending on which option was selected, the software will manipulate this angle and construct a G-Code line with additional information containing the value of the angle.

$$\begin{aligned}\tan \theta &= \frac{\textit{opposite}}{\textit{adjacent}}, \\ \theta &= \arctan \frac{\textit{opposite}}{\textit{adjacent}}.\end{aligned}\tag{3.1}$$

For the case of the “normal” alignment, the calculated angle from the G-Code is then rotated 90 degrees clockwise. In doing this, the magnetic dipole moves perpendicular to the concentric loops assuming that the deposition direction is counterclockwise. The “Inline” alignment means that the magnetic dipole follows the calculated angle between the neighboring points, subsequently the angle is added to the extended G-Code as a command. Finally, the “Fix” alignment reads the input angle value and constructs the G-Code command using the same value to construct all the G-Code lines where the deposition is to be made.

Once the algorithm iterates through the original file, the extended G-Code file is completed and the user receives a prompt that the process is finished successfully. The new file contains the needed additional instructions to modify the angle of the magnetic dipole at the same time that it performs the point-to-point linear interpolations. A comparison of a line of code before and after the post-processing is presented. The main difference can be seen after the identifier “E” in relation to the selected dispensing nozzle (“U” and “V” identifiers are available for adding additional dispensing nozzles in the future). A binary value of 1 after the identifier “E” means that the dispensing mechanism is being triggered. The identifier “A” next to it is related to the angle followed by the numeric value of the angle itself.

Original: G1 X98.364 Y97.933 E2.00840

Extended: G1 X98.364 Y97.933 E1 A49

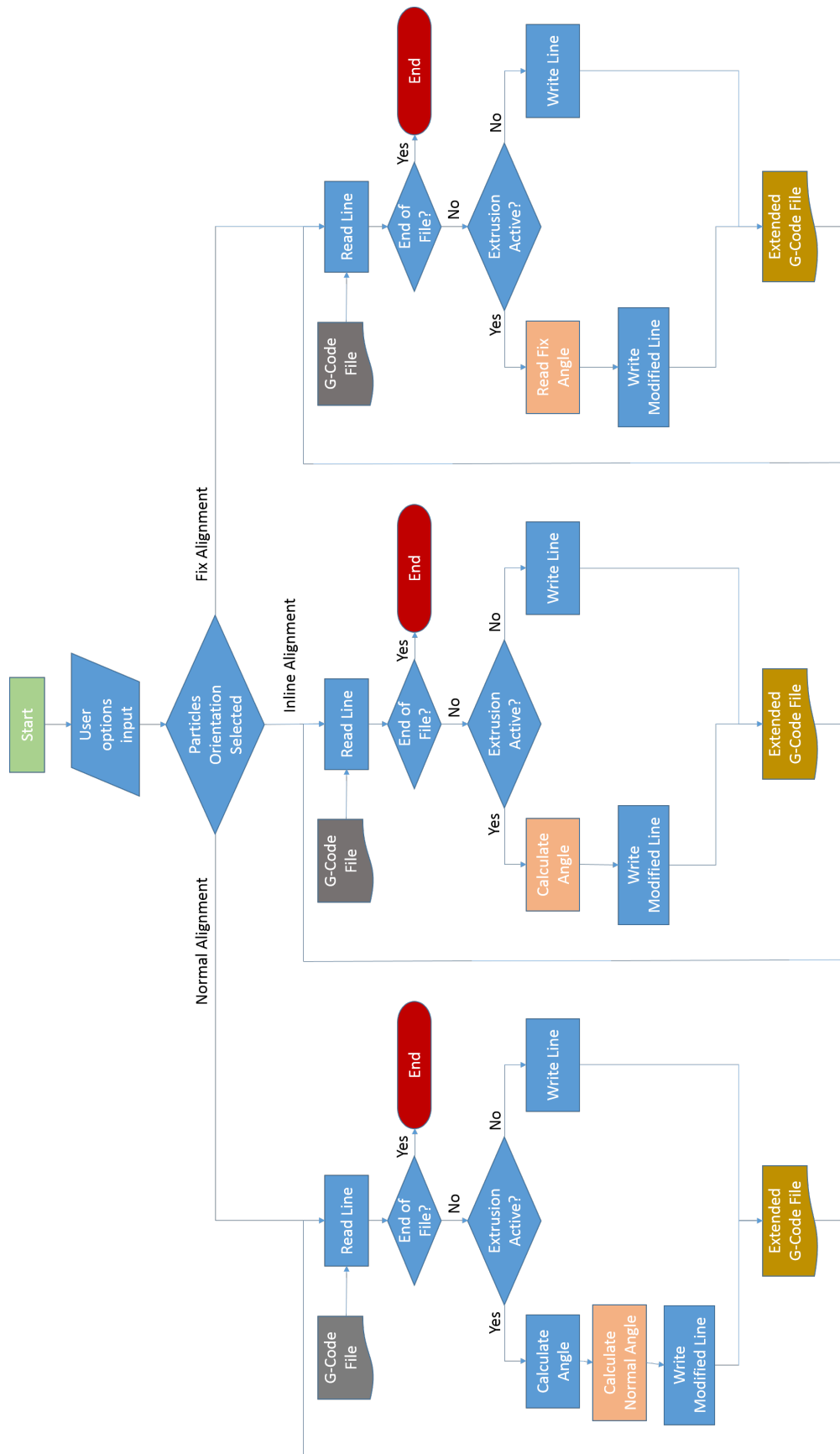


Figure 3.5: Post-processing algorithm.

3.2 ADaM Lab - Motion Control Center

Along with the design of the magnetic material deposition platform, a control interface that is equally flexible and customizable was developed to operate it. This software called “ADaM Lab - Motion Control Center” was designed to give complete control of all the components of the magnetic printer. Developed in LabView, this software takes advantage of the high-performance FPGA hardware control and features a graphical user interface running in the real-time processor of the cRIO. Taking advantage of the FPGA’s features, the Motion Control Center is capable of controlling coordination of all the axes of the magnetic printer, retriggering the dispensing mechanism, repositioning of the magnetic alignment, activation and changing of the intensity of the LED, as well as other capabilities. In this section, a detailed description of the hardware which was used and the development environment is given. Along with it, a detailed description of the construction blocks of our software is presented and the software structure is explained.

3.2.1 CompactRIO and LabView

The compactRIO or cRIO is a platform composed of a series of embedded controllers that features two processing targets [15]. First, a real-time processor is used to perform signal processing and communications tasks. The second is a programmable FPGA designed to perform high-speed control, precise timing, and trigger programmable hardware. FPGA stands for field-programmable gate array; in simple terms, an FPGA is a reprogrammable silicon chip [18]. This kind of system offers the performance and reliability of dedicated hardware with the flexibility of a software programmable system.

LabView is a development environment for a visual programming language called “G”. To roughly understand this language, we can start with one of its fundamental elements, the virtual instruments (VIs) [17]. A VI is the equivalent of a sub-routine in other languages, and it is composed of three elements; a connector pane, a front panel, and a block diagram. A connector pane is a graphical way to represent a VI in the block diagram of other VIs.

The front panel is the equivalent of a GUI. Built upon controls and indicators, the front panel is the one in charge of capturing the inputs and displaying the outputs of a VI. LabView offers pallets full of buttons, switches, knobs, graph indicators, plot indicators, and various input boxes for different types of variables. The block diagram, also known as the back panel, is where the visual programming language is located. Here, all the elements created in the front panel appear as terminals. Furthermore, structures and functions are available in the functions pallets. All the elements in the block diagram are also referred to as nodes. Nodes are connected through wires, so two controls and an indicator can be wired to a division function to show the result of the operation between those numbers. Finally, a VI can be dropped as a node in another's VI block diagram and the front panel of the dropped VI will define the inputs and the outputs for that node through the connector pane. Figure 3.6 shows an example of a VI.

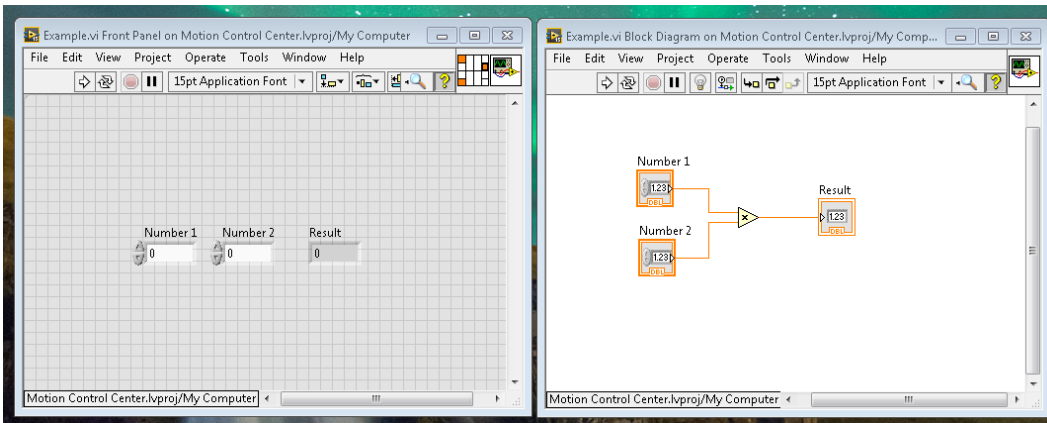


Figure 3.6: VI front panel, connector pane and back panel.

The LabView coding paradigm is based on data availability; a node can be executed when it has all the necessary inputs. When this node is executed, it generates output data which are passed to the next node. This flow of inputs and outputs through the nodes determines the execution order [17]. Figure 3.7 shows an example of the LabView execution flow. In this example, number 1 and number 2 are first added, then 50 is subtracted from the result and finally, the result is passed to the result node. It is important to understand that this code is not executed like this just because the nodes were placed in this order.

The reason is that the subtract function cannot be executed until the result from adding number 1 and number 2 is ready.

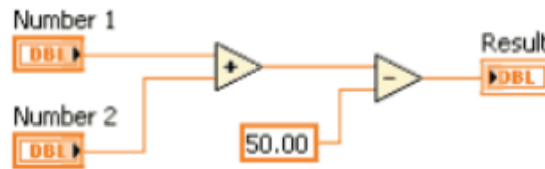


Figure 3.7: LabView data flow example.

The last aspect of the LabView’s programming paradigm to be presented is the design pattern used for our application. A design pattern is a standard architecture that can be re-used to solve certain kinds of problems. In this case, we followed a combined event-driven user interface and a state machine.

3.2.2 Software workflow

In this section, a general description of the Motion Control Center is given. Figure 3.8 shows a block diagram of the main VIs that integrates our LabView project and more importantly, in which hardware location each of them is being executed. This has very important results as explained in section 3.2.1 (CompactRIO and Labview). As it can be seen, there are three different instances where the VIs can run. These are: the host computer, the LabView real-time system, and the LabView FPGA. In the left side of Figure 3.8, we find the first component of the Motion Control Center. The FTP loader is a VI running in the host computer. The only purpose of this VI is to serve as a bridge between the host computer and the cRIO, allowing the user to transfer the previously generated G-Code file to the real-time system. In the central block, we have the main VI, running in the real-time system. This VI contains the main GUI through which our magnetic material deposition system can be controlled. Also, in the back panel of this VI, we can find the main algorithm that handles the user’s inputs, interprets the G-Code, and sends instructions to the FPGA. Finally, in the last block, we have the motion control VI or FPGA VI. Here, we can find the function blocks for the most basic motion and

control operations. These are the control loops to generate the step/direction signals to control the stepper motors, and the timing loop to generate the PWM signal to control the LED. The reasons why this application runs in the FPGA are because of the higher performance and the precise timing that can be achieved. These characteristics are required for controlling the coordinate axes of the motion platform and for accurately positioning the printing head in place.

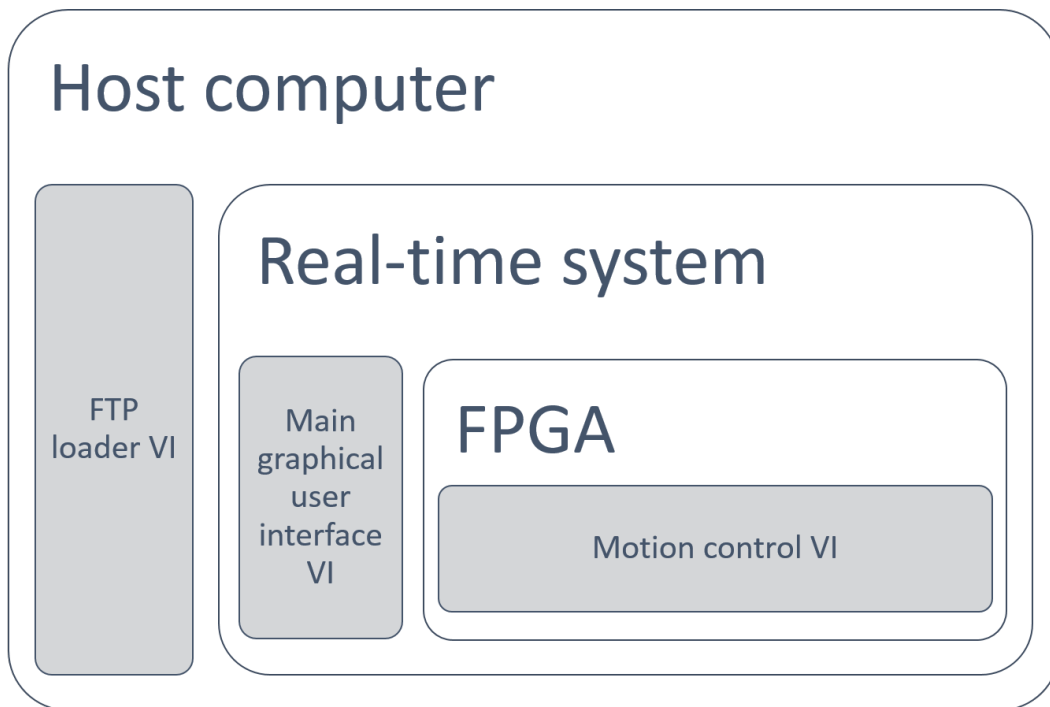


Figure 3.8: VI's block diagram.

3.2.3 Project Explorer files tree

Based on the previous discussion, it is necessary to identify all of the VIs inside of the LabView environment. Figure 3.9 shows the file structure of the LabView project itself. At the very top of the tree, we can identify the name of our project. Due to the available hardware, there are two platforms where VIs and many other programming elements can be created. These two platforms are the host computer marked with the label, "My computer," and the compactRIO, identified with the label, "NI-cRIO9066." Inside of the compactRIO, we will find our chassis. Any module physically plugged into

the cRIO’s chassis will appear in this sub-menu beside other items like VIs, dependencies, build specifications, and the FPGA target.

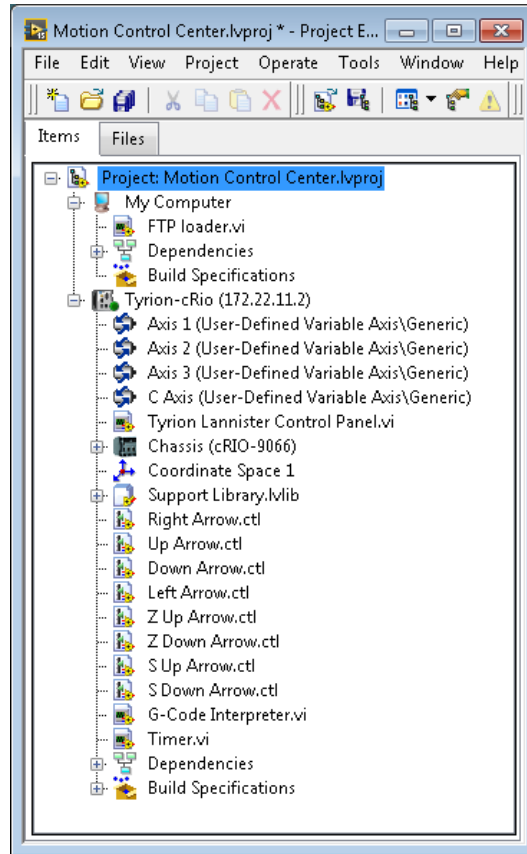


Figure 3.9: Project explorer files tree.

With the structure explained, it is easy to understand that any VI located under “My Computer” will be running on the local host; a VI located one level under the label “NI-cRIO9066,” will be running in the real-time system; and finally, a VI running under the FPGA target will be compiled and run in the FPGA. Results beyond the scope of this work explain in detail all the different implications of creating VIs in the different levels of the platform. It is also beyond this work to explain what kind of operations can or cannot be performed in the different levels of the platform. In order to understand this, we recommend following a tutorial on how to develop real-time applications and FPGA applications in a LabView compactRIO.

3.3 VIs internal description

In this section, a detailed description of the algorithms implemented in the different VIs and their functionalities are presented. Along with it, all the configurations done to match the properties and settings of the different external components are explained as well.

3.3.1 Motion control

As stated in Section 2.6.1, the stepper motor interface SISU-1004 was integrated with the cRIO to handle the control of the four motion axes in our platform. To do this, the SISU-1004 requires a LabView software module called Softmotion. In this module, different sub-VIs and configuration elements are available to specify the characteristics of the physical mechanism.

Axis configuration

The first task to configure the motion system is to create Softmotion axis objects inside of the LabView Project Explorer, more specifically, under the cRIO's chassis. Once that one axis object is created for each of the four outputs available in the SISU-1004, it can proceed to do the configuration. Inside of the properties of each of the axes, a number of parameters are available. Such parameters include the type of motor to be controlled, the loop mode, initial status, units to be used, type of interpolation to be used, the timing characteristics of the step/direction signals, and the desired polarity of the output signals, just to mention some of them. As expected, the configuration of each axis has to reflect the desired behavior and mechanical characteristics of the physical axis.

In our design, there are five stepper motors running on four different axes with three different kinds of actuators. Next, we present the configuration done for each of those axes. We started with the XY axes. As described in Section 2.5, three C-Beam linear actuators were combined to create the XY axes of the gantry configuration. Two of the actuators are used to run the Y-axis, but for the software, such actuators have to be controlled as a single

one. This was achieved by wiring the same output for the Y-axis from the SISU-1004 module to both of the stepper motor drivers. The third actuator was used to run the X-axis by itself. Due to their shared characteristics, both axes were configured as described in Table 3.1.

Axis tab	Setting	Configured value
General Settings	Axis	Type: Stepper Driver / Interface: Open Loop
Trajectory	Forward Software Limit	Position: 250 mm / Stop Mode: Immediate
	Reverse Software Limit	Position: -250 mm / Stop Mode: Immediate
Limits and Home	Reverse Limit	Enable / Stop mode: Immediate / Reverse Limit Input: Active State High
Stepper	Units	Units: mm / Steps per mm: 100

Table 3.1: XY common configurations.

A standard three-dimensional Cartesian coordinate system was implemented to determine the positive direction of the motion axis. Figure 3.10a shows a representation of the coordinate system adopted and Figure 3.10b shows our platform with matching orientation coordinates for better understanding.

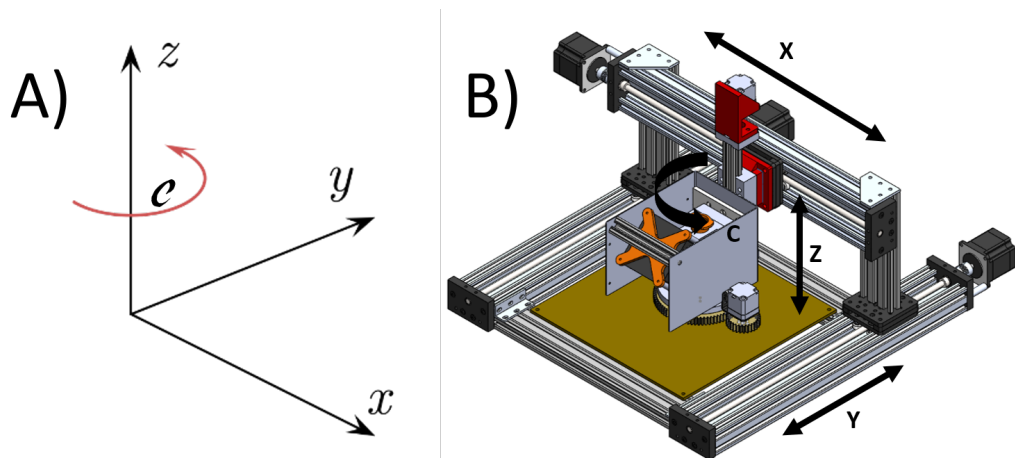


Figure 3.10: Machine coordinate system.

To account for the specific direction of the physical X-axis, the configura-

tion was set as shown in Figure 3.11.

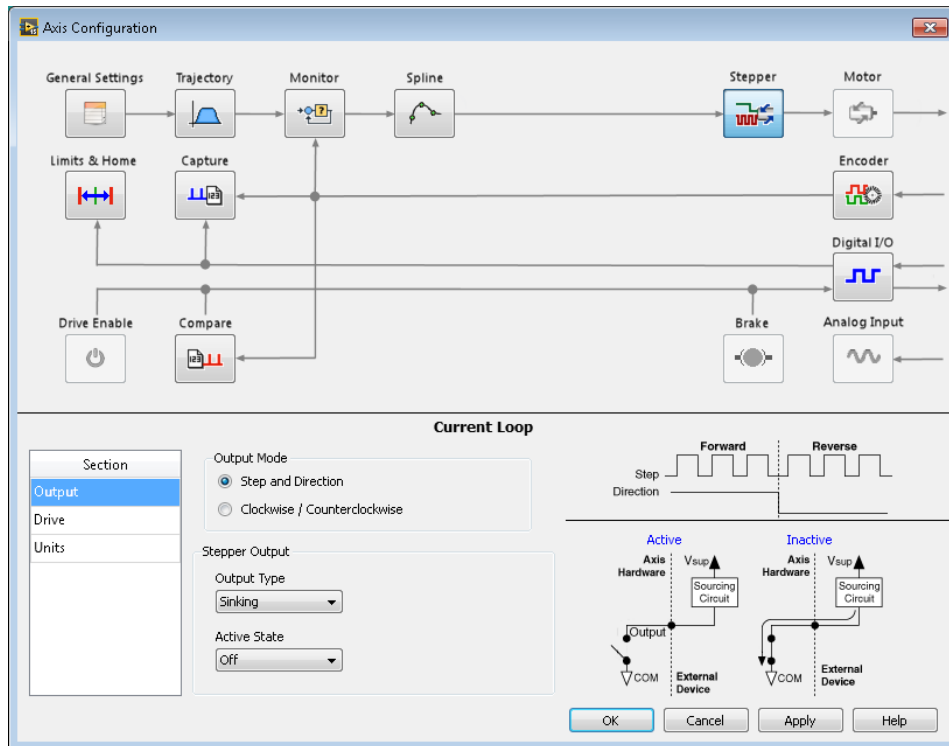


Figure 3.11: X-axis direction configuration.

To account for the different direction of the physical Y-axis the configuration was set as shown in Figure 3.12.

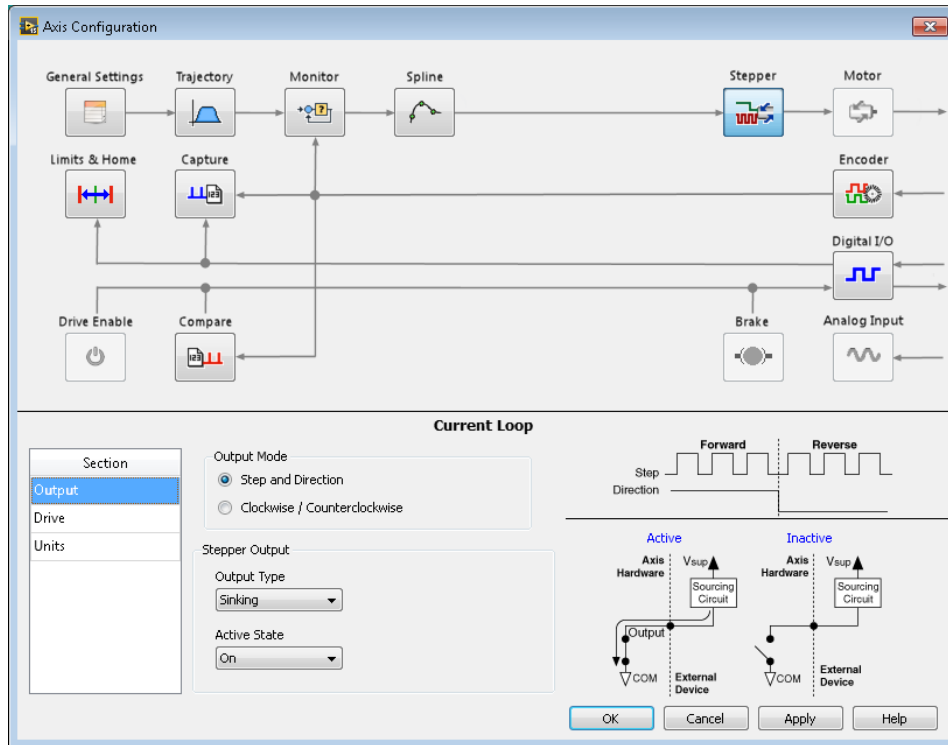


Figure 3.12: Y-axis direction configuration.

The Z-axis is driven by a much smaller linear actuator with different mechanical characteristics, which is a 6 mm diameter lead screw with a pitch of 1 mm. Considering the different mechanical properties and the vertical orientation within the motion platform, the configuration of this axis was performed as shown in Table 3.2.

Axis tab	Setting	Configured value
General Settings	Axis	Type: Stepper Driver / Interface: Open Loop
Trajectory	Forward Software Limit	Position: 100 mm / Stop Mode: Immediate
	Reverse Software Limit	Position: -100 mm / Stop Mode: Immediate
Limits and Home	Reverse Limit	Enable / Stop mode: Immediate / Reverse Limit Input: Active State High
Stepper	Units	Units: mm / Steps per mm: 200.0

Table 3.2: Z axis configurations.

Finally, the C-axis, which is the one that manages the rotation of the magnetic jig was configured as described in Table 3.3.

Axis tab	Setting	Configured value
General Settings	Axis	Type: Stepper Driver / Interface: Open Loop
Trajectory	Forward Software Limit	Position: 360 degree / Stop Mode: Decelerate
	Reverse Software Limit	Position: -360 degree / Stop Mode: Decelerate
Limits and Home	Reverse Limit	Enable / Stop mode: Immediate / Reverse Limit Input: Active State High
Stepper	Units	Units: degree / Steps per degree: 0.2

Table 3.3: C axis configurations.

3.3.2 Essential function blocks

In this section, a brief description of the most important VIs used in our application is presented.

Softmotion functions pallet

The Softmotion module offers a series of express VIs that can be used to perform different kinds of movements and operations. Figure 3.13a shows the available VIs. Based on the fact that the input G-Code file is a series of linear movements, the main function used from this pallet is the Straight-Line Move VI. As its name describes, this VI performs a straight line over an axis or over a coordinate system. Taking a single axis coordinate or an array with XY coordinates as an input, this VI defines the acceleration and deceleration time series for the movement and selects if the input coordinates belong to an absolute or a relative coordinate system. Along with this function, other functions like Read, Write, Stop and Reset Positions were used across the main VI. Figure 3.13b shows the properties window for the Straight-Line Move function used during the homing procedure.

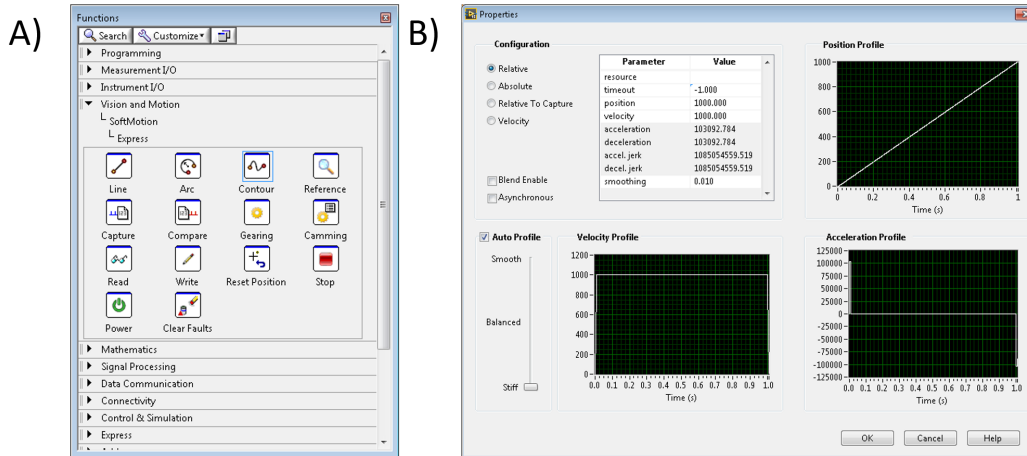


Figure 3.13: Softmotion VI's pallet.

Dispensing system VI

As mentioned in Section 2.1 (dispensing system), one of the reasons that the Ultimus V system was selected, was that the platform offered by Nordson has a high degree of compatibility with LabView. Furthermore, the supplier provides prebuilt LabView demos, which show how to control the Ultimus V from a LabView front panel. Using these demos allowed us to easily integrate this dispensing system with our platform. Among all the different VIs offered to interact with this system, two kinds are the fundamental ones to complete a dispensing cycle. The configuration VIs are the first of them. Shown in Figure 3.14a, these VIs allows us to set all the parameters related to the dispensing process; this includes the dispense mode, pressure, vacuum setting, pressure units, vacuum units, and others used to configure the system when it is running in different modes. The action-status VIs are the second kind, shown in Figure 3.14b. The action-status VIs allow the dispensing system to operate. The Initiate Dispense VI is the most important. Depending the selected mode, this VI will have different behaviors. For the selected, “steady” mode, the VI triggers the dispensing cycle and when the VI is activated again and stops it.

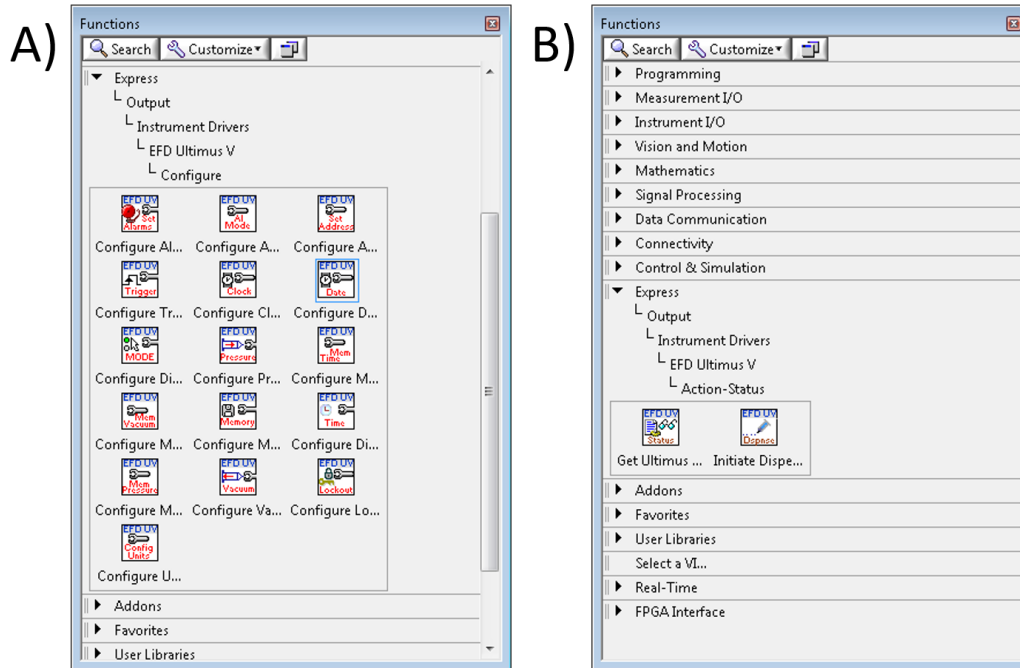


Figure 3.14: Ultimus V VI pallets.

PWM generation for UV LED driver

There are many ways to implement a PWM in a platform such as the cRIO. For our application, the PWM signal used to control the light intensity of the LED was implemented using a simple state machine running in the FPGA. Figure 3.15 shows the block diagram with the code used. A case structure is evident which becomes true when the input “UV Source On” is set to true. Inside the case structure, a while loop with a state shift register (characteristic of a state machine) switches back and forth between the true and false states. In each of the states, the digital output is activated and deactivated for different amounts of time, depending on the set values for the Low Period and the High Period variables.

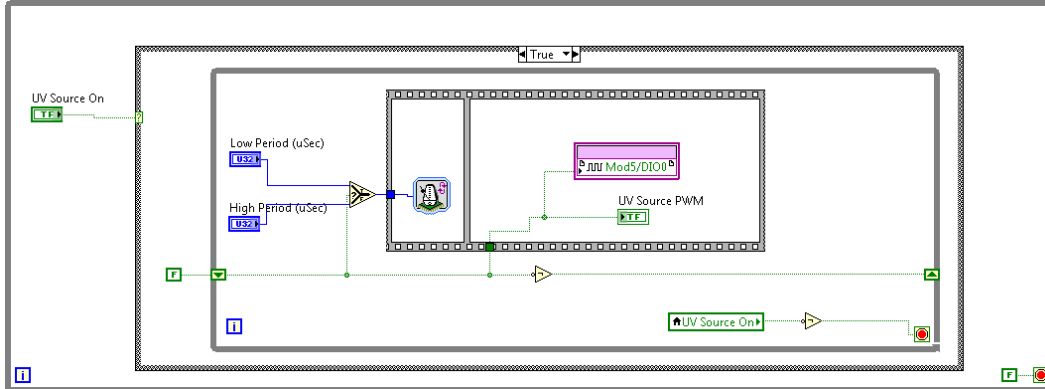


Figure 3.15: PWM block diagram.

3.4 VI description

3.4.1 FTP Loader VI

As described in Section 3.2.2 the FTP loader is a VI that helps the user to send the previously generated extended G-Code to the real-time system in the cRIO. This is achieved by using a communication protocol called File Transfer Protocol or FTP. This is a standard network protocol designed to send files between a server and a client. We implemented this protocol because it is supported in both; the real-time system that is basically a Linux-based operating system, and the host computer that runs a Windows operating system.

Figure 3.16 shows the front panel of this VI. A sub-VI invokes an open file argument. Using the open file window, the user can navigate through the Windows file system and find the G-Code file that needs to be uploaded to the cRIO. Once the file is selected, an upload button sends the file to the designated folder with the file name “currentGcode.gcode”.

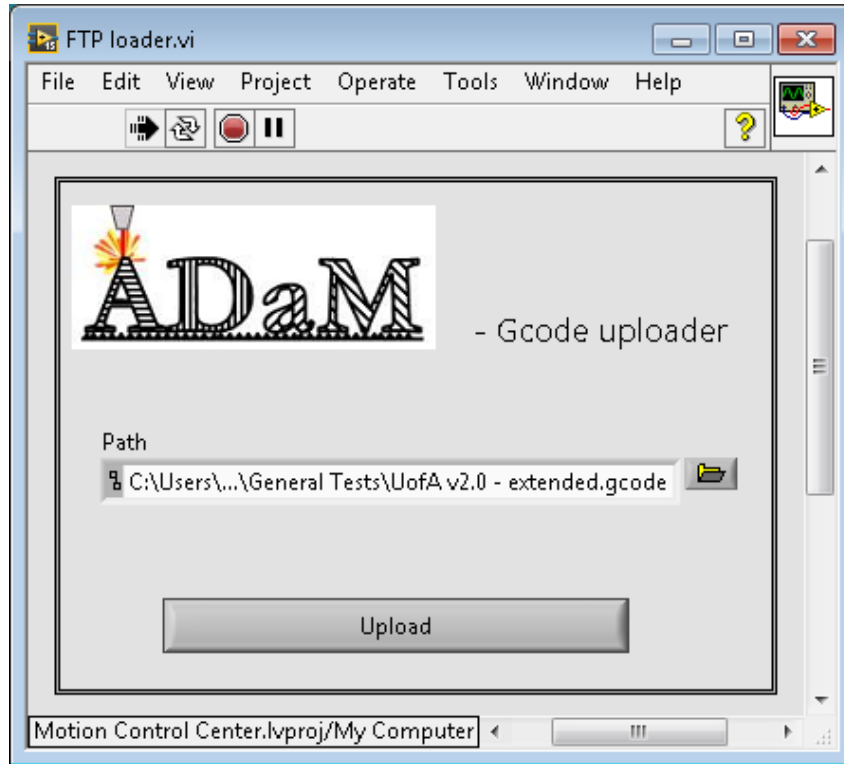


Figure 3.16: FTP VI front panel.

In the block diagram of this VI shown in Figure 3.17, we can see that once the user has selected a valid G-Code file, a function called *ftp-put* file is activated. Using the IP address for the cRIO, the host computer can generate a communication channel and copy the selected G-Code file to the desired location in the real-time system of the cRIO. This file will be retrieved later in the main VI from the specific folder.

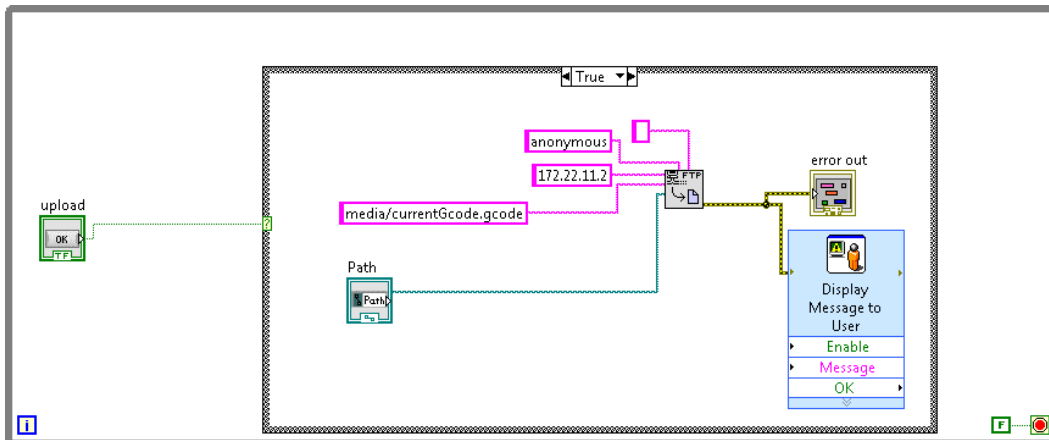


Figure 3.17: FTP VI back panel.

3.4.2 Main VI

This VI represents the main interaction center between the user and our platform. Through this GUI, the user is capable of activating all the different external devices and positioning the motion platform at any given point. Under the hood of this application, we can find the case-based algorithm to perform the magnetic-deposition material and alignment process. Furthermore, user event-driven function blocks to trigger axis specific linear movements, activate the dispensing system, and start the PWM signal generation are found here. In Figure 3.18, there is a screenshot of the Motion Control Center main VI. This GUI is divided into four different sections with specific functionalities used in the workflow.

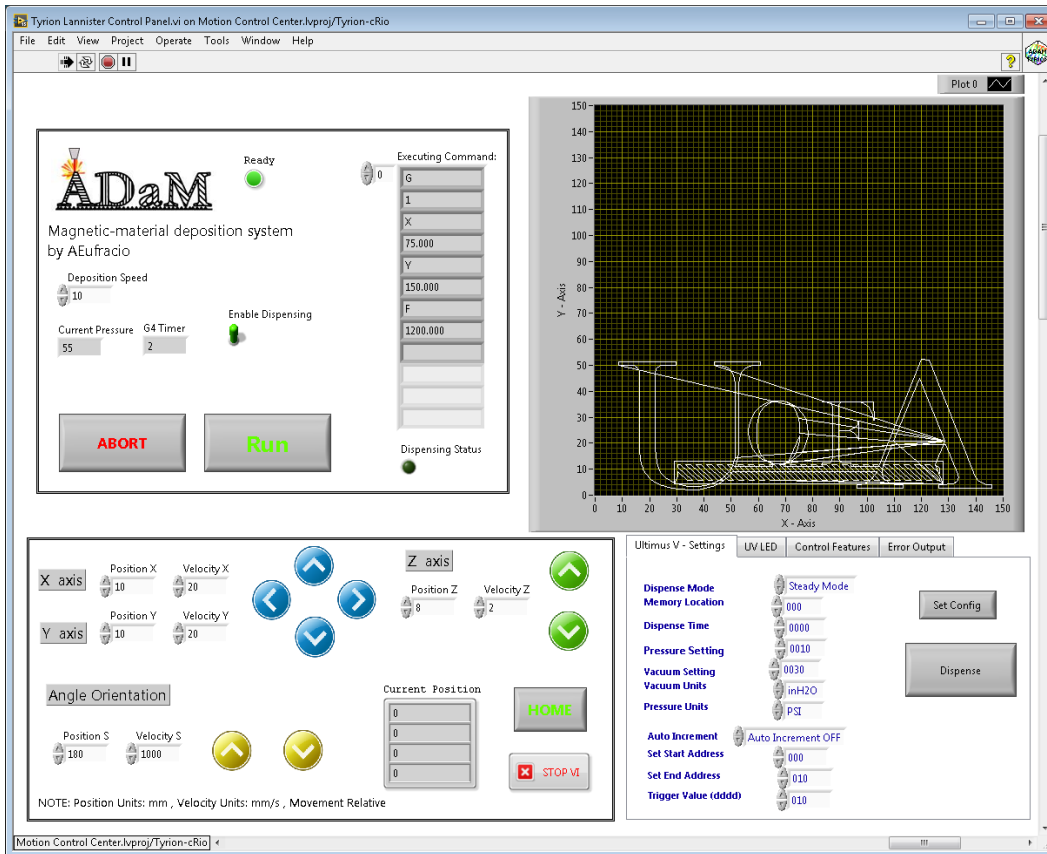


Figure 3.18: Main VI front panel.

Manual Control Interface

Figure 3.19 shows the manual control interface. This section of the panel allows the user to manually operate each of the axes separately. Tagged with a label, every axis is identified and followed by two numeric inputs. Such numeric inputs are position and velocity for the XYZ axes; and angle and velocity for the C-axis. As specified in the footnote from the main screen in the software, the units used are millimeters for the position and mm/sec for velocity. In the case of the angle orientation, the units are degrees for position and degrees/sec for velocity. Next to the position/velocity inputs, the user can find different colored arrows. These arrows indicate the direction of the movement to be performed.

A home button can be found inside this interface. This button controls the running of a user triggered homing procedure. Homing, in this kind of application, refers to the action of bringing the motion axes to an initial condition. This initial position has the coordinates $[0,0,0]$ for the X, Y, and Z axes, respectively. It is important to understand that the initial condition is defined as the position of the axes on which all the limit switches have been activated.

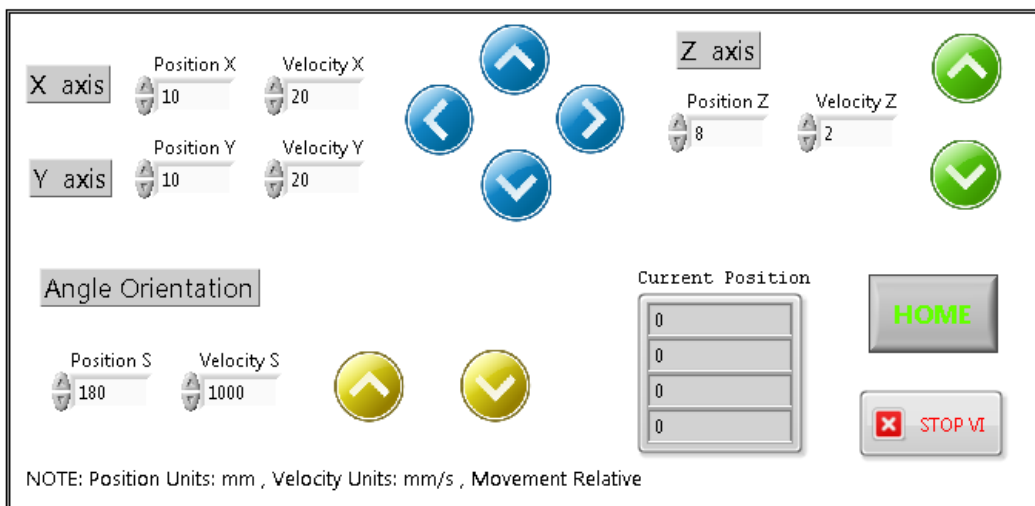


Figure 3.19: Manual control interface.

Based on the coordinate system shown in Figure 3.10, the arrows are configured as follows. Four blue arrows are used to control the XY positioning.

From this set of arrows, the one pointing to the right actuates the X-axis in the positive direction, and the one pointing to the left actuates the X-axis in the negative direction. The up and down arrows actuate the Y-axis in the positive and negative direction, respectively. A separate set of green arrows operates the Z-axis. Again, the up arrow activates the motion of the axis in the positive direction, and the down arrow activates it in the negative direction. To control the angle of the C-axis, two yellow arrows are used. The up arrow rotates the magnetic-jig in the counterclockwise direction or positive angle displacement, and the down arrow generates a clockwise rotation.

The final consideration for these controls is that the axes are configured for relative movement. This means that for a given position, the axis will move the distance in the selected direction, despite the initial position. As an example, if a value of 10 is introduced for the Position X, and then, the right blue arrow is pressed once, the X-axis will move 10 mm to the right. If the same right blue arrow is pressed again, the X-axis will move another 10 mm to the right from the current position.

Figure 3.20 shows the section of the main block diagram behind this manual control panel. The main aspect to understand in this code is that the four axes are represented as elements inside an array. This is how referring to an element of this array is equivalent to selecting that specific axis. The axes are enumerated from 0 to 3 and correspond to the X, Y, Z, and C axes, respectively. The inputs related to the different direction arrows and the position/velocity values from the front panel are represented as nodes in this diagram. When the user activates one of the control arrows, these inputs are sent to a *Straight-Line Move* sub-VI (described in Section 3.3.2). Doing this, the VI sends the needed instructions and information to the FPGA to generate the step/direction signals for the stepper motor driver.

As the last component of this block, the homing code is shown in Figure 3.21. As stated before, the home position requires that all the limit switches are activated by the moving carriages of the different axes. To guarantee this, the axes are moved into the negative direction, a magnitude of distance greater than the maximum travel distance of the different actuators. Doing this, it can

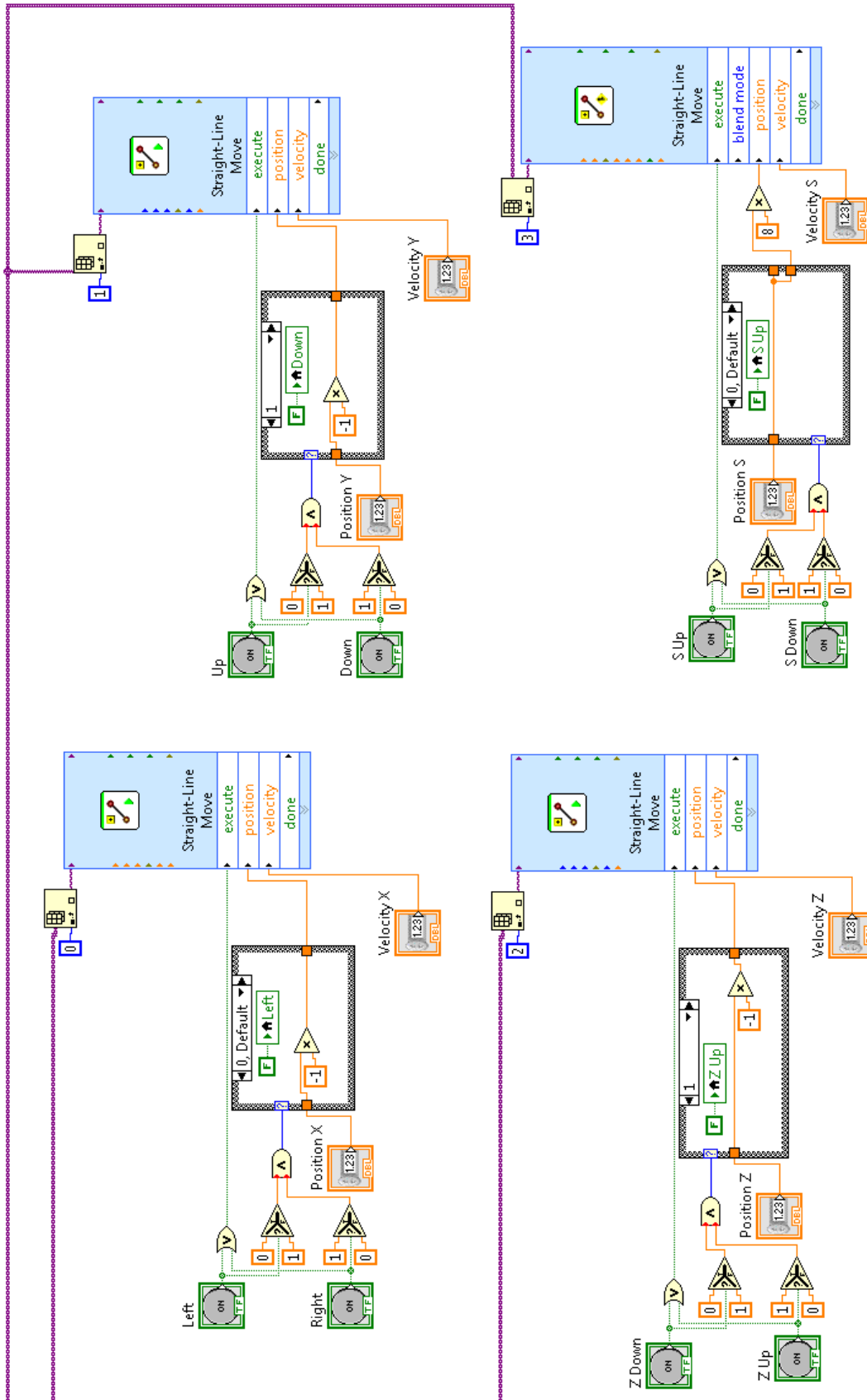


Figure 3.20: Manual control block diagram.

be guaranteed that all the limit switches are activated. Once all the reverse limit signals from the *Straight-Line Move* VIs are received, the current position is resealed.

Printing Interface

The block located in the upper left corner of the main GUI shown in Figure 3.22 is the one controlling the triggering the printing process. This GUI features four different controls. These controls are used to set the deposition speed (mm/s), enable the material dispensing, initiate the print, and abort the print. Setting the deposition speed to a value different than zero overrides the printing speed set in the G-Code. The “Enable Dispensing” control is used to allow the user to do a dry run of the uploaded G-Code with the purpose of corroborating the set parameters without wasting magnetic resin. When pressed, the “Run” control opens a prompt window to confirm if the print should be started. Finally, the “Abort” control halts the system if is required once the print has already been initiated.

The indicators in this section give real-time feedback about the current print, as well as the status of the system. Starting with the “Ready” light at the top of the block, this indicator shows if the system has successfully initiated the FPGA and if the axes faults were cleared successfully. A current pressure indicator shows the pressure value set up in the dispensing system. In the case that a waiting instruction (G4) is executed, an indicator shows the countdown value so the user will know that the system is not “hanging”. On the right side of the block, an array indicator shows the individual parsed string from the G-Code has been executed at a given time, and under it, a light indicator shows if the dispensing system is triggered or not.

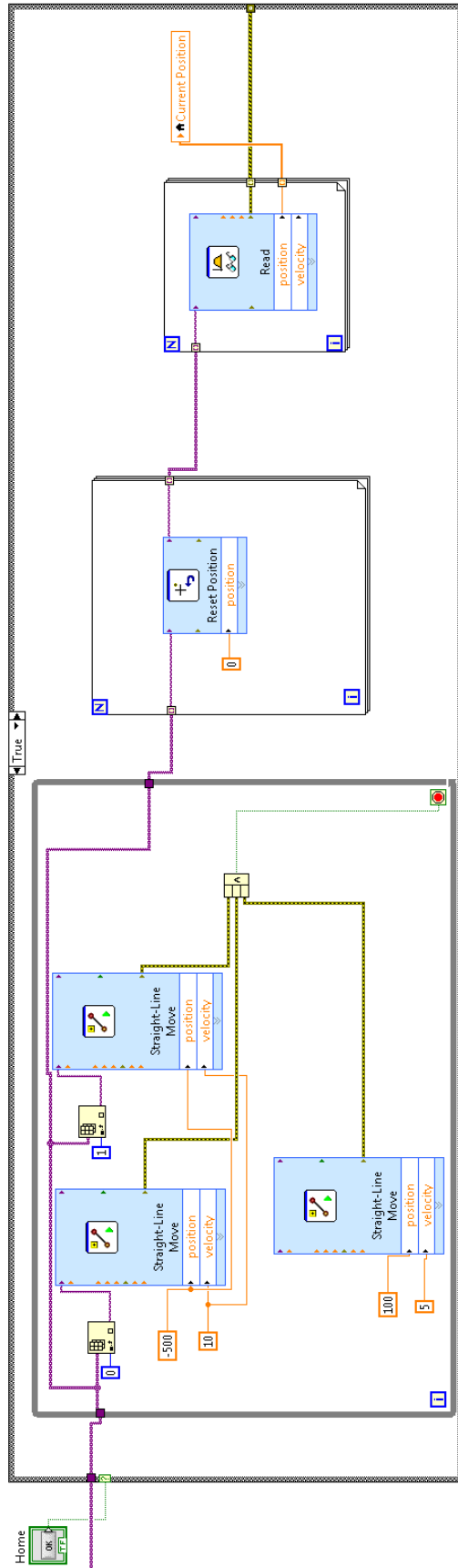


Figure 3.21: Homing block diagram.

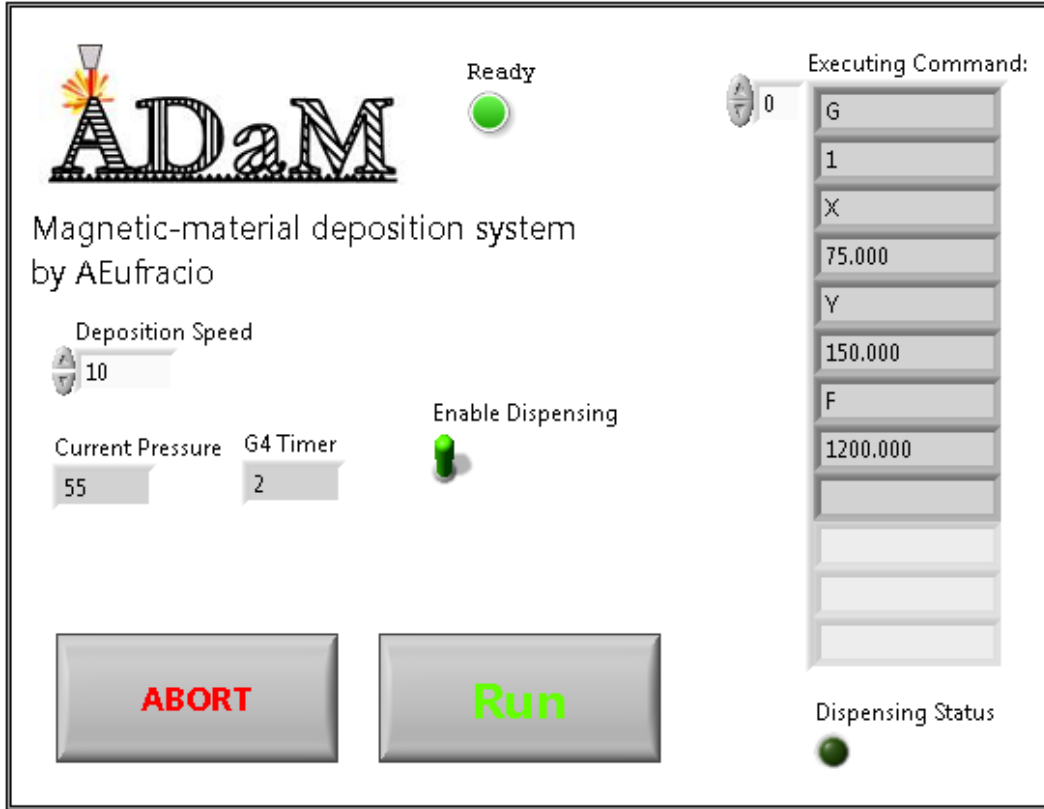


Figure 3.22: Printing control interface.

Once that the print has been started, the deposition, alignment, and curing processes take place. The first step is to retrieve the G-Code file uploaded by the user into the real-time system. A read file operation fetches the latest G-Code file with the pre-defined name `currentGcode.gcode` in the designated local folder `/media/` as shown in the Figure 3.23. The output of this reading operation is an array of strings, and each element of the array contains a line of text from the G-Code.

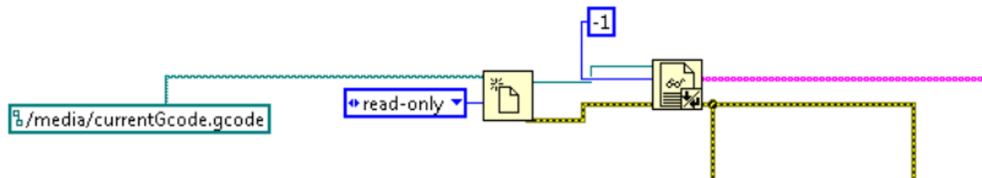


Figure 3.23: Read file block diagram.

This array of strings is then connected to the main *For*-loop of the printing algorithm. There are two main blocks inside of this loop; a parsing block and a

case based block where depending on the command identified, different actions are taken. The *For*-loop iterates through all the G-Code text lines and stops when an end of file is found, concluding the print.

The parsing block shown in the Figure 3.24 takes a single text line from the array of strings and uses a *Scan String for Tokens* function. This function takes as inputs the G-Code string to be analyzed and an array of strings called operators. If any of the operators appeared inside of the input string, the function identifies them as tokens. Once the string is analyzed, the function returns a token string. This token string is an array of all the matched tokens.

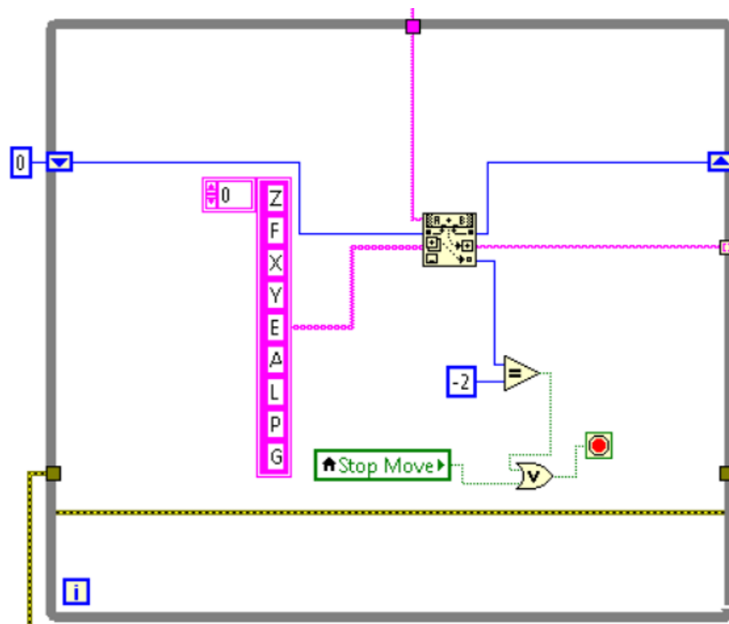


Figure 3.24: String parsing block diagram.

To define the set of operators for this function, it is necessary to understand all the cases that can be found in the G-Code. Listed in Table 3.4 we can find all the possible cases present in our custom extended G-Codes.

Based on these scenarios, a set of nested case-structures was created. The diagram shown in Figure 3.25 gives a clear picture of these cases and how they were structured to perform the printing process.

Case #	G-Code	Description
1	G1 X1.0 Y1.0 F10.0	This case represents a simple XY coordinate movement (X1.0 Y1.0) with a determined velocity (F10.0).
2	G1 Z0.10 F10.0	This case represents a Z linear movement (Z0.10) with a determined velocity (F10.0).
3	G1 X1.0 Y1.0 E1 A90	This case represents an XY coordinate movement, with the dispensing system "On" (E1), and a rotational movement of the magnetic jig (A90).
4	G1 L50 P5 F10.0	This case represents a configuration command with settings for light intensity percentage (L50), pressure value in psi (P5), and velocity (F10.0).
5	G28	This case represents a homing command.
6	G4 P10	This case represents a dwell instruction with a value in seconds (P10). This command was included to allow the user to idle the system in a given state as required. This routine is useful in the case that a sample wants to be exposed to the magnetic field or to the light for a determined period of time.

Table 3.4: G-Codes cases.

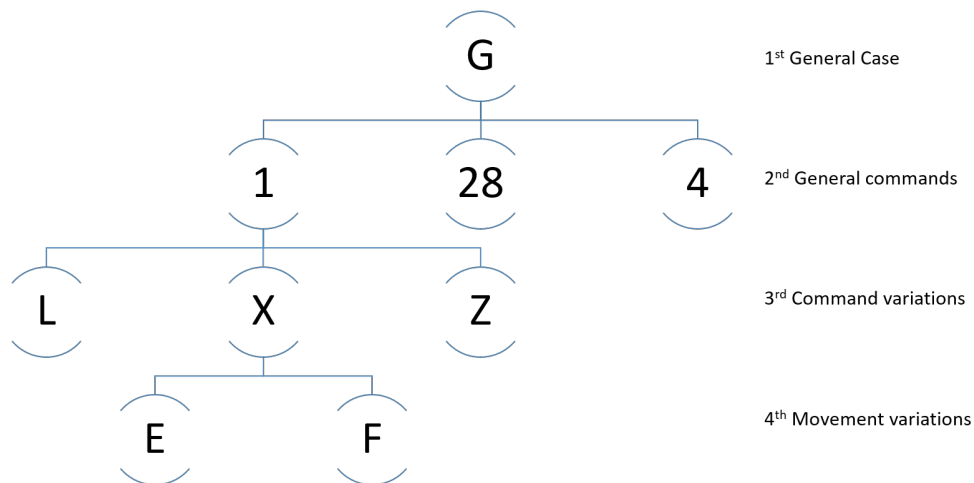


Figure 3.25: Cases diagram.

All cases in this structure are described below. Starting at the top of the diagram, to consider a G-Code command to be valid, the string itself must start with a letter G. This characteristic of G-codes is important because this first requirement helps to segregate any comment text or unsupported commands right away. Then, three general commands are identified. These are, G1 - linear motion, G28 - return to home, and G4 - dwell.

For the G1 command, four different variations were created. It is also important to understand that all the movements done hereafter use an absolute coordinate system. The first variation corresponds to Case 1 (F). As described before, this command represents a coordinate movement without any dispensing. The block diagram of this case is shown in Figure 3.26. At the beginning of the sub-routine, the status of the dispensing system is checked. If the dispensing was activated in a previous loop, then it is deactivated before starting the coordinate movement. The aspect to pay attention to in this sub-routine is the coordinate movement done. Instead of sending position/velocity values to each of the axes separately as done before, the XY axes were combined into a coordinate axis object and then actuated as a single object. With this, the system can make a linear interpolation between the start and end point using both axes simultaneously.

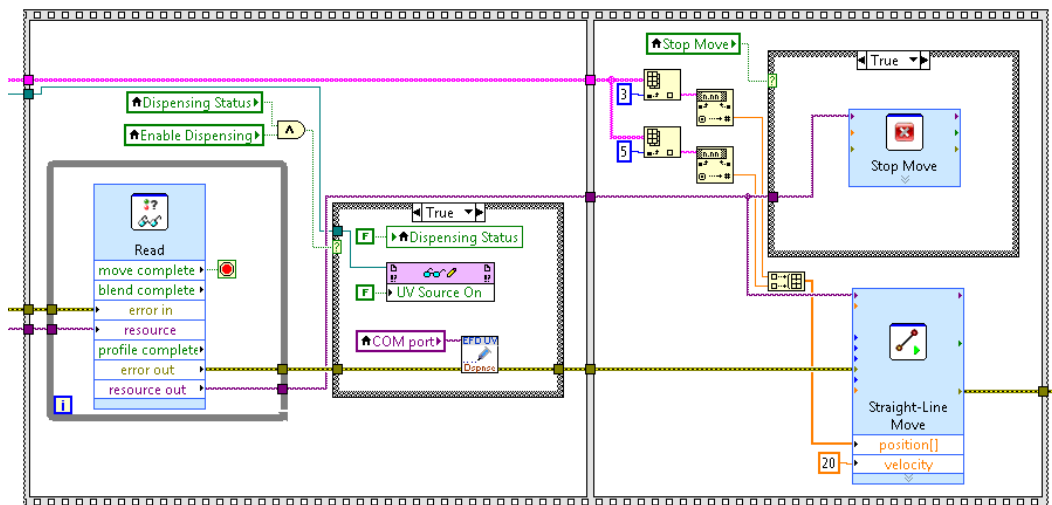


Figure 3.26: Case F block diagram.

The second variation of the G1 command corresponds to Case 3 (E). In

this case, a dispensing instruction E1 is combined with a coordinate linear movement. As shown in Figure 3.27, the first step in this sub-routine is to rotate the magnetic jig to the angle indicated next to the operator A (A90). Modifying the angle of the magnetic jig induces a new orientation of the particles within the deposited resin, as was explained in the previous chapters. Once the magnetic jig reaches the indicated angle, the dispensing system is triggered, and the coordinated linear movement is finally executed. This process results in a line of magnetic resin deposited over the printing bed. Due to the presence of the magnetic dipole, internal particle alignment should be simultaneously achieved. Another item found here is an array of all the executed positions. This array is then fed to an XY graph described next in the printing visualization interface Section 3.4.2.

Case 2 (Z) is the third variation of the G1 command. This case represents a simple linear movement over the Z-axis. The primary consideration, as shown in Figure 3.28, is to stop the dispensing cycle if it was triggered in a previous loop.

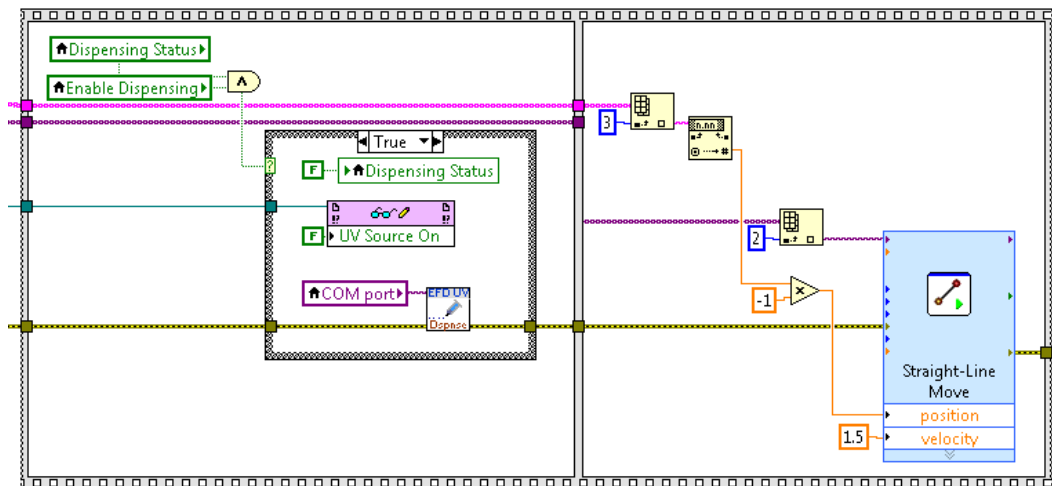


Figure 3.28: Case Z block diagram.

Finally, the fourth variation is represented by Case 4 (L). Figure 3.29 shows the block diagram for this case where no movements are performed. On the other hand, the configuration settings for the Ultimius V and the light intensity value are set.

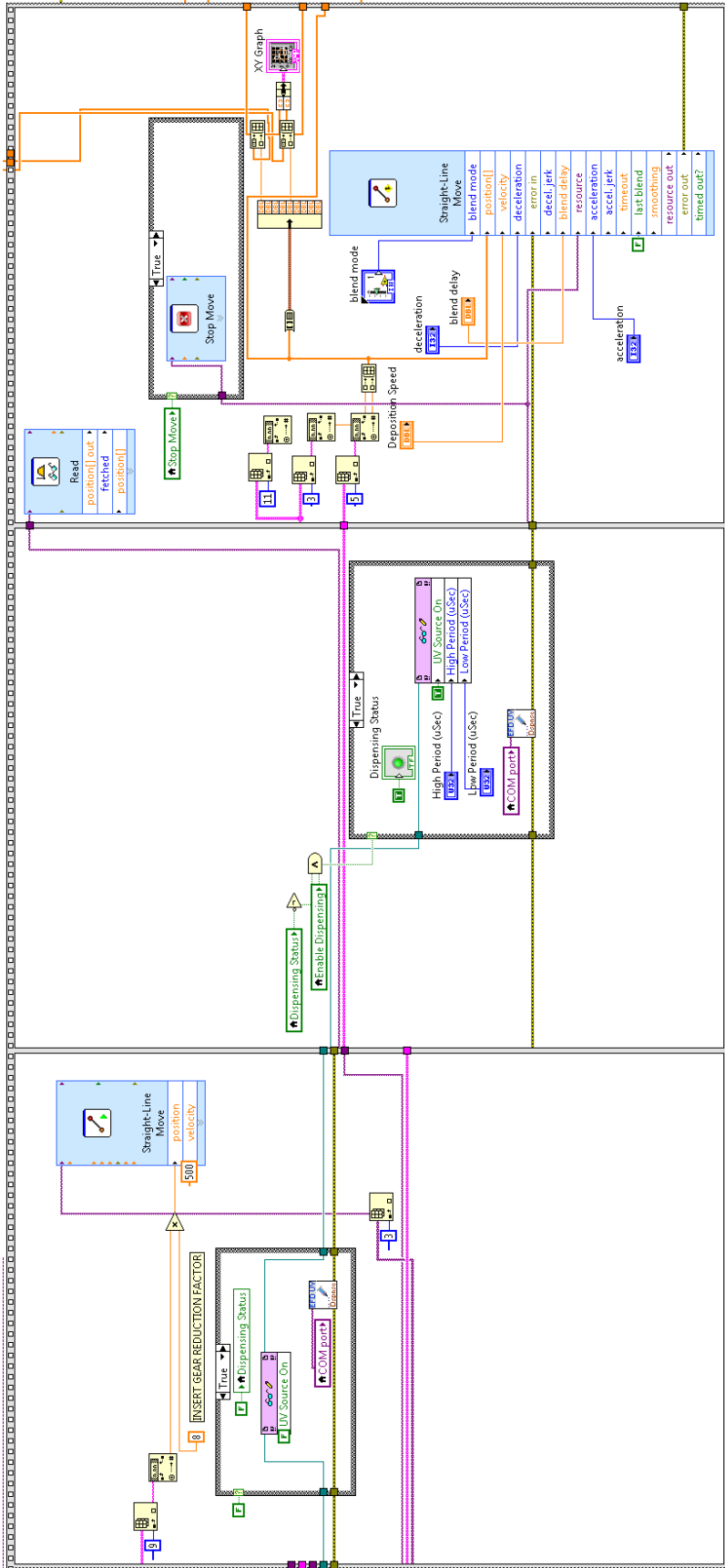


Figure 3.27: Case E block diagram.

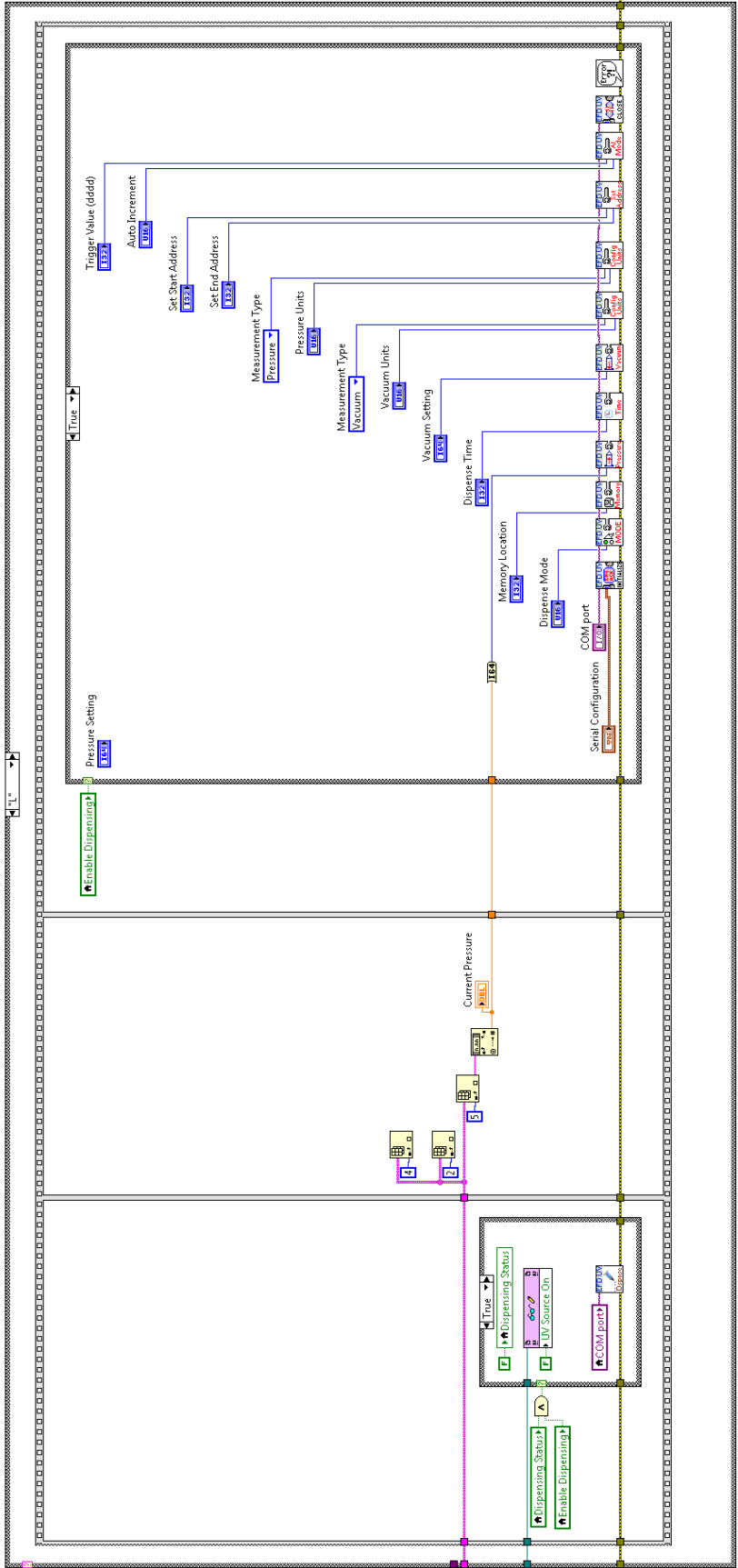


Figure 3.29: Case L block diagram

The commands G28 and G4 are examples of the Cases 5 and 6. Identical to the homing procedure found in the manual control interface, the G28 command moves the machine to the initial condition $[0,0,0]$ for the axes X, Y and Z. G4, on the other hand, generates a time delay defined by the argument of the token P (P10). This value is measured in seconds.

Printing Visualization Interface

As its name indicates, this part of the user interface gives a graphical representation of the dispensing linear movements performed during the printing process itself. With this indicator, the user can monitor and identify the geometry being printed. Figure 3.30 shows an example of the graphical output for a given print.

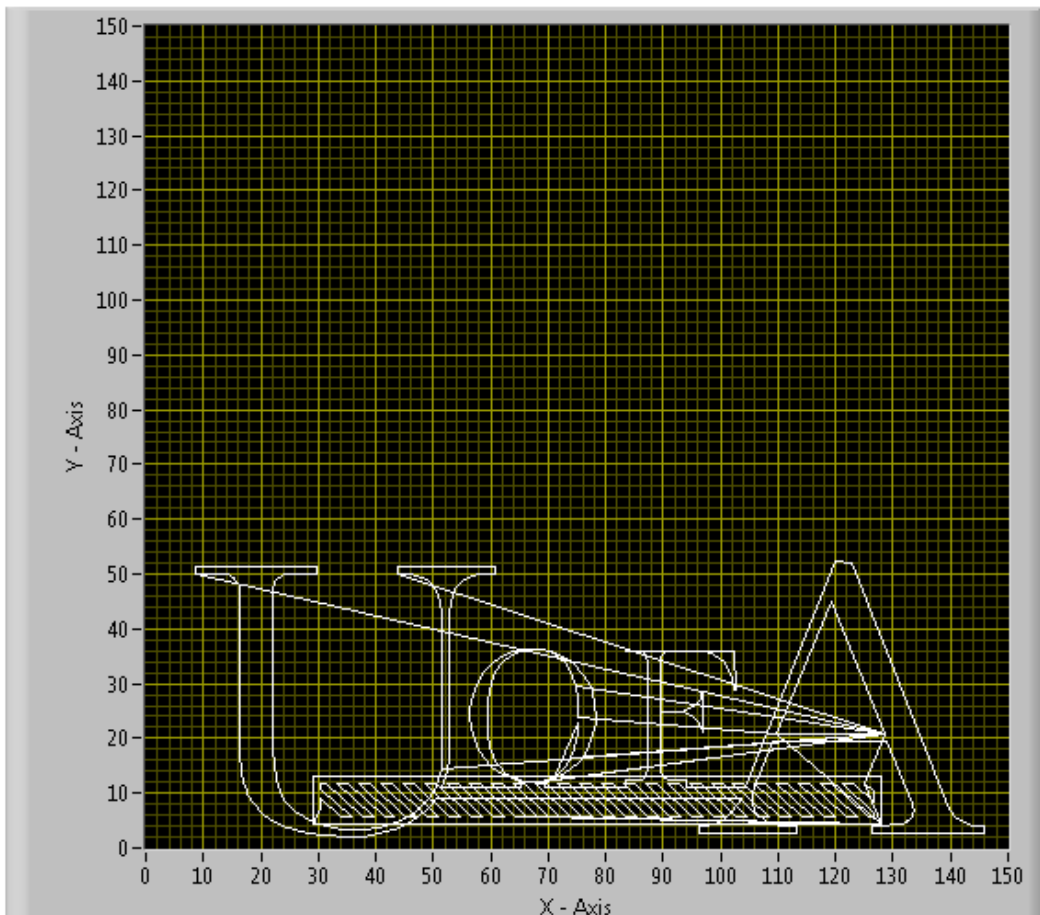


Figure 3.30: Main VI graph indicator.

Additional Controls Interface

This last block of the main VI shown in Figure 3.31 was created with two purposes. First, to allow the user to access the configuration settings for the different devices, like the dispensing system, the LED, and the movement profile for the printing algorithm. Second, to leave some room inside of the application to create new custom features necessary to perform specific research tasks. An example of this is the tab, “UV LED,” where the user can activate the light for a determined amount of time. It is recommended to use this section to include any new feature that is not related to the main printing process.

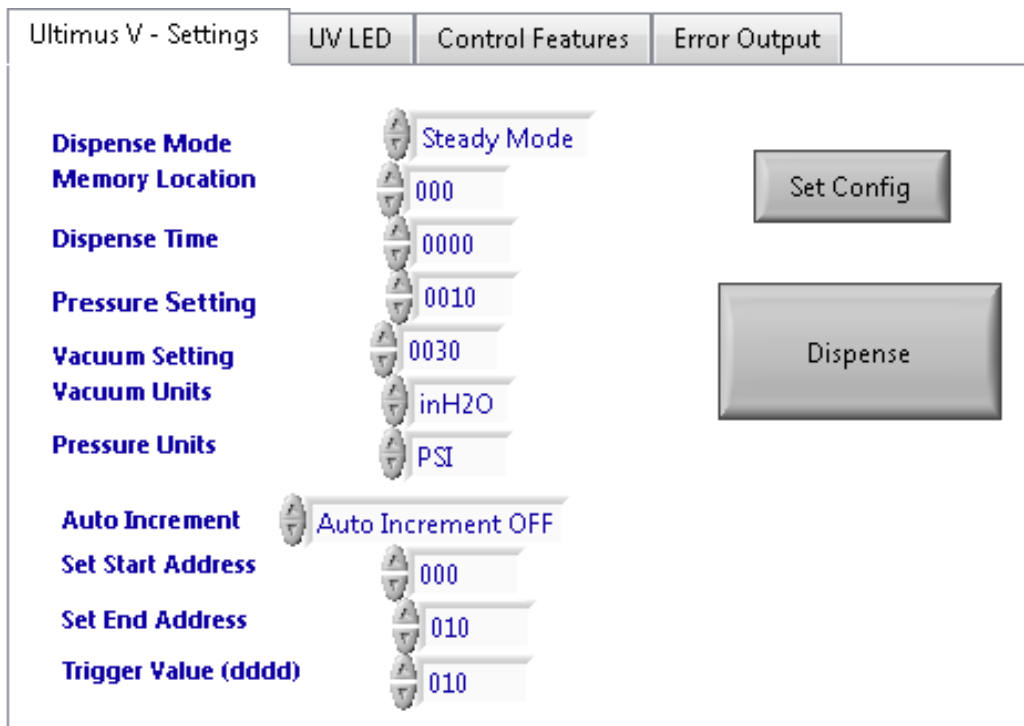


Figure 3.31: Main VI additional controls.

3.4.3 FPGA VI

The last VI to be analyzed is the SISU FPGA VI. This is the VI running directly inside of the FPGA. The front panel of this VI includes controls and indicators that allow the Softmotion functions to describe the status of the four different motion axes. These indicators include lights for: enable status,

direction, faults, and limit switches triggered. Besides that, the inputs and controls to drive the PWM signal generation for the LED can be also found in the front panel. These are Low Period and High Period, a UV source on control, and a UV source on/off indicator. Figure 3.32 shows the described front panel.

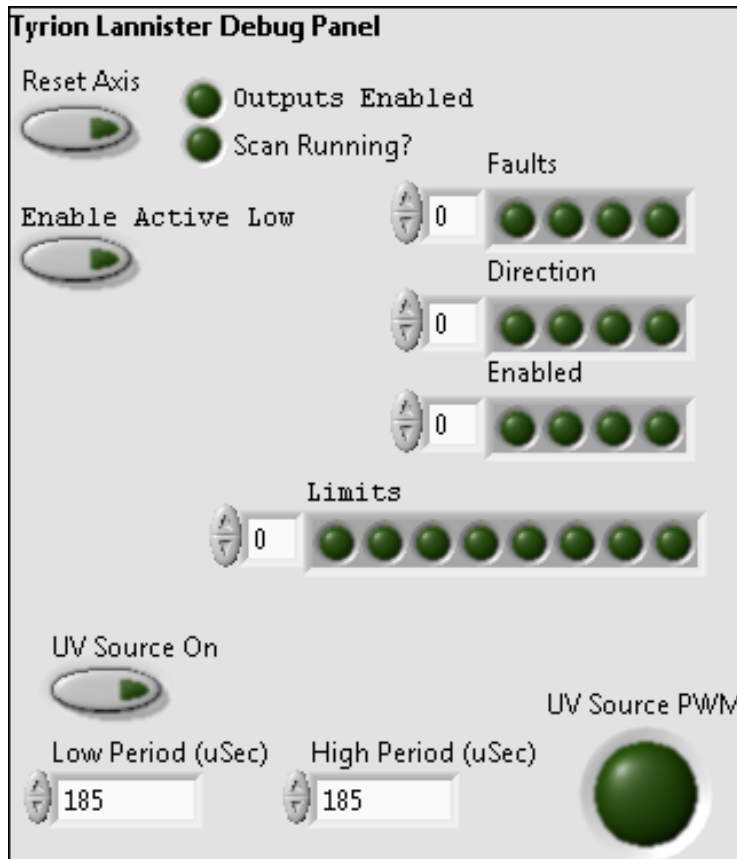


Figure 3.32: FPGA front panel.

All the functions used to generate the different signals for the stepper motor and to manage all the inputs from the stepper drives themselves are located in the back panel of this VI. It is important to mention that these functions were directly taken from the SISU-1004 examples database and it is not necessary to modify them at this level. Figure 3.33 shows the block diagram code for the PWM signal generation as described in Section 3.3.2, the SISU-1004 functions from this VI can be found in Section A.5 of the Appendix.

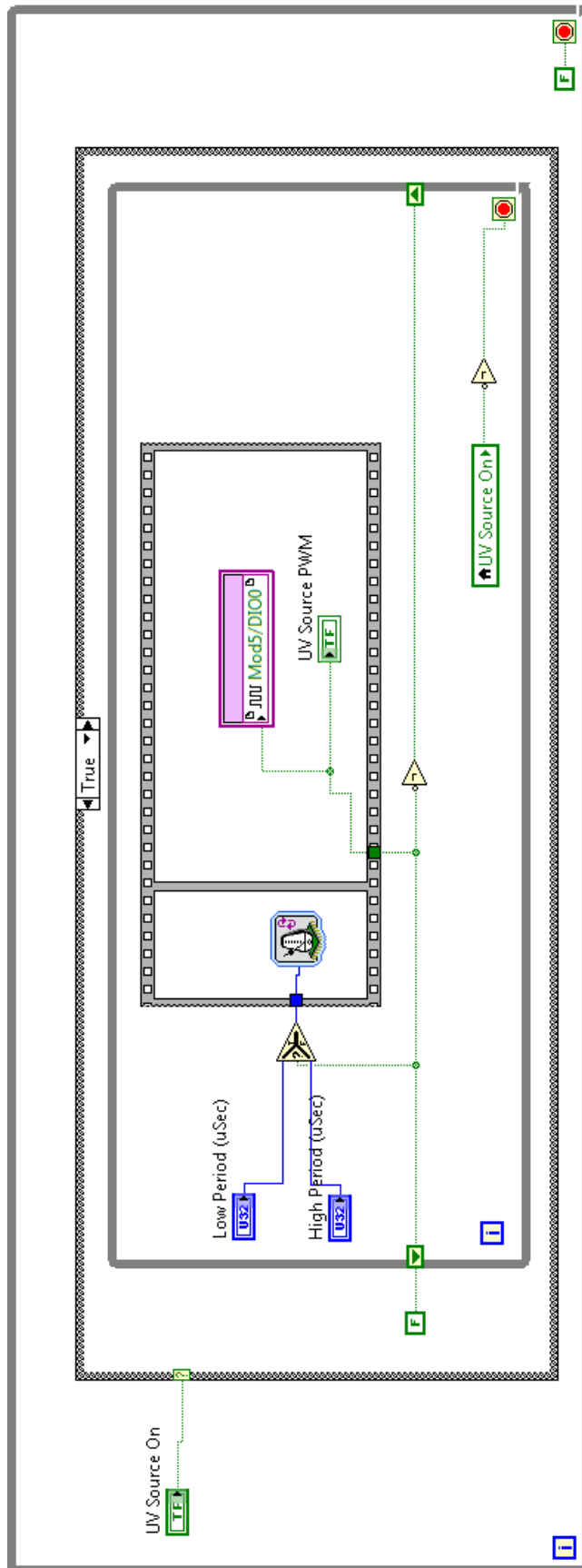


Figure 3.33: FPGA back panel.

Chapter 4

Experimental validation

There are two critical capabilities that this system required. First, it had to be able to dispense magnetic resin in a controllable way following an input G-Code. Second, considering that such magnetic resin is loaded with particles magnetically responsive, the system had to be capable of manipulating the angle of a magnetic jig in a programmable way. By modifying the angle of the magnetic jig, the orientation of the magnetic particles inside of the resin should change accordingly. To prove these two capabilities, two different tests were conducted.

4.1 Printing test

The first test was related to the capability of the system to perform a basic print. For this, the CAD model shown in Figure 4.1 was generated and processed in Slic3r to create an initial G-Code. Then, this G-Code was customized through our software ADaM - Lab Particles Control Center to obtain an extended G-Code compatible with our control software.

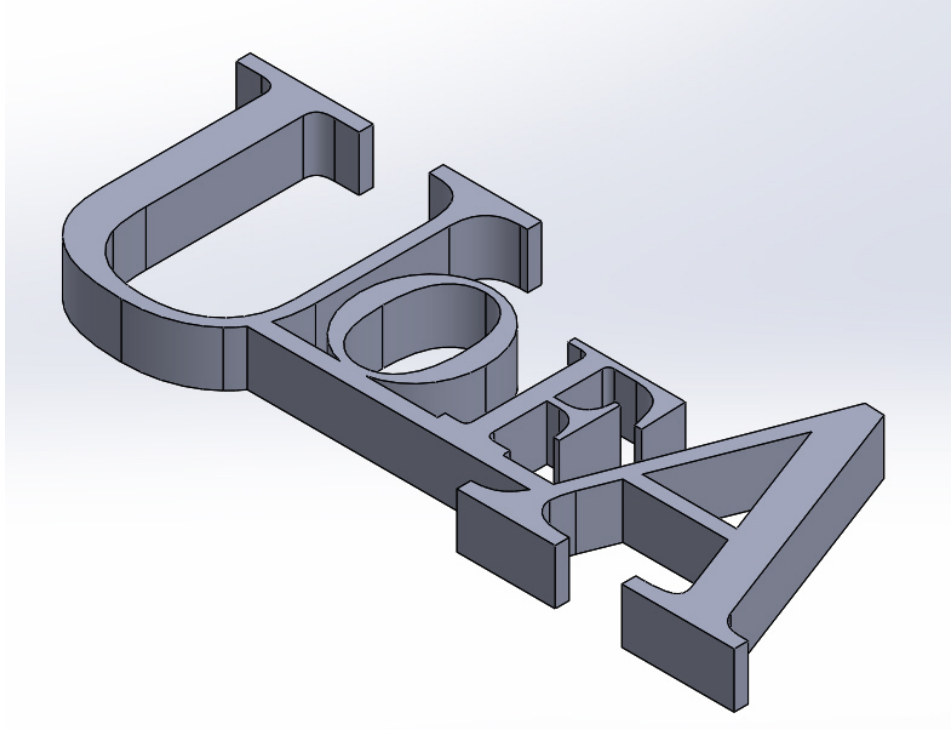


Figure 4.1: UofA CAD model.

Due to the early development stage of our magnetic resin, the deposition parameters were roughly estimated through simple deposition tests. For these tests, lines of the magnetic resin were dispensed at different deposition speeds and different pressures. Once they were cured, they were visually analyzed to evaluate the amount of resin dispensed and the quality of the line. Figure 4.2 shows a picture taken during the deposition test. A table with the results of these initial tests is included in the Section A.6 of the dix. It is important to understand that these results are reference values, due to several factors discussed in the conclusion section.

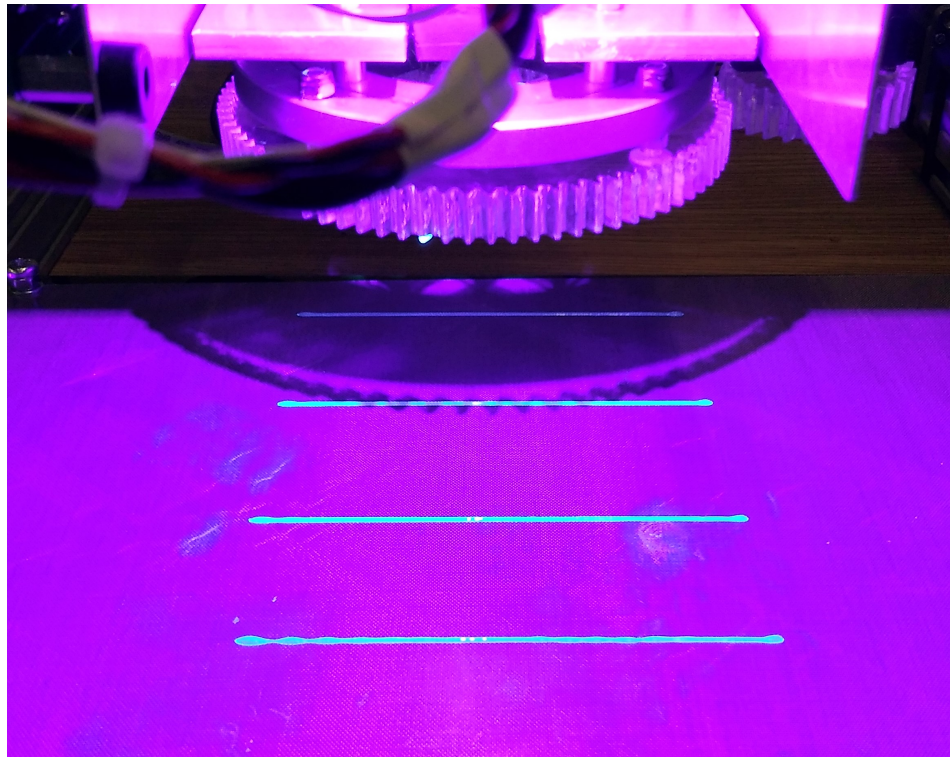


Figure 4.2: Deposition test.

With initial settings selected, the dispensing systems barrel was loaded with the magnetic resin. More details about this filling process can be found in Section A.1 of the Appendix. With the dispensing system ready, the extended G-Code was loaded to the printer and the process initiated. The requirement for this test was that the system had to have the ability to replicate the geometry created in the CAD model. For doing this, the system had to deposit the magnetic resin only when needed and to correctly execute all the commands in the G-Code. A single layer of the model was deposited. Figure 4.3 shows the result of this test. It is possible to see that the printer successfully performed the needed operations to deposit the resin as expected.



Figure 4.3: UofA logo printing test.

As part of further tests, other variations of the magnetic resin were tested using the same G-Code. These tests showed that the results are highly dependent on the physical properties of the resin being used. Figure 4.4 shows a test using a variation of the resin with a high concentration of the magnetic particles.

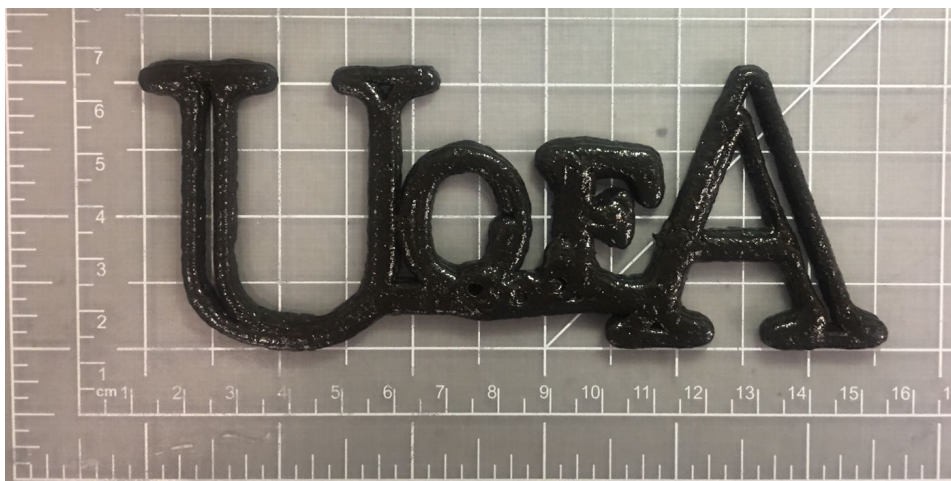


Figure 4.4: Grid used for directionality test

4.2 Particles alignment test

The second test involved the creation of a custom G-Code to dispense resin inside of a grid and then to align the suspended particles to a given orientation. The G-Code used for this test can be found in Section A.7 of the Appendix. For the test, a 3x3 grid was cut out of a 1/8 inch thick acrylic sheet. Figure 4.5 shows an image of the grid used. The procedure consisted of positioning the printing head into each of the nine locations on the grid and then depositing a single drop of the magnetic resin. With the magnetic resin deposited, the magnetic jig was rotated to a different angle depending on the position in the grid. The test began at 0 degrees, then the magnetic jig was rotated 45 degrees every time in the next sample until it reached 360 degrees. The magnetic jig was kept in the different angles exposing the sample to the uniaxial magnetic field for 1 minute to align the particles.

Using previous optical microscopy studies it was observed that the magnetic orientation is a two steps process. In the first step the magnetic particles, in this case the strontium ferrite, behave like individual magnetic dipoles that become magnetize under the presence of the uniaxial magnetic field. In the second step these polarized individual particles start to aggregate to form the chain-like micro-structures align with the magnetic flux lines from the magnetic field. Further analysis also showed that once the particles are magnetized a relative small magnetic field is sufficient to rotate the chain-like micro-structures to any desired orientation angle.

Once that the alignment process was completed the LED was activated to cure the magnetic resin for 2 minutes. The aligning/curing process was then repeated for every sample in the grid. Once that all the samples were printed, the grid was removed from the printing bed and the particles' orientation of each sample was characterized via image processing as explained in the next subsection.

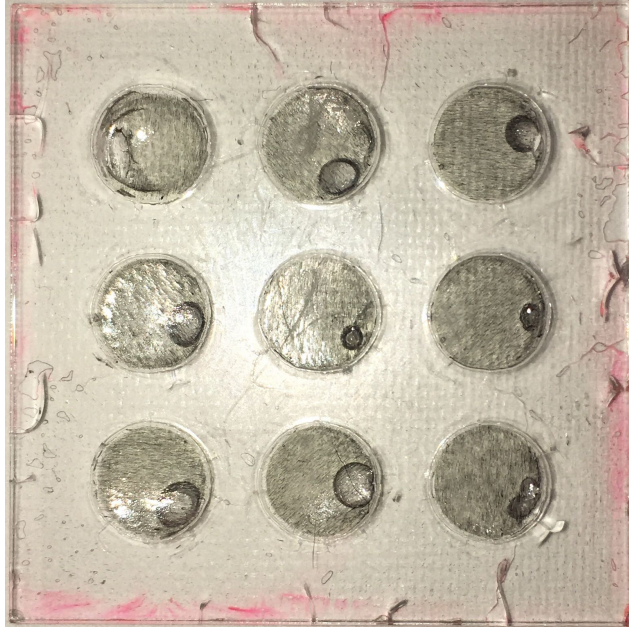


Figure 4.5: Grid used for directionality test

4.2.1 Alignment characterization

The degree of particle alignment within the magnetic resin was evaluated using optical microscopy. A PR48 suspension was loaded with 0.5 wt% strontium ferrite. The low percentage of particles was a key factor while using optical microscopy to analyze the samples. The reason is that when the particles' weight percentage is increased, the resin turns into a dark liquid where the alignment cannot be characterized using standard visual methods.

With the samples cured inside the grid, the whole grid was removed and placed under an optical microscope. Then using interface software for the microscope at a magnification of 4.5X, images of the samples were captured. The acquired images were converted to gray scale and then digitally enhance. Figure 4.6 shows some of the images taken from the optical microscopy analysis. In these images, it is possible to observe the chain-like micro-structures formed by the ferrite powder. This is possible to prove if they are compared with the image presented by Martin et al. [12] of their field structured composite. Using the magnetic field generated by the Halbach array and controlled by the magnetic jig mechanism the particles' alignment was modified with respect to

the programmed angle. For the directionality analysis the platform was programmed to generate samples with a particle angular orientation of -30, 30, -45 and 45 degrees. Other images taken can be found in Section A.8 of the Appendix.

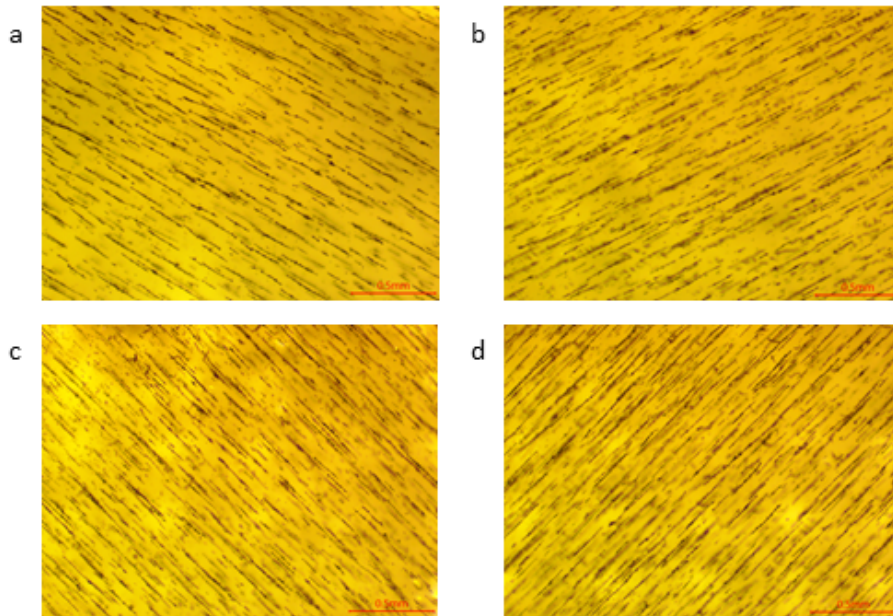


Figure 4.6: Optical microscopy images of aligned particles in cured resin. (a) -30 degrees; (b) 30 degrees; (c) -45 degrees; (d) 45 degrees.

A software called Fiji ImageJ [21] was used to measure the angles of the particles in the images taken. This analysis was performed Using the “directionality” feature of the software. This tool uses an algorithm that counts the number of structures oriented in certain direction, using the local gradient orientation method. Figure 4.7 shows the result of the analysis. The data obtained describe a Gaussian curve with a sharp peak at the set orientation angle. This sharp peak represents that there is a high number of oriented structures at that particle angular orientation, in comparison an isotropic sample produce results in the shape of a flat curve, where the structures don’t present a particular orientation. From these directionality curves, it is also evident that the standard deviation results are the same for all orientation angles.

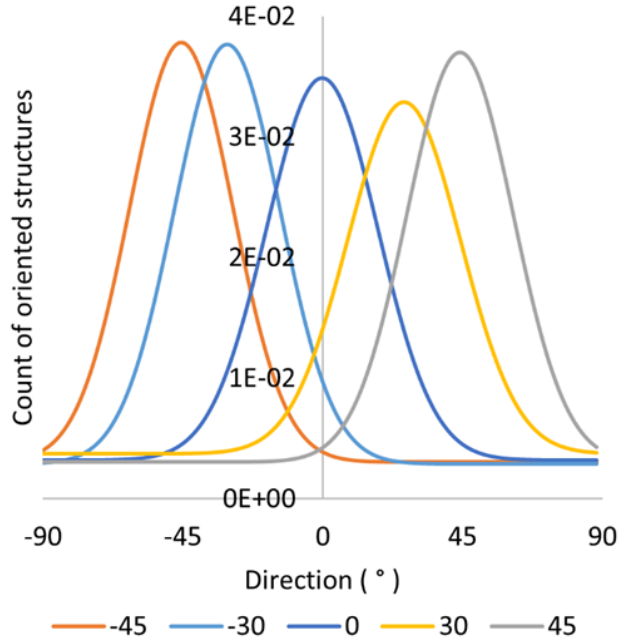


Figure 4.7: Magnetic particles directionality data for -45,-30,0,30,45 degrees.

4.3 Conclusion

In the present work, an additive manufacturing process aimed to create custom permanent magnets was presented. The AM process was selected over other traditional manufacturing method, due to its unique capability to create complex geometries and its flexibility to allow localized properties to be tailored. As studied by Martin et al. [12] the presence of anisotropic chainlike structures within a magnetic composite increases the magnitude of remanent magnetization. This is how generating localized anisotropic particle arrangement became a goal for this project.

As presented in this document a material jetting based platform was built to experiment with a magnetically loaded light sensitive resin. This platform integrates a custom designed rotating magnetic jig, a precision dispensing system, a light based curing system, and a 3-axis Cartesian motion platform. The machine was designed to be capable of dispensing a magnetic resin and aligning the magnetic particles suspended inside of it. A pre-programmed set of instructions called G-Code was followed.

The selected dispensing system proved to be a flexible tool, allowing to customize a series of parameters like pressure and vacuum. The disadvantage of this platform resulted to be the very limited reservoir with a maximum capability of 30 cc of resin at a time. This limitation will create a bottle neck in the printing process, making it a primary feature to be modify in the next design iteration.

With the selected positioning of the dispensing system across the Halbach array, new challenges arose. Fluctuations in the amount of the deposited resin were observed. Different printing settings like pressure and printing speed were varied in an attempt to correct the fluctuations. It was concluded that in the magnetic resins with particles concentration higher than 0.5 wt%, the magnetic field was attracting too many particles at a given time and clogging the dispensing tip.

In the current design, the dispensing tip used to deposit the magnetic resin is located in the center of the magnetic jig causing a direct interaction between the magnetic particles and the magnetic field from the permanent magnets. Reaching this conclusion allow us to understand that in order to have a constant flow, the area around the dispensing tip must be shielded from the present magnetic field. Possible solutions include shielding the dispensing tip with a high permeability material. The dimensions and the necessary amount of shielding will have to be defined. Nevertheless, with this modification, other changes would have to take place, including the position of the LED and possible machining of the aluminum support angle to hold the shielding.

Once that a constant flow is achieved, the true capabilities of the XYZ gantry configuration can be exploited. Setting like micro-stepping and different motion feed rates can be tested in order to optimize the printing quality and minimize the operation time accordingly. This design resulted to be sensitive to the perfect alignment of the parallel slides in charge of actuating the Y-axis. Failing to precisely align the carriages of both linear actuators caused uneven displacement and immediate jamming. Although not ideal, this scenario does not diminish the overall positive performance of the design.

Based on the first set of experiments, it was concluded that further under-

standing of the curing process has to be developed for the different variations of the magnetic resin. Furthermore, in this experiment, the same G-Code and same parameters were run using magnetic resins with higher particle concentration. It was observed that increasing the particles' weight percentage in the resin had a direct effect on the curing time, showing less curing in magnetic resin with higher concentrations.

Another important factor to consider is the location and orientation of the curing light, in the current design the light is meant to flood the area around the dispensing tip. This way of exposing the resin to the curing light resulted to be not the most effective. Due to the fact that depending the direction of movement the resin was not exposed to the same amount of light.

It is important to understand that this analysis was qualitative. Adequate equipment should be used in the future to obtain quantitative measurements of the curing degree for the different levels of particle concentration and light intensities.

From the second set of experiments, results are clear that two factors have to be accounted for during the optimization process. These are the curing time and the alignment time. Therefore, a full optimization study must be performed, including the curing time, the alignment time, the printing parameters, and the printing quality. This last task is related to achieving a constant and repeatable stream of magnetic resin being deposited. The ultimate test would be related to determining the anisotropy achieved through the manufacturing process. Lastly, the results of this study indicate the industrial applications of the technology developed.

Along with the mechatronic system, two different software programs were created; the first one to post-process a standard G-code, and the second one to control the actuation of the mechanism itself. Once the system was manufactured and programmed, initial tests were performed to evaluate its printing and alignment capabilities.

In summary, in this work, a novel mechatronic system comprising software, hardware and a control system capable of creating 3D printed composites with internal, local, and programmable magnetic particles orientation has been

developed. Then, the major contributions of this research are:

A system level design of a 4 dimensional ferromagnetic printing platform. Addition of an extra rotation axis (4D) enabling the orientation of magnetic particles within an (X-Y) printing plane. Development of an extended G-Code to enable 4D printing. Development of an extensible, scalable, and open firmware for 4D printing of magnetic composites.

References

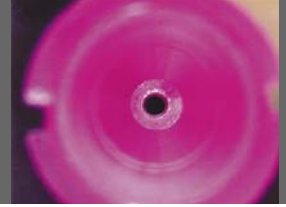
- [1] A. 52900:2015, “Standard Terminology for Additive Manufacturing – General Principles – Terminology,” *ASTM International*, vol. i, pp. 1–9, 2015, ISSN: 1882-675X. DOI: 10.1520/F2792-12A.2. arXiv: arXiv:1011.1669v3. [Online]. Available: http://compass.astm.org/EDIT/html%7B%5C_%7Dannot.cgi?ISOASTM52900+15. 3–6
- [2] I. Aleph Objects, *Lulzbot TAZ 6 user manual*. 2016, pp. 1–90, ISBN: 978-0-9893784-8-2. [Online]. Available: <http://download.lulzbot.com/TAZ/6.0/documentation/manual/TAZ-6-Manual.pdf>. 24
- [3] Alessandro Ranellucci, *Slic3r - About*, 2011. [Online]. Available: <http://slic3r.org/about> (visited on 03/12/2018). 39
- [4] A. de Almeida, P. Bertoldi, and W. Leonhard, *Energy efficiency improvements in electric motors and drives*. Springer Science & Business Media, 2012. 2
- [5] S. S. Detection and P.-m. Motor, “EM705,” pp. 1–7, 31
- [6] O. Gutfleisch, M. A. Willard, E. Brück, C. H. Chen, S. G. Sankar, and J. P. Liu, “Magnetic materials and devices for the 21st century: Stronger, lighter, and more energy efficient,” *Advanced Materials*, vol. 23, no. 7, pp. 821–842, 2011, ISSN: 09359648. DOI: 10.1002/adma.201002180. 2
- [7] D. Kokkinis, M. Schaffner, and A. R. Studart, “Multimaterial magnetically assisted 3D printing of composite materials,” *Nature Communications*, vol. 6, p. 8643, 2015, ISSN: 2041-1723. DOI: 10.1038/ncomms9643. [Online]. Available: <http://www.nature.com/doifinder/10.1038/ncomms9643>. 6
- [8] L. Li, B. Post, V. Kunc, A. M. Elliott, and M. P. Paranthaman, “Additive manufacturing of near-net-shape bonded magnets: Prospects and challenges,” *Scripta Materialia*, vol. 135, pp. 100–104, 2017, ISSN: 13596462. DOI: 10.1016/j.scriptamat.2016.12.035. [Online]. Available: <http://dx.doi.org/10.1016/j.scriptamat.2016.12.035>. 6
- [9] L. Li, A. Tirado, I. C. Nlebedim, O. Rios, B. Post, V. Kunc, R. R. Lowden, E. Lara-Curzio, R. Fredette, J. Ormerod, T. A. Lograsso, and M. P. Paranthaman, “Big Area Additive Manufacturing of High Performance Bonded NdFeB Magnets,” *Scientific Reports*, vol. 6, no. 1, p. 36212,

- 2016, ISSN: 2045-2322. DOI: 10.1038/srep36212. [Online]. Available: <http://www.nature.com/articles/srep36212>. 11, 12
- [10] F. Lundh, *TkInter - Python Wiki*. [Online]. Available: <https://wiki.python.org/moin/TkInter> (visited on 03/12/2018). 40
- [11] O. Manual, “Ultimus V High Precision Fluid Dispenser Srimi Subramanian,” 17, 41
- [12] J. E. Martin, E. Venturini, J. Odinek, and R. Anderson, “Anisotropic magnetism in field-structured composites,” *Physical Review E*, vol. 61, no. 3, pp. 2818–2830, 2000, ISSN: 1063-651X. DOI: 10.1103/PhysRevE.61.2818. 7, 81, 83
- [13] Micromo, “Stepper Motor Technical Note: Microstepping Myths and Realities,” *White Papers*, pp. 1–4, 2014. 32
- [14] S. I. Module, “SISU-1004,” pp. 1–13, 30
- [15] C. S. Modules, “NI cRIO-9066,” pp. 1–8, 29, 45
- [16] B. Nagarajan, A. F. E. Aguilera, A. Qureshi, and P. Mertiny, “Additive manufacturing of magnetically loaded polymer composites: An experimental study for process development,” V002T02A032–V002T02A032, 2017. 20
- [17] National Instruments, *LabVIEW Programming Fundamentals - National Instruments*, 2012. [Online]. Available: <http://www.ni.com/white-paper/14187/en/> (visited on 03/12/2018). 45, 46
- [18] —, *NI FPGA - National Instruments*, 2018. [Online]. Available: <http://www.ni.com/fpga/> (visited on 03/12/2018). 45
- [19] M. P. Paranthaman, C. S. Shafer, A. M. Elliott, D. H. Siddel, M. A. McGuire, R. M. Springfield, J. Martin, R. Fredette, and J. Ormerod, “Binder Jetting: A Novel NdFeB Bonded Magnet Fabrication Process,” *Jom*, vol. 68, no. 7, pp. 1978–1982, 2016, ISSN: 15431851. DOI: 10.1007/s11837-016-1883-4. 9–11
- [20] Pololu, *Pololu - A4988 Stepper Motor Driver Carrier*. [Online]. Available: <https://www.pololu.com/product/1182> (visited on 03/12/2018). 33
- [21] J. Schindelin, I. Arganda-Carreras, E. Frise, V. Kaynig, M. Longair, T. Pietzsch, S. Preibisch, C. Rueden, S. Saalfeld, B. Schmid, J.-Y. Tinevez, D. J. White, V. Hartenstein, K. Eliceiri, P. Tomancak, and A. Cardona, “Fiji: an open-source platform for biological-image analysis,” *Nature Methods*, vol. 9, no. 7, pp. 676–682, Jun. 2012, ISSN: 1548-7091. DOI: 10.1038/nmeth.2019. arXiv: 1081–8693. [Online]. Available: <http://www.nature.com/doifinder/10.1038/nmeth.2019>. 82
- [22] SimCom, “Development Kit Manual,” *Solutions*, pp. 1–30, 2011. 19

- [23] H. Song, J. Spencer, A. Jander, J. Nielsen, J. Stasiak, V. Kasperchik, and P. Dhagat, "Inkjet printing of magnetic materials with aligned anisotropy," *Journal of Applied Physics*, vol. 115, no. 17, 17E308, 2014, ISSN: 0021-8979. DOI: 10.1063/1.4863168. [Online]. Available: <http://scitation.aip.org/content/aip/journal/jap/115/17/10.1063/1.4863168>. 13, 14
- [24] P. Test, A. Average, D. Actual, and R. Accuracy, "OpenBuilds Actuator Testing Data," pp. 1–7, 25
- [25] X. lei ZHANG, M. yuan ZHU, Y. LI, Q. ping YANG, H. ming JIN, J. JIANG, Y. TIAN, and Y. LUO, "Study on Fabrication Process of Anisotropic Injection Bonded Nd-Fe-B Magnets," *Journal of Iron and Steel Research International*, vol. 13, no. SUPPL. 1, pp. 286–288, 2006, ISSN: 1006706X. DOI: 10.1016/S1006-706X(08)60196-X. 8

Appendix A

A.1 Ultimus V



Dispensing Tips

EFD produces the highest quality dispensing tips in the industry. All tips are produced in our own silicone-free facilities, and subjected to stringent quality control inspections throughout the entire manufacturing process.

Features and Benefits

- Free of flash, burrs and contaminants
- Package labels include lot numbers for process control and traceability
- Consistent from style to style and lot to lot
- 360° SafetyLok™ thread ensures safe, positive attachment to syringe barrel
- Engineered hub flats for easy twist on, twist off



Precision Stainless Steel Passivated stainless steel tips handle a wide range of fluids and applications.

Tapered Smooth flow for application of medium- to high-viscosity fluids – especially thick or particle-filled materials like epoxies, RTVs and braze pastes.

Flexible Polypropylene shafts reach into hard-to-access areas and will not scratch delicate surfaces. Easily cut to size or angled as needed.

Angled Stainless steel tips are available with 45° and 90° bends.

Brush For spreading glues and greases. Available with soft or stiff bristles.

Specialty For specific applications: chamfered, ESD-safe, PTFE-coated and PTFE-lined, microdot tips and oval tips.










PRECISION STAINLESS STEEL TIPS

Gauge	6.35 mm (0.25")	12.7 mm (0.50")	25.4 mm (1.0")	38.1 mm (1.5")	45° Bend/12.7 mm (0.5")	90° Bend/12.7 mm (0.5")	45° Bend/38.1 mm (1.5")	Color
14	7018029	7018043	7018032	7018035	7018044	7018045	7016906	Olive
15	7018056	7018068	7018059	7018062	7018069	7018070	n/a	Amber
18	7018107	7018122	7018110	7018113	7018123	7018124	7016908	Green
20	7018163	7018178	7018166	7018169	7018179	7018180	n/a	Pink
21	7005005	7018233	7018222	7018225	7018234	7018235	7016910	Purple
22	7018260	7018272	7018263	7018266	7018273	7018274	n/a	Blue
23	7018302	7018314	7018305	7018308	7018315	7018316	n/a	Orange
25	7018333	7018345	7018336	7018339	7018346	7018347	n/a	Red
27	7018395	7005008	n/a	n/a	7018404	7018405	n/a	Clear
30	7018424	7018433	n/a	n/a	7018434	7018435	n/a	Lavender
32	7018462	n/a	n/a	n/a	n/a	n/a	n/a	Yellow





Burr-free, polished, passivated stainless steel dispensing tips with polypropylene SafetyLok hubs for a secure fit to barrel reservoirs. Packaged 50 tips per box.
 • 6.35 mm (0.25") tips: Fast point-to-point dispensing. • 12.7 mm (0.50") tips: Standard all-around precision dispensing tips. • 45° and 90° bent tips: Easy access into hard-to-reach areas.

SMOOTHFLOW TAPERED TIPS

Gauge	Standard	Opaque Rigid	Color
14	7018052	7018049	Olive 
16	7018100	7018097	Grey 
18	7018158	7018147	Green 
20	7005009	7005006	Pink 
22	7018298	7005007	Blue 
25	7018391	7018370	Red 
27	7018417	n/a	Clear 





Use with gel cyanoacrylates, UV-cure adhesives, sealants, and particle-filled materials or any medium- to high-viscosity fluid. Molded of polyethylene with UV-light block additive. Packaged 50 tips per box.

FLEXIBLE TIPS

Gauge	12.7 mm (0.50")	38.1 mm (1.5")	Color
15	7018085	7018080	Amber 
18	7018143	7018138	Green 
20	7018205	7018201	Pink 
25	7018366	7018362	Red 

Flexible polypropylene tubing for application into difficult-to-access areas. Easily drags along edges and around corners and prevents scratching. Tubing can be cut to length. Packaged 50 tips per box.


CHAMFERED TIPS

Gauge	12.7 mm (0.50")	Color
18	7018129	Green 
23	7018321	Orange 
25	7018352	Red 
33	7018482**	Clear 

Use for microdot application of low viscosity fluids. Packaged 50 tips per box.



**7018482 is 6.35 mm (0.25") long and packaged 25 tips per box.

OVAL TIPS

Gauge	12.7 mm (0.50")	Color
15	7018078	Amber 

Flat ribbon deposits of thick pastes, sealants & epoxies. Outlet size is 1.98 x 0.41 mm (.078" x .016"). Packaged 50 tips per box.

TIP SHIELDS

Size	Part #	Color
3cc	7017715	Red 
5cc to 55cc	7017717	Black 

Reusable tip shields for light-sensitive and UV-cure adhesives. Fits over dispensing tip hub. Packaged 10 tip shields per box.



BRUSH TIPS

Style	Standard	High Flow
soft bristle	7018490	7018491
stiff bristle	7018494	7018495

Spread glues and greases. Nylon bristles, 50.8 mm (2") length. Sold individually.





PTFE-COATED TIPS

Gauge	ID	OD	12.7 mm (0.50")	Color
21	0.020	0.033	7018243	Purple 
23	0.013	0.026	7018326	Orange 

Controls wicking to stop drips in optical media applications. Packaged 20 tips per box.

PTFE-LINED TIPS

ID	12.7 mm (0.50")	25.4 mm (1.0")	Color
0.020"	7018256	7005003	Grey 
0.006"	7018388	7005004	Pink 

Resists clogging of cyanoacrylates. Use for microdot application of low viscosity fluids. Packaged 50 tips per box.

POLYETHYLENE NOZZLES

Size	Part #
6.35 x .318 cm (2.5 x .125")	7018555
6.35 x .157 cm (2.5 x .062")	7018557
10.6 x .157 cm (4.0 x .062")	7018559
10.6 x .08 cm (4.0 x .031")	7018561

Polyethylene nozzles thread into all cartridge sizes and 725 Series and 736HPA-NV valves. 1/4 NPT (6.35 mm) thread. Packaged 10 nozzles per bag.

METAL NOZZLES

Gauge	Part #	ID mm	ID inch
7	7017630	3.8	.150
8	7017633	3.4	.135
10	7017638	2.7	.106
12	7017643	2.2	.085
14	7017651	1.6	.063
16	7017660	1.2	.047

38.1 mm (1 1/2") long metal nozzles with 1/4 NPT to fit 725 Series and 736HPA-NV valves.



EFD[®] TIP RECOMMENDATIONS

A NORDSON COMPANY

APPLICATIONS	DISPENSING TIPS			
	Tapered	Stainless Steel	PTFE-Lined	Flexible
Very Low Viscosity Fluids	X	●	●	●
Particle-Filled Pastes	●	●	▲	X
Microdot Deposits	X	●	▲	●
Fluid is Reactive to Metal	●	X	●	●
Depositing in Recesses	▲	●	●	▲
Spreading/Smearing	●	▲	●	▲
Fast-Curing Glues	●	▲	●	●
Beading, Striping	●	●	●	▲
Easily Scratched Substrates	●	▲	●	●
FLUIDS				
Adhesives	●	●	●	●
Anaerobics	●	▲	●	▲
Conformal Coatings	●	▲	▲	X
Cyanoacrylates	●	▲	●	●
Gel Cyanoacrylates	●	▲	●	▲
Epoxies	●	●	●	X
Greases	●	●	●	X
Light-Cure Adhesives	X	▲*	▲*	X
Oils	▲	●	●	▲
Paints	▲	●	●	X
Sealants	●	▲	▲	X
Silver Epoxy	X	▲ ⁺	X	X
Solder Paste/Braze Pastes	●	●	▲	X
Solder Masks	●	●	▲	X
Solvents	X	●	●	●
UV-Cure Adhesives	●	▲*	▲*	-

Key
● Recommended
▲ Satisfactory
X Do not use

* OK if used with tip shield, part #7017715 or 7017717.

⁺ Chamfered tips are recommended for best results.



COLOR CODING FOR TIP SIZES

Color	Gauge	Inner Diameter		Outer Diameter	
		mm	inch	mm	inch
● Olive	14	1.54	.060	1.83	.072
● Amber	15	1.36	.053	1.65	.065
● Grey	16	1.19	.047	n/a	n/a
● Green	18	0.84	.033	1.27	.050
● Pink	20	0.61	.024	0.91	.036
● Purple	21	0.51	.020	0.82	.032
● Blue	22	0.41	.016	0.72	.028
● Orange	23	0.33	.013	0.65	.025
● Red	25	0.25	.010	0.52	.020
○ Clear	27	0.20	.008	0.42	.016
● Lavender	30	0.15	.006	0.31	.012
● Yellow	32	0.10	.004	0.24	.009

Note: OD dimensions are for stainless tips only.

Whatever tip style, all sizes are color-coded to ensure the specified size is used.

Free Syringe & Tip Poster for Adhesive Dispensing

Quickly identify the right dispensing components for your fluid application process.

Call 800-556-3484 to request a free copy.

Specifications

Cabinet Dimensions: 111 mm (4.36") H x 225 mm (10.04") W x 214 mm (8.43") D

Weight: 3.36 kg (7 lb, 6.5 oz) with feet

Input AC: 100–240 VAC \pm 10%, 0.5 Amp, 50/60Hz

Output DC (from power supply): 24 VDC, 1.66 Amp maximum

Internal Voltage: 24 VDC

Footswitch: 24 VDC

Cycle Initiate: Foot Pedal, Finger Switch, I/O

Air Input Requirements: 1.4 bar (15 psi) minimum to 6.9 bar (100 psi) maximum

Air Output: 0–6.9 bar (0–100 psi)

Approvals: RoHS, WEEE & China RoHS Compliant, CE

Ambient Operating Conditions

Temperature: 5° C to 50° C (41° F to 122° F)

Humidity: 85% RH at 30° C non-condensing

Height above sea level: 2000 m max (6562 ft)

This unit is intended for indoor use only

Product Classification

Installation: Category II

Pollution: Degree 2

RoHS标准相关声明 (China RoHS Hazardous Material Declaration)

产品名称 Part Name	有害物质及元素 Toxic or Hazardous Substances and Elements					
	铅 Lead (Pb)	汞 Mercury (Hg)	镉 Cadmium (Cd)	六价铬 Hexavalent Chromium (Cr6)	多溴联苯 Polybrominated Biphenyls (PBB)	多溴联苯醚 Polybrominated Diphenyl Ethers (PBDE)
外部接口 External Electrical Connectors	X	0	0	0	0	0
<p>0: 表示该产品所含有的危险成分或有害物质含量依照EIP-A, EIP-B, EIP-C 的标准低于SJ/T11363-2006 限定要求。 Indicates that this toxic or hazardous substance contained in all the homogeneous materials for this part, according to EIP-A, EIP-B, EIP-C is below the limit requirement in SJ/T11363-2006.</p> <p>X: 表示该产品所含有的危险成分或有害物质含量依照EIP-A, EIP-B, EIP-C 的标准高于SJ/T11363-2006 限定要求。 Indicates that this toxic or hazardous substance contained in all the homogeneous materials for this part, according to EIP-A, EIP-B, EIP-C is above the limit requirement in SJ/T11363-2006.</p>						

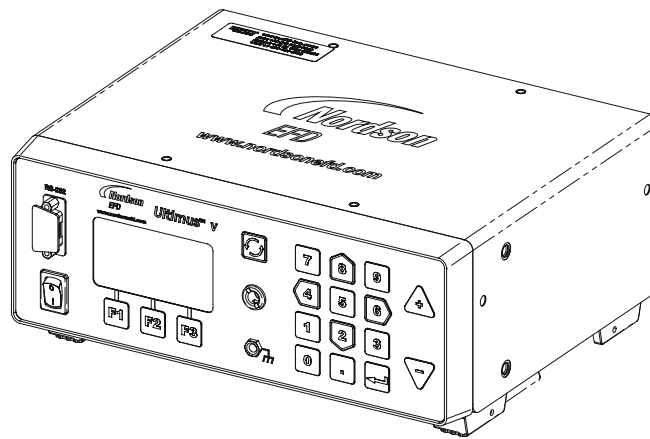
WEEE Directive



This equipment is regulated by the European Union under WEEE Directive (2012/19/EU). Refer to www.nordsonefd.com/WEEE for information about how to properly dispose of this equipment.

Ultimus V Features

- Electronically change / adjust dispensing Time, Pressure, and Vacuum
- Simultaneously display dispensing Time, Pressure, and Vacuum
- Auto Increment mode to adjust dispensing parameters after a certain number of shots or a specific lapsed time
- Auto Sequence mode that allows deposit patterns to be repeated automatically
- 400 individual memory storage cells
- Scroll or select cells via front panel keypad or external PC / PLC control
- Switching between Steady, Timed, and Teach modes
- Front panel Manual Cycle key
- Teach function
- Multi-level operator lockout
- Alarm indicators
- End of Cycle Feedback loop
- Soft button data input 0–9 keypad
- Operator control of LCD display brightness
- Easy UP / DOWN arrow key navigation
- External PC interface for data input
- Display cycle counter
- RS-232 interface compatible with standard RS-232 protocol
- ESD-safe via connection with external ESD grounding plug
- 0–6.9 bar (0–100 psi) air regulation range; 0–18 H₂O vacuum regulation range
- Internal universal power supply
- D-sub I/O (15-pin) and communication (9-pin) connections
- Alarm input / output I/O signals



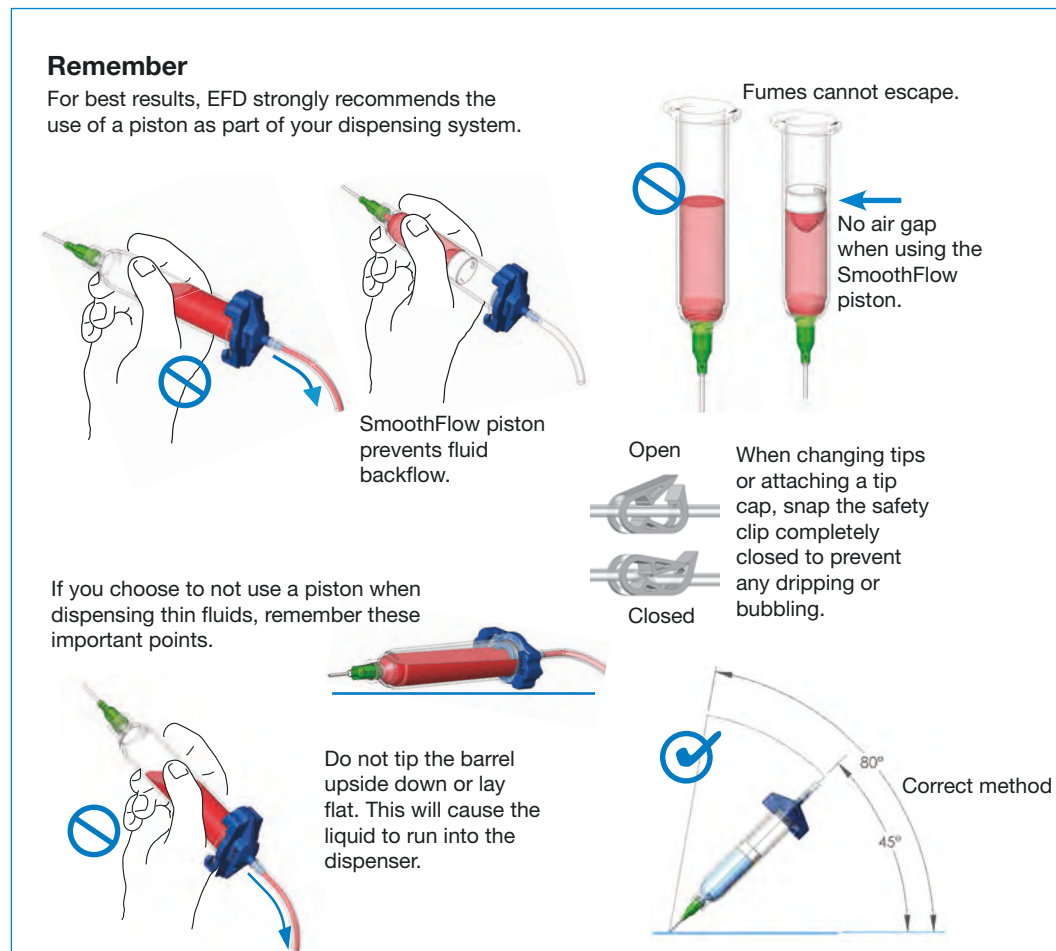
Filling the Syringe Barrel

Caution: Do not completely fill syringe barrels. The optimum fill is a maximum 2/3 of the barrel capacity and 1/2 of the barrel capacity when using the EFD blue LV Barrier™ piston.

For best results, we strongly recommend that you use a piston as part of your dispensing system. The white EFD SmoothFlow piston is appropriate for most fluids and has several advantages.

- First, vacuum adjustment is less sensitive.
- Second, the piston prevents fumes from the fluid being exhausted into the work environment.
- Third, the piston prevents fluid backflow into the dispenser if the syringe barrel is inadvertently turned upside down.
- Fourth, the piston makes it easy and safe to change tips without dripping.

For watery solvents and cyanoacrylates, request the blue EFD LV Barrier piston, available in 3cc, 10cc, and 30 / 55cc sizes. If you are dispensing an RTV silicone and find that the piston bounces and causes stringing, request EFD's assistance in selecting a suitable piston.



A.2 UV LED Driver

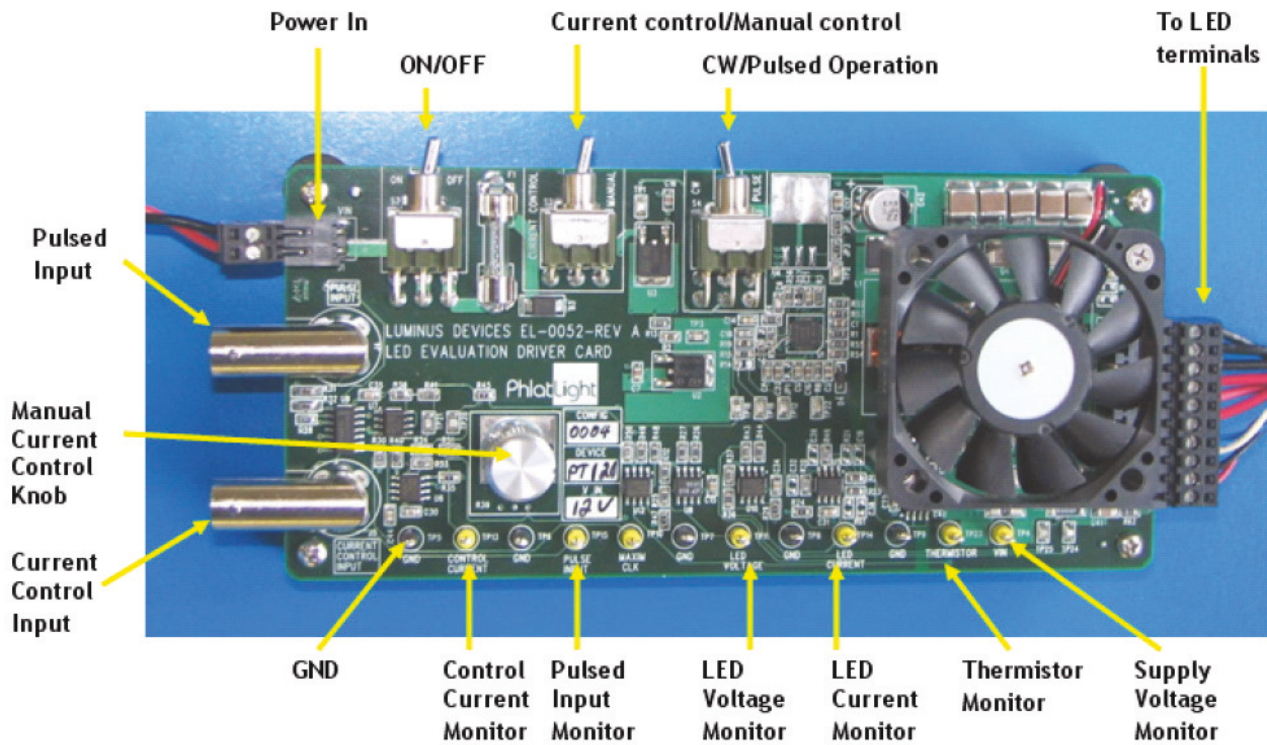


Figure 8: Driver board pin layout.

4. Use Instructions

4.1 Mounting the LED to the heat sink

Ineffective heat sinking may lead to premature LED degradation or failure. The following steps explain how an LED is mounted on the heat sink while ensuring good thermal contact between the copper core-board and the heat sink.

1. Use a thermal pad of an area slightly larger than the area of the core board (Figure 9).
2. Place the thermal pad on the heat sink with pre-drilled holes matching the hole pattern on the heat sink (Figures 10 and 11).

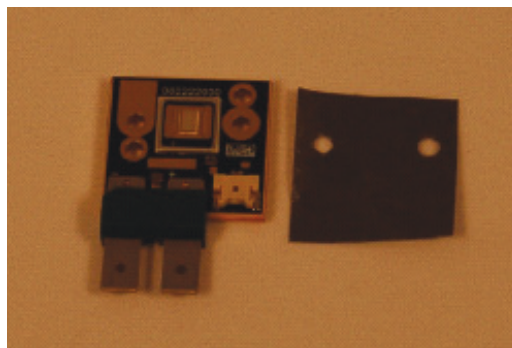


Figure 9: Thermal pad and device

3. Place the LED on the thermal pad such that the hole patterns match (Figure 12).
4. Insert screws in the holes of the coreboard and tighten. To ensure equal pressure is exerted by all screws, alternate tightening each screw until the board is securely fastened. The use of a torque wrench, with a torque setting of 40 Oz-Inches, is recommended.

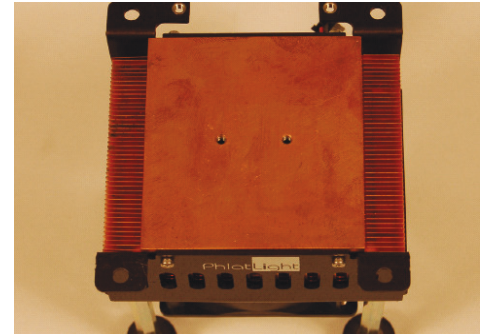


Figure 10: Pre-drilled holes

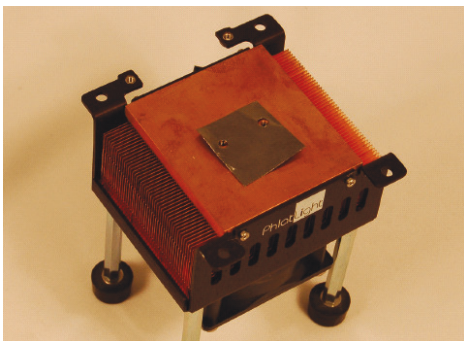


Figure 11: Thermal pad on heat sink

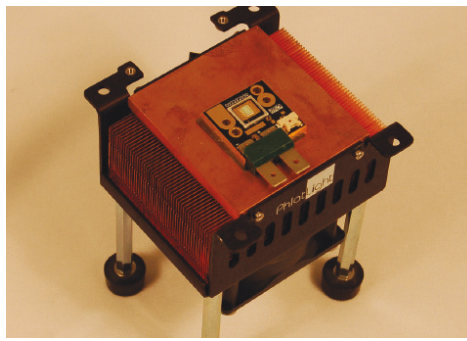


Figure 12: Device aligned on heat sink

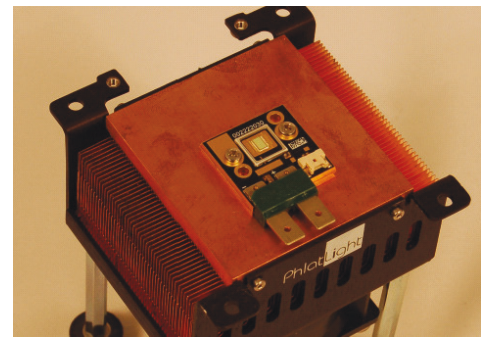


Figure 13: Device mounted on heat sink and is now ready for electrical connections

4.2 Additional Lab Equipment Needed By User

Additional lab equipment such as a 12 V laboratory power supply, an oscilloscope, a waveform generator, a multimeter and a photodetector are required to power and use the DK-136M. Table 1 lists a recommended model for the equipment. The Lambda power supply recommended in Table 1 assumes operation of one device at a time.

Lab Equipment	Luminus Recommendation
12 V Lab Power Supply	Lambda ZUP20-20
Oscilloscope	Tektronix TDS 3024B
Waveform Generator	Agilent 33220A
Multimeter	Fluke 187
Photodetector	Thorlabs PDA10A

Table 1: Additional lab equipment

4.3 Driver Board Operation

Arrange the evaluation kit, required lab power supplies and measurement equipment (e.g. digital multimeters, oscilloscope) preferably on one table. Refer to Figure 16 for an example of equipment set up for evaluation (no wire connections shown). It is recommended that the table is equipped with ESD (Electrostatic Sensitive Device) safe arrangement. Please refer to Appendix B for ESD precautions.

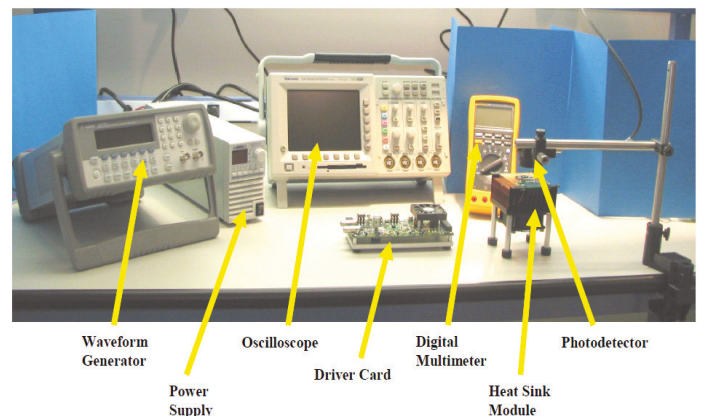


Figure 14: Equipment set up for Big Chip LED evaluation (example).

Mount the devices on heat sinks as discussed in section 4.1.

1. Make sure power supply is OFF and the power switch (ON/ OFF switch in Figure 8) on the driver board is OFF.
2. Connect driver board to heat sink module on which device is mounted.
3. Connect power supply to driver board using the cable supplied with the kit.
4. Turn the Current Control Knob on the driver board all the way counter clockwise.
5. Set middle switch (Current Control/Manual Control switch in Figure 8) to "Manual".
6. Set right switch (CW/Pulsed switch in Figure 8) to "CW" for continuous operation.
7. Turn on power supply and set to the output voltage to 12 V, as specified for the driver board.
8. Turn power switch on driver board to "ON". The device may turn on at this point.
9. Check to make sure that the two fans, one on driver board and one on heat sink module, are running.
10. Using a digital voltmeter (DVM) check that the supply voltage on the driver board is correct using test point "TP4", labeled "VIN", at the lower right corner of board. If this voltage is zero check to see if the fuse is blown.
11. Connect DVM to "GND" and "LED CURRENT" test points to monitor current through the device. The output is 10 mV/ A. Monitoring this output to ensures that the LED is always driven within its limits.
12. Turn the knob on the driver board clockwise while monitoring the current. This will drive more current in the device.
13. To operate in pulse mode, connect a pulse generator to "Pulse Input" BNC. Pulse Generator should have an output signal set to TTL levels or 0-5 V. Using an oscilloscope, monitor the pulse generator output at the "PULSE INPUT" test point.
14. Turn the current control knob all the way counter clockwise and set the right switch to "PULSE". The driver board is now operating the device in pulse mode. The "Current Control" knob sets the amplitude of the current and the pulse generator sets the width of the pulse. Proper operation is best monitored by using a photodetector to monitor device's light output. Current amplitude can still be monitored using the "LED CURRENT" test point.

NOTE: The output voltage of the power supply should not exceed 12 V, doing so may damage the driver board. During pulsed operation, the output voltage of the power supply can overshoot the 12 V limit. To prevent voltage over shoot and consequent damage to the driver, connecting a capacitor across the output of the power supply (and thus, across the input to the driver) is recommended. Two capacitors, such as Nichicon UHE1V392MHD 3900 μ F or equivalent may be used.

15. Device current amplitude can also be controlled using an external signal. Connect a signal source (0-5 V max) to the "CURRENT CONTROL INPUT" BNC. Monitor using the "CURRENT CONTROL" test point. Switch the middle switch to "CURRENT CONTROL" and the driver now uses the input signal instead of the current control knob to set the LED current amplitude. This input can be used both in CW and Pulse mode. Note that the max output current corresponds to 5V input and is the maximum level specified for the specific driver board regardless of whether operation is CW or Pulse.

Figures 15, 16 and 17 show oscilloscope traces for a GREEN Big Chip LED™ PT-120 device operated at 30A, 50% duty cycle and 2.88kHz frequency. The pink trace is the input pulse and the green trace is the photo detector output. These traces are shown for reference; actual waveforms may depend on individual driver boards, devices and settings. Figure 17 shows the input and output pulse. Figure 16 and Figure 17 show the rise time (1 μ s) and fall time (1 to 2 μ s) of the output pulse

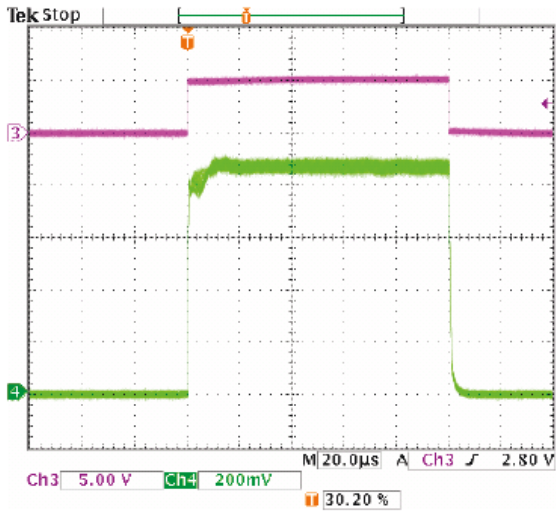


Figure 15: Input and output pulse (example).

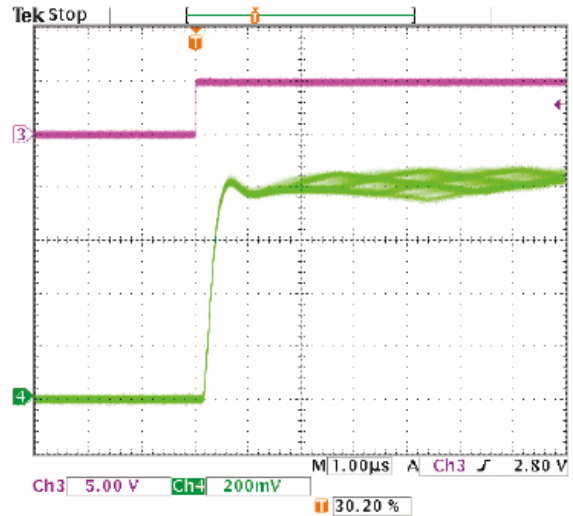


Figure 15: Rise time (example).

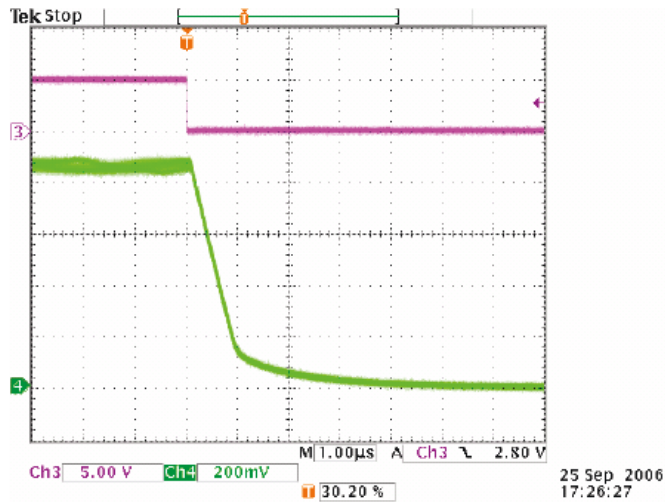


Figure 17: Fall time (example).

A.3 Permanent Magnets Setup

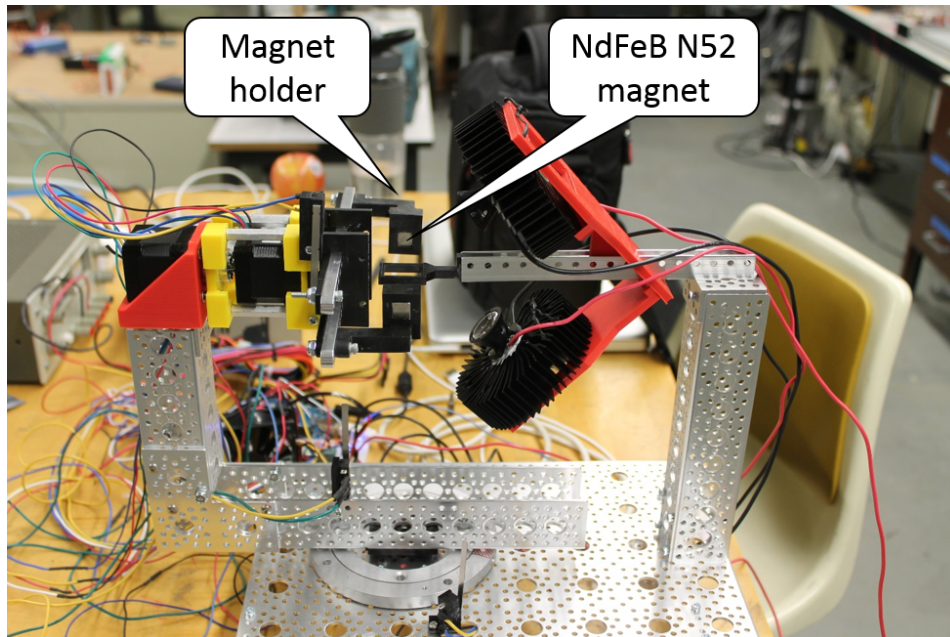


Figure A.1: Permanent magnets setup side view

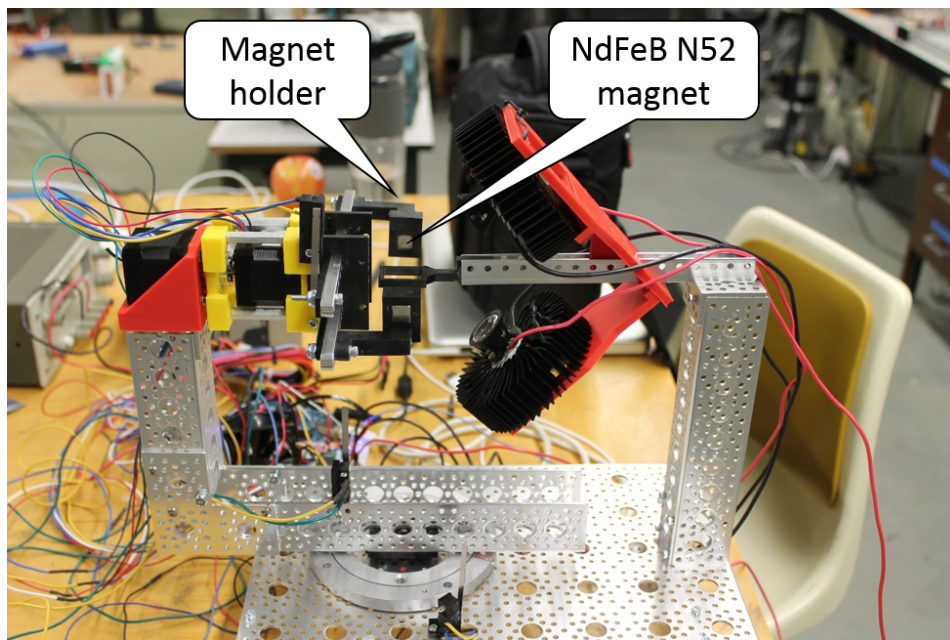


Figure A.2: Permanent magnets setup top view

A.4 Final Assembly Images

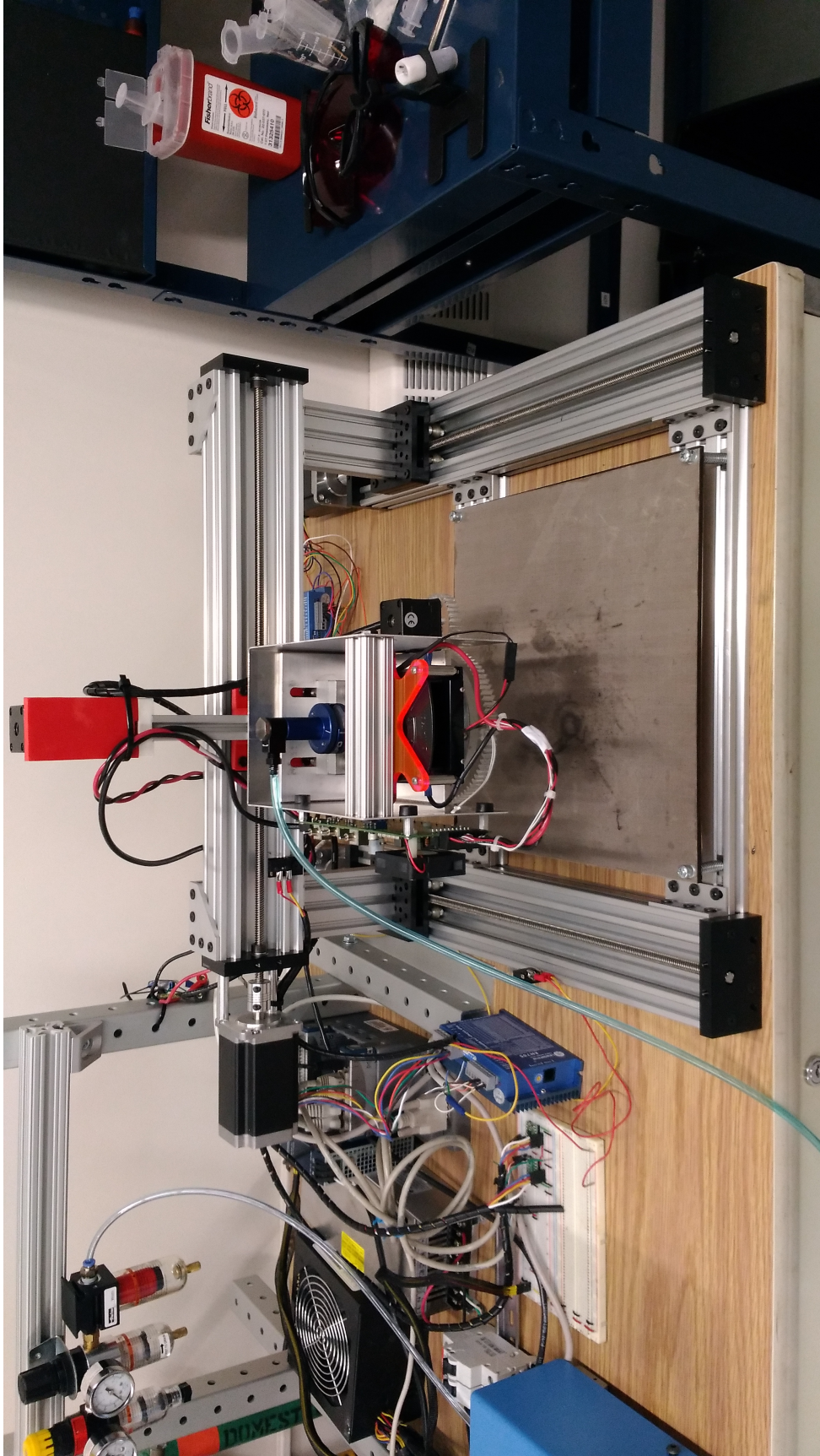


Figure A.3: Assembly view 1

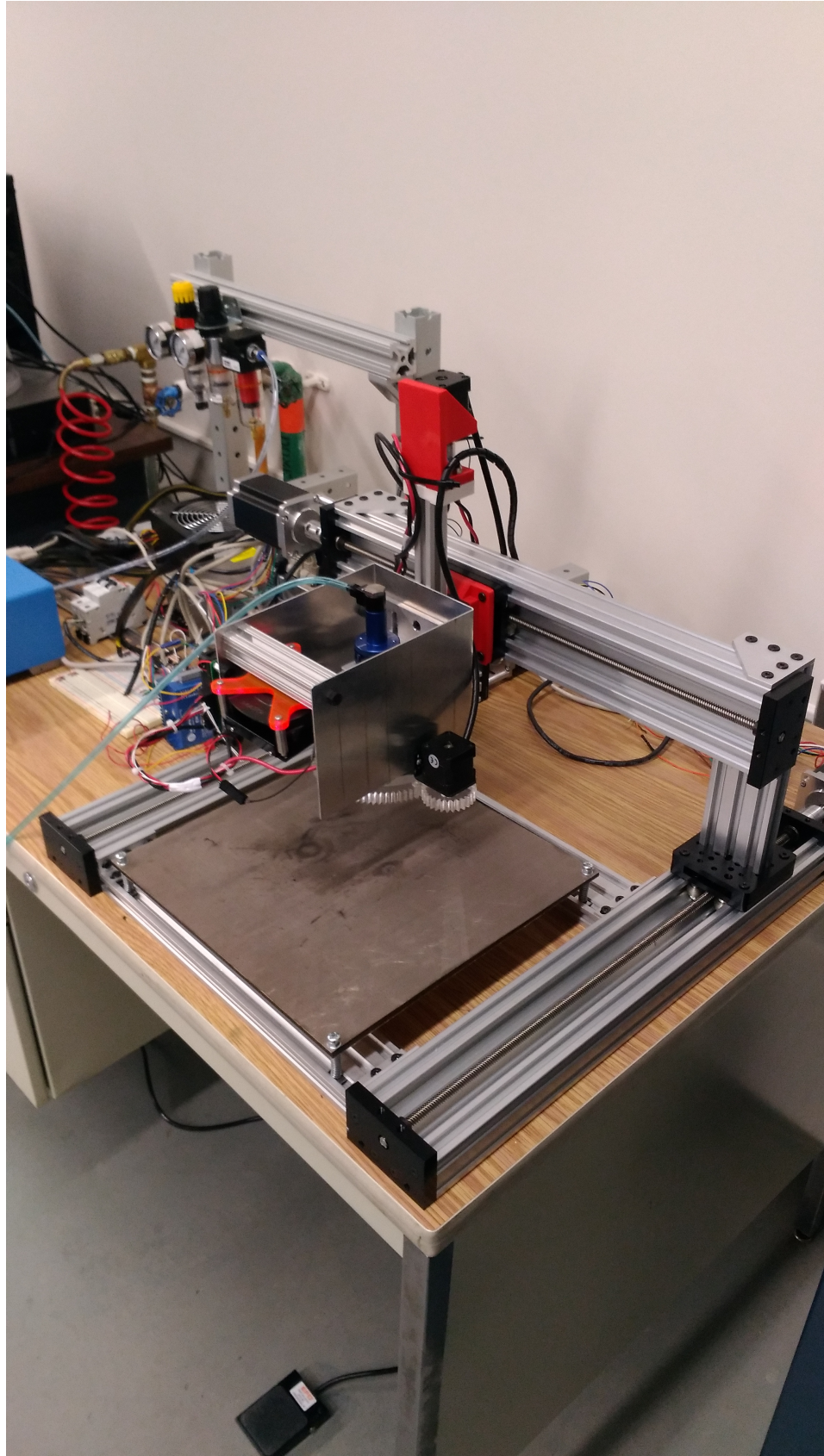


Figure A.4: Assembly view 2
106

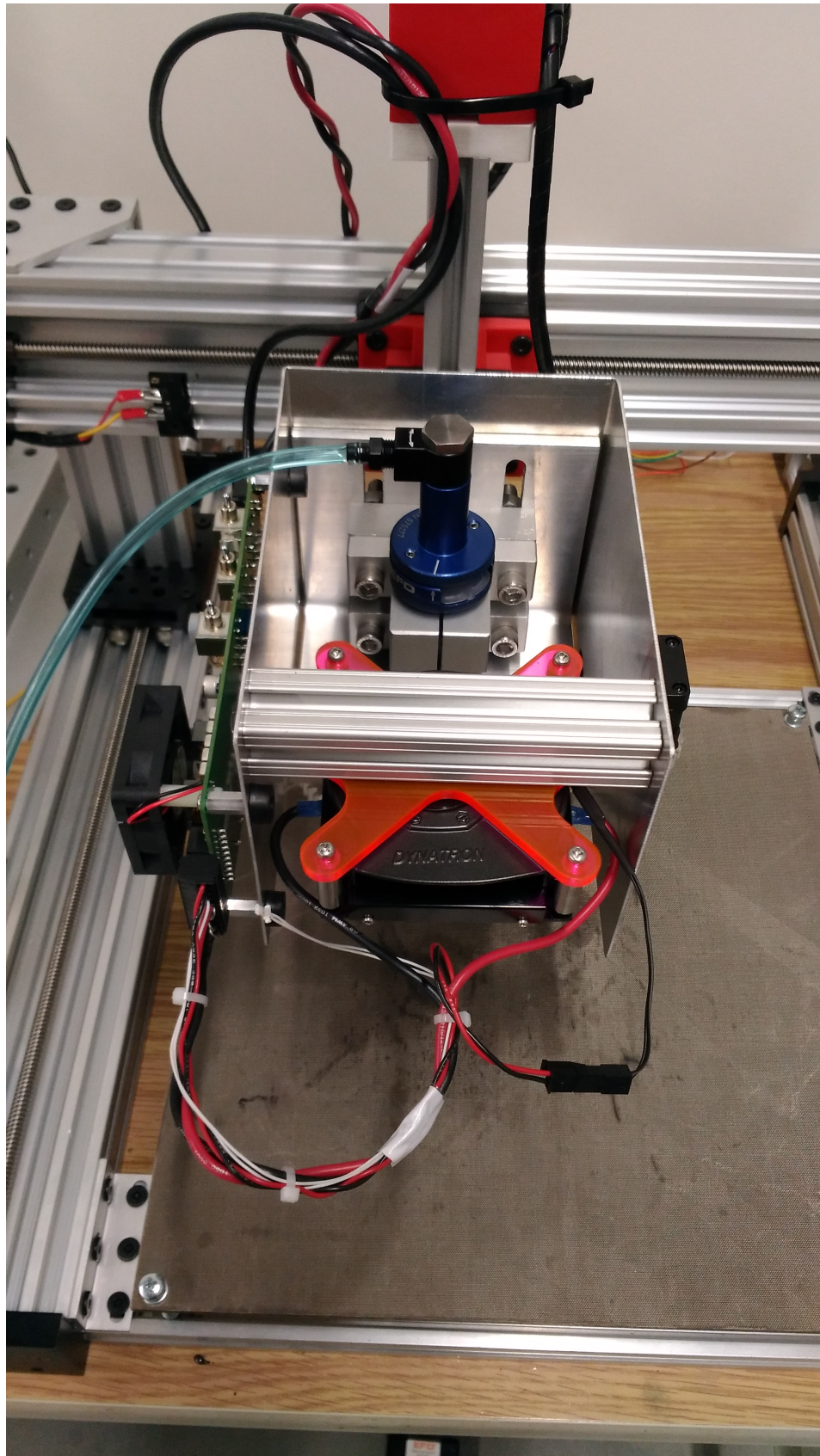


Figure A.5: Assembly view 3
107

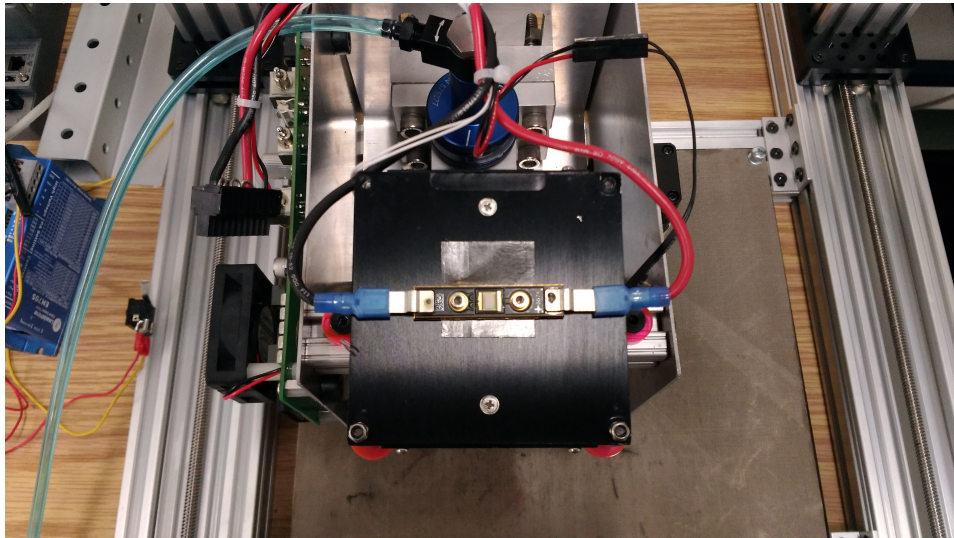


Figure A.6: Assembly view 4

A.5 SISU-1004 FPGA VI code

SISU-1004 FPGA Example for NI SoftMotion

Connects the SISU-1004 4-Axis Stepper Interface Module to the NI SoftMotion RT engine through User-Defined Variables (UDVs).

UDVs must have the same prefix as the SoftMotion axis when bound as a User Define Variable Axis (i.e. NI SoftMotion "Axis 1" must have User Defined Variables that begin with "Axis 1" like "Axis 1.Control Register")

Fault Monitoring Loop

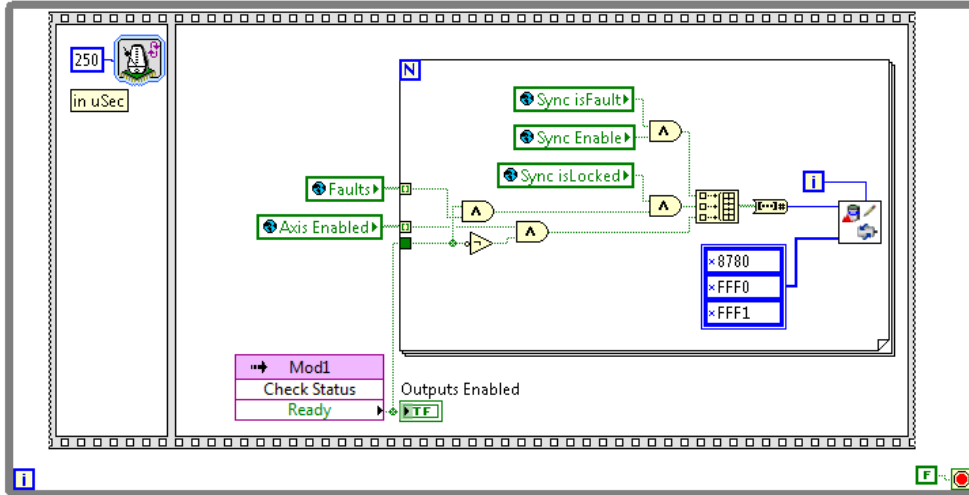


Figure A.7: FPGA VI - section 1.

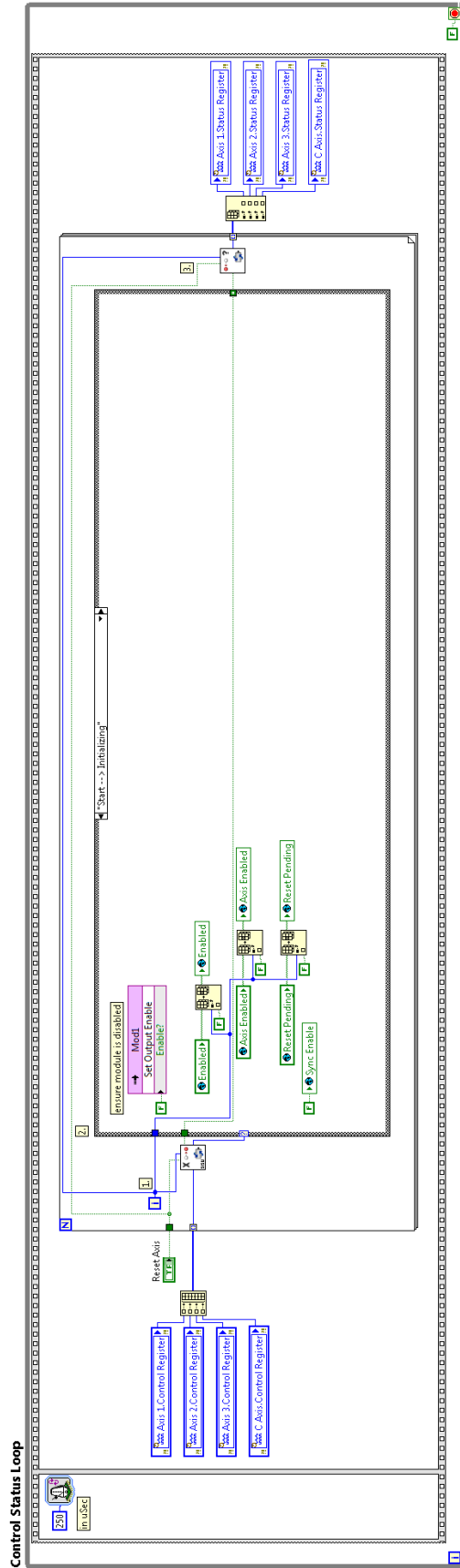


Figure A.8: FPGA VI - section 2.

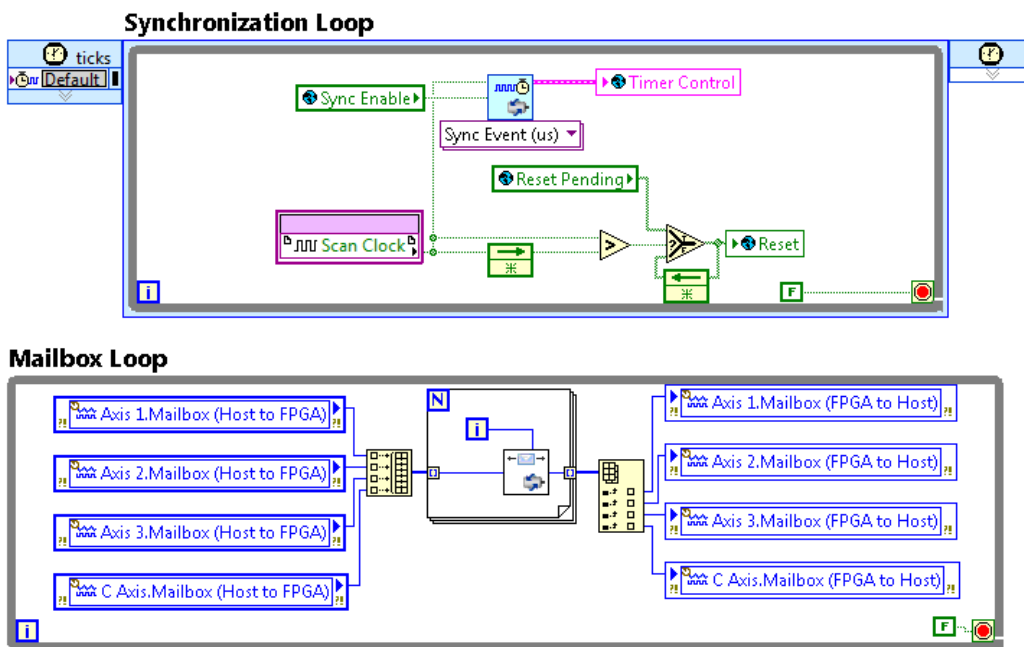


Figure A.9: FPGA VI - section 3.

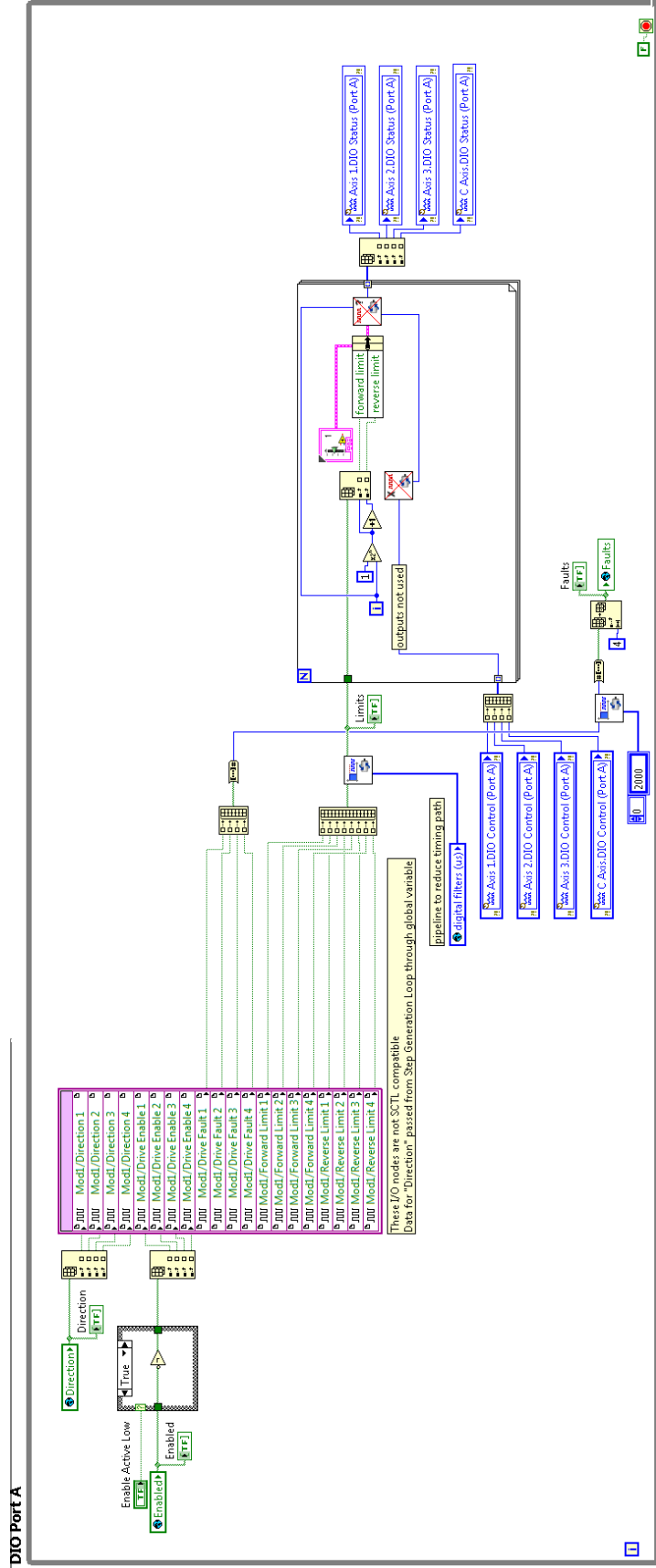


Figure A.10: FPGA VI - section 4.

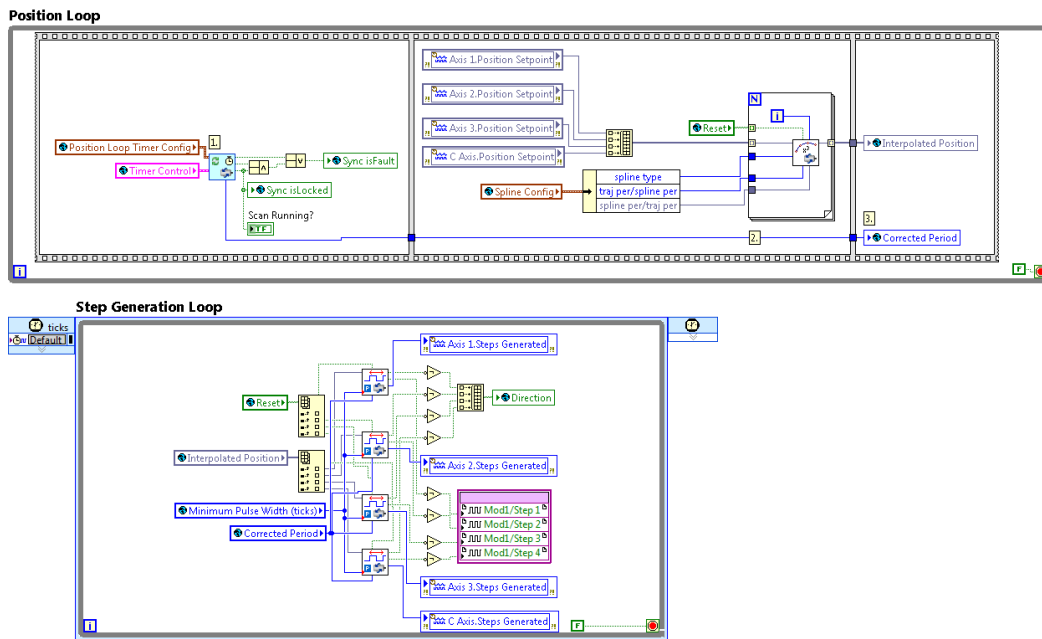


Figure A.11: FPGA VI - section 5.

A.6 Deposition Test

Particles wt%	Initial Z-offset	Pressure (psi)	Feed rate (mm/sec)	Positive Results (Steady defined resin line)
5%	0.7 mm	P15	F9	no
	0.3 mm	P15	F6	no
	0.5 mm	P14	F6	no
	0.7 mm	P14	F6	no (resin inside the stream is not cure and accumulation presented)
	0.5 mm	P13	F5	no (inconsistent line)
	0.5 mm	P13	F9	no (inconsistent line)
	0.5 mm	P13	F9	no (initial flow)
	0.5 mm	P13	F9	no (resin not flowing due to magnetic field)
20%	1.0 mm	P25	F9	no (initial flow)
	1.0 mm	P30	F9	positive results (filament width visually too thin)
	1.0 mm	P30	F5	positive results (filament width 1.4 mm with overflow around it)

A.7 Particles orientation test G-Code

G28 %Homing G1 X0.000 Y6.700 E1 A0 F10.0 %Curing G1 X127.200
Y6.700 F20.0 %Move to First Position G4 P60.0 %Alignment G1 X127.200
Y6.700 E1 A0 F10.0 %Curing G4 P120.0

G1 X75.000 Y150.000 F20.0 %Move Away G4 P10.0 G1 X75.000 Y150.000
E1 A45 F10.0 %New Angle

G1 X135.2 Y6.700 F20.0 %Move to Second Position G4 P60.0 %Alignment
G1 X135.2 Y6.700 E1 A45 F10.0 %Curing G4 P120.0

G1 X75.000 Y150.000 F20.0 %Move Away G4 P10.0 G1 X75.000 Y150.000
E1 A90 F10.0 %New Angle

G1 X143.2 Y6.700 F20.0 %Move to Third Position G4 P60.0 %Alignment
G1 X143.2 Y6.700 E1 A90 F10.0 %Curing G4 P120.0

G1 X75.000 Y150.000 F20.0 %Move Away G4 P10.0 G1 X75.000 Y150.000
E1 A135 F10.0 %New Angle

G1 X143.2 Y13.400 F20.0 %Move to Fourth Position G4 P60.0 %Alignment
G1 X143.2 Y13.400 E1 A135 F10.0 %Curing G4 P120.0

G1 X75.000 Y150.000 F20.0 %Move Away G4 P10.0 G1 X75.000 Y150.000
E1 A180 F10.0 %New Angle

G1 X135.2 Y13.400 F20.0 %Move to Fifth Position G4 P60.0 %Alignment
G1 X135.2 Y13.400 E1 A180 F10.0 %Curing G4 P120.0

G1 X75.000 Y150.000 F20.0 %Move Away G4 P10.0 G1 X75.000 Y150.000
E1 A225 F10.0 %New Angle

G1 X127.200 Y13.400 F20.0 %Move to Sixth Position G4 P60.0 %Align-
ment G1 X127.200 Y13.400 E1 A225 F10.0 %Curing G4 P120.0

G1 X75.000 Y150.000 F20.0 %Move Away G4 P10.0 G1 X75.000 Y150.000
E1 A270 F10.0 %New Angle

G1 X127.200 Y20.100 F20.0 %Move to Seventh Position G4 P60.0 %Align-
ment G1 X127.200 Y20.100 E1 A270 F10.0 %Curing G4 P120.0

G1 X75.000 Y150.000 F20.0 %Move Away G4 P10.0 G1 X75.000 Y150.000
E1 A315 F10.0 %New Angle

G1 X135.2 Y20.100 F20.0 %Move to Eighth Position G4 P60.0 %Alignment
G1 X135.2 Y20.100 E1 A315 F10.0 %Curing G4 P120.0

G1 X75.000 Y150.000 F20.0 %Move Away G4 P10.0 G1 X75.000 Y150.000

E1 A360 F10.0 %New Angle

G1 X143.2 Y20.100 F20.0 %Move to Ninth Position G4 P60.0 %Alignment

G1 X143.2 Y20.100 E1 A360 F10.0 %Curing G4 P120.0

G1 X75.000 Y150.000 F20.0 %Move Away G4 P10.0

A.8 Alignment characterization images

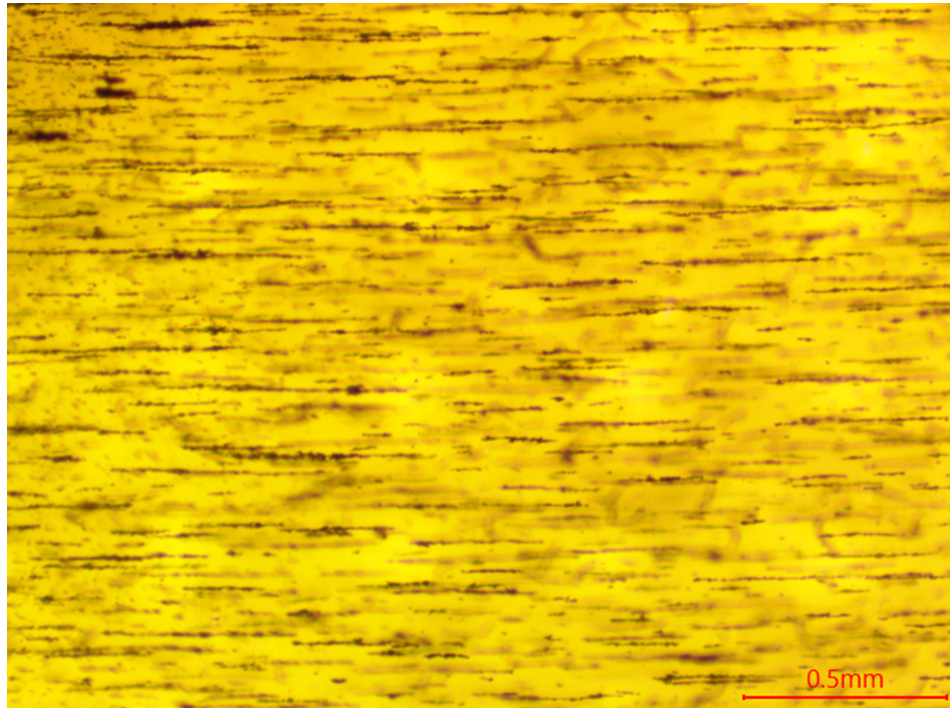


Figure A.12: Zero degree alignment.

A.9 Permission letters



2018-03-15

Univeristy of Alberta
116 St & 85 Ave,
Edmonton, AB
T6G 2R3

Subject: Content Reproduction from ISO 17296-2:2015, Additive manufacturing -- General principles -- Part 2: Overview of process categories and feedstock and ISO/ASTM 529000:2015, Additive manufacturing -- General principles -- Terminology (the "Publication(s)").

Dear Alejandro Eufrazio Aguilera,

In response to your recent request and based on the information that you have provided to us, the Standards Council of Canada is pleased to grant Robert Sauvé Research Institute in Occupational Heart and Safety (the "Requestor") permission to reproduce the following:

- The specific content from the Publication(s) listed below;
- Reproduction of the content in: Development of a Material Jetting 3D Printer with Magnetic Orientation Capabilities.
- Date of the reproduction: April 2018

Please note that the following conditions apply, as per ISO's Policy for the Distribution, Sales and Reproduction of ISO Publications and the Protection of ISO's Copyright (ISO POCOSA) Agreement and/or IEC Sales Policy:

1. The content represents less than 10% of the total content of the Publication(s) referenced; and
2. These permissions are based on the condition that recognition will be given by the Requestor in all reproductions of the Content, by the inclusion of the attached notation: April 2018

"Copied by Alejandro Eufrazio Aguilera at the University of Alberta with the permission of the Standards Council of Canada (SCC) on behalf of ISO."

Content:

ISO 17296-2:2015

- Figure 1 — Schematic diagram of two alternative principles for vat photopolymerization
- Figure 2 — Schematic diagram of material jetting
- Figure 3 — Schematic diagram of binder jetting

ISO/ASTM 52900:2015

- Figure A.1 – Single-step and multi-step AM process principles
- Figure A1.3 – Overview of single-step AM processing principles for polymer materials



Please confirm via signature below, your understanding and acceptance of the conditions and permissions outlined above.

Sincerely,

Patrick Bonnilla
Manager, Canadian Standards Development

2018-03-16

Date

Requestor: I have read, understood, and will comply with the Conditions:

Alejandro Eufrazio Aguilera
MSc Student
University of Alberta

16-03-2018

Date

15-Feb-2018

This license agreement between the American Physical Society ("APS") and Alejandro Eufrazio ("You") consists of your license details and the terms and conditions provided by the American Physical Society and SciPris.

Licensed Content Information

License Number: RNP/18/FEB/001556
License date: 15-Feb-2018
DOI: 10.1103/PhysRevE.61.2818
Title: Anisotropic magnetism in field-structured composites
Author: James E. Martin et al.
Publication: Physical Review E
Publisher: American Physical Society
Cost: USD \$ 0.00

Request Details

Does your reuse require significant modifications: No
Specify intended distribution locations: United States,Canada
Reuse Category: Reuse in a thesis/dissertation
Requestor Type: Author of requested content
Items for Reuse: Figures/Tables
Number of Figure/Tables: 1
Figure/Tables Details: FIG. 1. Field-structured composites of particles structured by a uniaxial magnetic field.
Format for Reuse: Electronic

Information about New Publication:

University/Publisher: University of Alberta
Title of dissertation/thesis: Development of a Material Jetting 3D Printer with Magnetic Orientation Capabilities.
Author(s): Alejandro Federico Eufrazio Aguilera
Expected completion date: Mar. 2018

License Requestor Information

Name: Alejandro Eufrazio
Affiliation: Individual
Email Id: eufrazio@ualberta.ca
Country: Canada

TERMS AND CONDITIONS

The American Physical Society (APS) is pleased to grant the Requestor of this license a non-exclusive, non-transferable permission, limited to Electronic format, provided all criteria outlined below are followed.

1. You must also obtain permission from at least one of the lead authors for each separate work, if you haven't done so already. The author's name and affiliation can be found on the first page of the published Article.
2. For electronic format permissions, Requestor agrees to provide a hyperlink from the reprinted APS material using the source material's DOI on the web page where the work appears. The hyperlink should use the standard DOI resolution URL, <http://dx.doi.org/{DOI}>. The hyperlink may be embedded in the copyright credit line.
3. For print format permissions, Requestor agrees to print the required copyright credit line on the first page where the material appears: "Reprinted (abstract/excerpt/figure) with permission from [(FULL REFERENCE CITATION) as follows: Author's Names, APS Journal Title, Volume Number, Page Number and Year of Publication.] Copyright (YEAR) by the American Physical Society."
4. Permission granted in this license is for a one-time use and does not include permission for any future editions, updates, databases, formats or other matters. Permission must be sought for any additional use.
5. Use of the material does not and must not imply any endorsement by APS.
6. APS does not imply, purport or intend to grant permission to reuse materials to which it does not hold copyright. It is the requestor's sole responsibility to ensure the licensed material is original to APS and does not contain the copyright of another entity, and that the copyright notice of the figure, photograph, cover or table does not indicate it was reprinted by APS with permission from another source.
7. The permission granted herein is personal to the Requestor for the use specified and is not transferable or assignable without express written permission of APS. This license may not be amended except in writing by APS.
8. You may not alter, edit or modify the material in any manner.
9. You may translate the materials only when translation rights have been granted.
10. APS is not responsible for any errors or omissions due to translation.
11. You may not use the material for promotional, sales, advertising or marketing purposes.
12. The foregoing license shall not take effect unless and until APS or its agent, Aptara, receives payment in full in accordance with Aptara Billing and Payment Terms and Conditions, which are incorporated herein by reference.
13. Should the terms of this license be violated at any time, APS or Aptara may revoke the license with no refund to you and seek relief to the fullest extent of the laws of the USA. Official written notice will be made using the contact information provided with the permission request. Failure to receive such notice will not nullify revocation of the permission.
14. APS reserves all rights not specifically granted herein.
15. This document, including the Aptara Billing and Payment Terms and Conditions, shall be the entire agreement between the parties relating to the subject matter hereof.

**ELSEVIER LICENSE
TERMS AND CONDITIONS**

Feb 15, 2018

This Agreement between University of Alberta -- Alejandro Eufrazio ("You") and Elsevier ("Elsevier") consists of your license details and the terms and conditions provided by Elsevier and Copyright Clearance Center.

License Number	4290010526701
License date	Feb 15, 2018
Licensed Content Publisher	Elsevier
Licensed Content Publication	Journal of Iron and Steel Research, International
Licensed Content Title	Study on Fabrication Process of Anisotropic Injection Bonded Nd-Fe-B Magnets
Licensed Content Author	Xiao-lei ZHANG,Ming-yuan ZHU,Ying LI,Qiu-ping YANG,Hong-ming JIN,Juan JIANG,Ye TIAN,Yang LUO
Licensed Content Date	Jan 1, 2006
Licensed Content Volume	13
Licensed Content Issue	n/a
Licensed Content Pages	3
Start Page	286
End Page	288
Type of Use	reuse in a thesis/dissertation
Portion	figures/tables/illustrations
Number of figures/tables/illustrations	1
Format	electronic
Are you the author of this Elsevier article?	No
Will you be translating?	No
Original figure numbers	Fig. 1 Process of bonded Nd-Fe-B magnets by injection
Title of your thesis/dissertation	Development of a Material Jetting 3D Printer with Magnetic Orientation Capabilities
Expected completion date	Mar 2018
Estimated size (number of pages)	100
Requestor Location	University of Alberta 87nd Av edmonton, AB t6g0x6 Canada Attn: Alejandro Eufrazio
Publisher Tax ID	GB 494 6272 12
Total	0.00 CAD 126

Terms and Conditions

INTRODUCTION

1. The publisher for this copyrighted material is Elsevier. By clicking "accept" in connection with completing this licensing transaction, you agree that the following terms and conditions apply to this transaction (along with the Billing and Payment terms and conditions established by Copyright Clearance Center, Inc. ("CCC"), at the time that you opened your Rightslink account and that are available at any time at <http://myaccount.copyright.com>).

GENERAL TERMS

2. Elsevier hereby grants you permission to reproduce the aforementioned material subject to the terms and conditions indicated.

3. Acknowledgement: If any part of the material to be used (for example, figures) has appeared in our publication with credit or acknowledgement to another source, permission must also be sought from that source. If such permission is not obtained then that material may not be included in your publication/copies. Suitable acknowledgement to the source must be made, either as a footnote or in a reference list at the end of your publication, as follows:

"Reprinted from Publication title, Vol /edition number, Author(s), Title of article / title of chapter, Pages No., Copyright (Year), with permission from Elsevier [OR APPLICABLE SOCIETY COPYRIGHT OWNER]." Also Lancet special credit - "Reprinted from The Lancet, Vol. number, Author(s), Title of article, Pages No., Copyright (Year), with permission from Elsevier."

4. Reproduction of this material is confined to the purpose and/or media for which permission is hereby given.

5. Altering/Modifying Material: Not Permitted. However figures and illustrations may be altered/adapted minimally to serve your work. Any other abbreviations, additions, deletions and/or any other alterations shall be made only with prior written authorization of Elsevier Ltd. (Please contact Elsevier at permissions@elsevier.com). No modifications can be made to any Lancet figures/tables and they must be reproduced in full.

6. If the permission fee for the requested use of our material is waived in this instance, please be advised that your future requests for Elsevier materials may attract a fee.

7. Reservation of Rights: Publisher reserves all rights not specifically granted in the combination of (i) the license details provided by you and accepted in the course of this licensing transaction, (ii) these terms and conditions and (iii) CCC's Billing and Payment terms and conditions.

8. License Contingent Upon Payment: While you may exercise the rights licensed immediately upon issuance of the license at the end of the licensing process for the transaction, provided that you have disclosed complete and accurate details of your proposed use, no license is finally effective unless and until full payment is received from you (either by publisher or by CCC) as provided in CCC's Billing and Payment terms and conditions. If full payment is not received on a timely basis, then any license preliminarily granted shall be deemed automatically revoked and shall be void as if never granted. Further, in the event that you breach any of these terms and conditions or any of CCC's Billing and Payment terms and conditions, the license is automatically revoked and shall be void as if never granted. Use of materials as described in a revoked license, as well as any use of the materials beyond the scope of an unrevoked license, may constitute copyright infringement and publisher reserves the right to take any and all action to protect its copyright in the materials.

9. Warranties: Publisher makes no representations or warranties with respect to the licensed material.

10. Indemnity: You hereby indemnify and agree to hold harmless publisher and CCC, and their respective officers, directors, employees and agents, from and against any and all claims arising out of your use of the licensed material other than as specifically authorized pursuant to this license.

11. No Transfer of License: This license is personal to you and may not be sublicensed, assigned, or transferred by you to any other person without publisher's written permission.

12. **No Amendment Except in Writing:** This license may not be amended except in a writing signed by both parties (or, in the case of publisher, by CCC on publisher's behalf).

13. **Objection to Contrary Terms:** Publisher hereby objects to any terms contained in any purchase order, acknowledgment, check endorsement or other writing prepared by you, which terms are inconsistent with these terms and conditions or CCC's Billing and Payment terms and conditions. These terms and conditions, together with CCC's Billing and Payment terms and conditions (which are incorporated herein), comprise the entire agreement between you and publisher (and CCC) concerning this licensing transaction. In the event of any conflict between your obligations established by these terms and conditions and those established by CCC's Billing and Payment terms and conditions, these terms and conditions shall control.

14. **Revocation:** Elsevier or Copyright Clearance Center may deny the permissions described in this License at their sole discretion, for any reason or no reason, with a full refund payable to you. Notice of such denial will be made using the contact information provided by you. Failure to receive such notice will not alter or invalidate the denial. In no event will Elsevier or Copyright Clearance Center be responsible or liable for any costs, expenses or damage incurred by you as a result of a denial of your permission request, other than a refund of the amount(s) paid by you to Elsevier and/or Copyright Clearance Center for denied permissions.

LIMITED LICENSE

The following terms and conditions apply only to specific license types:

15. **Translation:** This permission is granted for non-exclusive world **English** rights only unless your license was granted for translation rights. If you licensed translation rights you may only translate this content into the languages you requested. A professional translator must perform all translations and reproduce the content word for word preserving the integrity of the article.

16. **Posting licensed content on any Website:** The following terms and conditions apply as follows: Licensing material from an Elsevier journal: All content posted to the web site must maintain the copyright information line on the bottom of each image; A hyper-text must be included to the Homepage of the journal from which you are licensing at <http://www.sciencedirect.com/science/journal/xxxxx> or the Elsevier homepage for books at <http://www.elsevier.com>; Central Storage: This license does not include permission for a scanned version of the material to be stored in a central repository such as that provided by Heron/XanEdu.

Licensing material from an Elsevier book: A hyper-text link must be included to the Elsevier homepage at <http://www.elsevier.com>. All content posted to the web site must maintain the copyright information line on the bottom of each image.

Posting licensed content on Electronic reserve: In addition to the above the following clauses are applicable: The web site must be password-protected and made available only to bona fide students registered on a relevant course. This permission is granted for 1 year only. You may obtain a new license for future website posting.

17. **For journal authors:** the following clauses are applicable in addition to the above:

Preprints:

A preprint is an author's own write-up of research results and analysis, it has not been peer-reviewed, nor has it had any other value added to it by a publisher (such as formatting, copyright, technical enhancement etc.).

Authors can share their preprints anywhere at any time. Preprints should not be added to or enhanced in any way in order to appear more like, or to substitute for, the final versions of articles however authors can update their preprints on arXiv or RePEc with their Accepted Author Manuscript (see below).

If accepted for publication, we encourage authors to link from the preprint to their formal publication via its DOI. Millions of researchers have access to the formal publications on ScienceDirect, and so links will help users to find, access, cite and use the best available

version. Please note that Cell Press, The Lancet and some society-owned have different preprint policies. Information on these policies is available on the journal homepage.

Accepted Author Manuscripts: An accepted author manuscript is the manuscript of an article that has been accepted for publication and which typically includes author-incorporated changes suggested during submission, peer review and editor-author communications.

Authors can share their accepted author manuscript:

- immediately
 - via their non-commercial person homepage or blog
 - by updating a preprint in arXiv or RePEc with the accepted manuscript
 - via their research institute or institutional repository for internal institutional uses or as part of an invitation-only research collaboration work-group
 - directly by providing copies to their students or to research collaborators for their personal use
 - for private scholarly sharing as part of an invitation-only work group on commercial sites with which Elsevier has an agreement
- After the embargo period
 - via non-commercial hosting platforms such as their institutional repository
 - via commercial sites with which Elsevier has an agreement

In all cases accepted manuscripts should:

- link to the formal publication via its DOI
- bear a CC-BY-NC-ND license - this is easy to do
- if aggregated with other manuscripts, for example in a repository or other site, be shared in alignment with our hosting policy not be added to or enhanced in any way to appear more like, or to substitute for, the published journal article.

Published journal article (JPA): A published journal article (PJA) is the definitive final record of published research that appears or will appear in the journal and embodies all value-adding publishing activities including peer review co-ordination, copy-editing, formatting, (if relevant) pagination and online enrichment.

Policies for sharing publishing journal articles differ for subscription and gold open access articles:

Subscription Articles: If you are an author, please share a link to your article rather than the full-text. Millions of researchers have access to the formal publications on ScienceDirect, and so links will help your users to find, access, cite, and use the best available version.

Theses and dissertations which contain embedded PJAs as part of the formal submission can be posted publicly by the awarding institution with DOI links back to the formal publications on ScienceDirect.

If you are affiliated with a library that subscribes to ScienceDirect you have additional private sharing rights for others' research accessed under that agreement. This includes use for classroom teaching and internal training at the institution (including use in course packs and courseware programs), and inclusion of the article for grant funding purposes.

Gold Open Access Articles: May be shared according to the author-selected end-user license and should contain a [CrossMark logo](#), the end user license, and a DOI link to the formal publication on ScienceDirect.

Please refer to Elsevier's [posting policy](#) for further information.

18. **For book authors** the following clauses are applicable in addition to the above:

Authors are permitted to place a brief summary of their work online only. You are not allowed to download and post the published electronic version of your chapter, nor may you scan the printed edition to create an electronic version. **Posting to a repository:** Authors are permitted to post a summary of their chapter only in their institution's repository.

19. Thesis/Dissertation: If your license is for use in a thesis/dissertation your thesis may be submitted to your institution in either print or electronic form. Should your thesis be published commercially, please reapply for permission. These requirements include permission for the Library and Archives of Canada to supply single copies, on demand, of the complete thesis and include permission for Proquest/UMI to supply single copies, on demand, of the complete thesis. Should your thesis be published commercially, please reapply for permission. Theses and dissertations which contain embedded PJAs as part of the formal submission can be posted publicly by the awarding institution with DOI links back to the formal publications on ScienceDirect.

Elsevier Open Access Terms and Conditions

You can publish open access with Elsevier in hundreds of open access journals or in nearly 2000 established subscription journals that support open access publishing. Permitted third party re-use of these open access articles is defined by the author's choice of Creative Commons user license. See our [open access license policy](#) for more information.

Terms & Conditions applicable to all Open Access articles published with Elsevier:

Any reuse of the article must not represent the author as endorsing the adaptation of the article nor should the article be modified in such a way as to damage the author's honour or reputation. If any changes have been made, such changes must be clearly indicated.

The author(s) must be appropriately credited and we ask that you include the end user license and a DOI link to the formal publication on ScienceDirect.

If any part of the material to be used (for example, figures) has appeared in our publication with credit or acknowledgement to another source it is the responsibility of the user to ensure their reuse complies with the terms and conditions determined by the rights holder.

Additional Terms & Conditions applicable to each Creative Commons user license:

CC BY: The CC-BY license allows users to copy, to create extracts, abstracts and new works from the Article, to alter and revise the Article and to make commercial use of the Article (including reuse and/or resale of the Article by commercial entities), provided the user gives appropriate credit (with a link to the formal publication through the relevant DOI), provides a link to the license, indicates if changes were made and the licensor is not represented as endorsing the use made of the work. The full details of the license are available at <http://creativecommons.org/licenses/by/4.0>.

CC BY NC SA: The CC BY-NC-SA license allows users to copy, to create extracts, abstracts and new works from the Article, to alter and revise the Article, provided this is not done for commercial purposes, and that the user gives appropriate credit (with a link to the formal publication through the relevant DOI), provides a link to the license, indicates if changes were made and the licensor is not represented as endorsing the use made of the work. Further, any new works must be made available on the same conditions. The full details of the license are available at <http://creativecommons.org/licenses/by-nc-sa/4.0>.

CC BY NC ND: The CC BY-NC-ND license allows users to copy and distribute the Article, provided this is not done for commercial purposes and further does not permit distribution of the Article if it is changed or edited in any way, and provided the user gives appropriate credit (with a link to the formal publication through the relevant DOI), provides a link to the license, and that the licensor is not represented as endorsing the use made of the work. The full details of the license are available at <http://creativecommons.org/licenses/by-nc-nd/4.0>. Any commercial reuse of Open Access articles published with a CC BY NC SA or CC BY NC ND license requires permission from Elsevier and will be subject to a fee.

Commercial reuse includes:

- Associating advertising with the full text of the Article
- Charging fees for document delivery or access
- Article aggregation
- Systematic distribution via e-mail lists or share buttons

Posting or linking by commercial companies for use by customers of those companies.

20. Other Conditions:

v1.9

Questions? customercare@copyright.com or +1-855-239-3415 (toll free in the US) or +1-978-646-2777.

SPRINGER NATURE LICENSE TERMS AND CONDITIONS

Feb 16, 2018

This Agreement between University of Alberta -- Alejandro Eufrazio ("You") and Springer Nature ("Springer Nature") consists of your license details and the terms and conditions provided by Springer Nature and Copyright Clearance Center.

License Number	4290910101348
License date	Feb 16, 2018
Licensed Content Publisher	Springer Nature
Licensed Content Publication	JOM Journal of the Minerals, Metals and Materials Society
Licensed Content Title	Binder Jetting: A Novel NdFeB Bonded Magnet Fabrication Process
Licensed Content Author	M. Parans Paranthaman, Christopher S. Shafer, Amy M. Elliott et al
Licensed Content Date	Jan 1, 2016
Licensed Content Volume	68
Licensed Content Issue	7
Type of Use	Thesis/Dissertation
Requestor type	academic/university or research institute
Format	electronic
Portion	figures/tables/illustrations
Number of figures/tables/illustrations	3
Will you be translating?	no
Circulation/distribution	<501
Author of this Springer Nature content	no
Title	Development of a Material Jetting 3D Printer with Magnetic Orientation Capabilities
Instructor name	n/a
Institution name	n/a
Expected presentation date	Mar 2018
Portions	Figures 1, 4 & 5
Requestor Location	University of Alberta 9211-116 Street NW edmonton, AB T6G 1H9 Canada Attn: Alejandro Eufrazio
Billing Type	Invoice
Billing Address	University of Alberta 87nd Av

Canada
Attn: Alejandro Eufrazio

Total 0.00 USD

Terms and Conditions

Springer Nature Terms and Conditions for RightsLink Permissions

Springer Customer Service Centre GmbH (the Licensor) hereby grants you a non-exclusive, world-wide licence to reproduce the material and for the purpose and requirements specified in the attached copy of your order form, and for no other use, subject to the conditions below:

1. The Licensor warrants that it has, to the best of its knowledge, the rights to license reuse of this material. However, you should ensure that the material you are requesting is original to the Licensor and does not carry the copyright of another entity (as credited in the published version).

If the credit line on any part of the material you have requested indicates that it was reprinted or adapted with permission from another source, then you should also seek permission from that source to reuse the material.

2. Where **print only** permission has been granted for a fee, separate permission must be obtained for any additional electronic re-use.
3. Permission granted **free of charge** for material in print is also usually granted for any electronic version of that work, provided that the material is incidental to your work as a whole and that the electronic version is essentially equivalent to, or substitutes for, the print version.
4. A licence for 'post on a website' is valid for 12 months from the licence date. This licence does not cover use of full text articles on websites.
5. Where **'reuse in a dissertation/thesis'** has been selected the following terms apply: Print rights for up to 100 copies, electronic rights for use only on a personal website or institutional repository as defined by the Sherpa guideline (www.sherpa.ac.uk/romeo/).
6. Permission granted for books and journals is granted for the lifetime of the first edition and does not apply to second and subsequent editions (except where the first edition permission was granted free of charge or for signatories to the STM Permissions Guidelines <http://www.stm-assoc.org/copyright-legal-affairs/permissions/permissions-guidelines/>), and does not apply for editions in other languages unless additional translation rights have been granted separately in the licence.
7. Rights for additional components such as custom editions and derivatives require additional permission and may be subject to an additional fee. Please apply to Journalpermissions@springernature.com/bookpermissions@springernature.com for these rights.
8. The Licensor's permission must be acknowledged next to the licensed material in print. In electronic form, this acknowledgement must be visible at the same time as the figures/tables/illustrations or abstract, and must be hyperlinked to the journal/book's homepage. Our required acknowledgement format is in the Appendix below.
9. Use of the material for incidental promotional use, minor editing privileges (this does not include cropping, adapting, omitting material or any other changes that affect the meaning, intention or moral rights of the author) and copies for the disabled are permitted under this licence.
10. Minor adaptations of single figures (changes of format, colour and style) do not require the Licensor's approval. However, the adaptation should be credited as shown in Appendix below.

Appendix — Acknowledgements:**For Journal Content:**

Reprinted by permission from [the Licensor]: [Journal Publisher (e.g. Nature/Springer/Palgrave)] [JOURNAL NAME] [REFERENCE CITATION (Article name, Author(s) Name), [COPYRIGHT] (year of publication)

For Advance Online Publication papers:

Reprinted by permission from [the Licensor]: [Journal Publisher (e.g. Nature/Springer/Palgrave)] [JOURNAL NAME] [REFERENCE CITATION (Article name, Author(s) Name), [COPYRIGHT] (year of publication), advance online publication, day month year (doi: 10.1038/sj.[JOURNAL ACRONYM].)

For Adaptations/Translations:

Adapted/Translated by permission from [the Licensor]: [Journal Publisher (e.g. Nature/Springer/Palgrave)] [JOURNAL NAME] [REFERENCE CITATION (Article name, Author(s) Name), [COPYRIGHT] (year of publication)

Note: For any republication from the British Journal of Cancer, the following credit line style applies:

Reprinted/adapted/translated by permission from [the Licensor]: on behalf of Cancer Research UK: : [Journal Publisher (e.g. Nature/Springer/Palgrave)] [JOURNAL NAME] [REFERENCE CITATION (Article name, Author(s) Name), [COPYRIGHT] (year of publication)

For Advance Online Publication papers:

Reprinted by permission from The [the Licensor]: on behalf of Cancer Research UK: [Journal Publisher (e.g. Nature/Springer/Palgrave)] [JOURNAL NAME] [REFERENCE CITATION (Article name, Author(s) Name), [COPYRIGHT] (year of publication), advance online publication, day month year (doi: 10.1038/sj.[JOURNAL ACRONYM])

For Book content:

Reprinted/adapted by permission from [the Licensor]: [Book Publisher (e.g. Palgrave Macmillan, Springer etc)] [Book Title] by [Book author(s)] [COPYRIGHT] (year of publication)

Other Conditions:

Version 1.0

Questions? customercare@copyright.com or +1-855-239-3415 (toll free in the US) or +1-978-646-2777.



RightsLink®

SPRINGER NATURE

Title: Big Area Additive Manufacturing of High Performance Bonded NdFeB Magnets
Author: Ling Li, Angelica Tirado, I. C. Nlebedim, Orlando Rios, Brian Post et al.
Publication: Scientific Reports
Publisher: Springer Nature
Date: Oct 31, 2016
Copyright © 2016, Springer Nature

Creative Commons

This is an open access article distributed under the terms of the [Creative Commons CC BY](#) license, which permits unrestricted use, distribution, and reproduction in any medium, provided the original work is properly cited.

You are not required to obtain permission to reuse this article.

Are you the [author](#) of this Springer Nature article?

To order reprints of this content, please contact Springer Nature by e-mail at reprintswarehouse@springernature.com, and you will be contacted very shortly with a quote.

AIP PUBLISHING LLC LICENSE TERMS AND CONDITIONS

Feb 16, 2018

This Agreement between University of Alberta -- Alejandro Eufracio ("You") and AIP Publishing LLC ("AIP Publishing LLC") consists of your license details and the terms and conditions provided by AIP Publishing LLC and Copyright Clearance Center.

License Number	4290911096474
License date	Feb 16, 2018
Licensed Content Publisher	AIP Publishing LLC
Licensed Content Publication	Journal of Applied Physics
Licensed Content Title	Inkjet printing of magnetic materials with aligned anisotropy
Licensed Content Author	Han Song, Jeremy Spencer, Albrecht Jander, et al
Licensed Content Date	May 7, 2014
Licensed Content Volume	115
Licensed Content Issue	17
Type of Use	Thesis/Dissertation
Requestor type	Student
Format	Electronic
Portion	Figure/Table
Number of figures/tables	3
Title of your thesis / dissertation	Development of a Material Jetting 3D Printer with Magnetic Orientation Capabilities
Expected completion date	Mar 2018
Estimated size (number of pages)	100
Requestor Location	University of Alberta 9211-116 Street NW edmonton, AB T6G 1H9 Canada Attn: ALEJANDRO EUFRACIO
Billing Type	Invoice
Billing Address	University of Alberta 87nd Av edmonton, AB t6g0x6 Canada Attn: Alejandro Eufracio
Total	0.00 CAD

Terms and Conditions

AIP Publishing LLC -- Terms and Conditions: Permissions Uses
136

AIP Publishing hereby grants to you the non-exclusive right and license to use and/or distribute the Material according to the use specified in your order, on a one-time basis, for the specified

term, with a maximum distribution equal to the number that you have ordered. Any links or other content accompanying the Material are not the subject of this license.

1. You agree to include the following copyright and permission notice with the reproduction of the Material: "Reprinted from [FULL CITATION], with the permission of AIP Publishing." For an article, the credit line and permission notice must be printed on the first page of the article or book chapter. For photographs, covers, or tables, the notice may appear with the Material, in a footnote, or in the reference list.
2. If you have licensed reuse of a figure, photograph, cover, or table, it is your responsibility to ensure that the material is original to AIP Publishing and does not contain the copyright of another entity, and that the copyright notice of the figure, photograph, cover, or table does not indicate that it was reprinted by AIP Publishing, with permission, from another source. Under no circumstances does AIP Publishing purport or intend to grant permission to reuse material to which it does not hold appropriate rights.
You may not alter or modify the Material in any manner. You may translate the Material into another language only if you have licensed translation rights. You may not use the Material for promotional purposes.
3. The foregoing license shall not take effect unless and until AIP Publishing or its agent, Copyright Clearance Center, receives the Payment in accordance with Copyright Clearance Center Billing and Payment Terms and Conditions, which are incorporated herein by reference.
4. AIP Publishing or Copyright Clearance Center may, within two business days of granting this license, revoke the license for any reason whatsoever, with a full refund payable to you. Should you violate the terms of this license at any time, AIP Publishing, or Copyright Clearance Center may revoke the license with no refund to you. Notice of such revocation will be made using the contact information provided by you. Failure to receive such notice will not nullify the revocation.
5. AIP Publishing makes no representations or warranties with respect to the Material. You agree to indemnify and hold harmless AIP Publishing, and their officers, directors, employees or agents from and against any and all claims arising out of your use of the Material other than as specifically authorized herein.
6. The permission granted herein is personal to you and is not transferable or assignable without the prior written permission of AIP Publishing. This license may not be amended except in a writing signed by the party to be charged.
7. If purchase orders, acknowledgments or check endorsements are issued on any forms containing terms and conditions which are inconsistent with these provisions, such inconsistent terms and conditions shall be of no force and effect. This document, including the CCC Billing and Payment Terms and Conditions, shall be the entire agreement between the parties relating to the subject matter hereof.

This Agreement shall be governed by and construed in accordance with the laws of the State of New York. Both parties hereby submit to the jurisdiction of the courts of New York County for purposes of resolving any disputes that may arise hereunder.

V1.1

Questions? customercare@copyright.com or +1-855-239-3415 (toll free in the US) or +1-978-646-2777.
